University of Thessaly
School of Engineering
Department of Mechanical Engineering

Diploma Thesis

Numerical methods for porous metals with deformation-induced anisotropy

by
Orestis-Athanasios Gkaintes
Supervisor: Professor Nikolaos Aravas

A thesis
submitted in partial fulfillment of the
requirements for the degree of
Diploma in Mechanical Engineering

Volos, June 2020

Acknowledgments

This diploma thesis is accomplished in the scope of the partial fulfilment of the requirement of degree of Diploma in Mechanical Engineering at University of Thessaly.

At the present moment I am writing this, my journey to my bachelor studies is coming to an end. It has been quite a rough and long journey, since I entered as a freshman to the bachelor program in mechanical engineering. However, as the poet K. Kavafis said "What matters is the journey and not the destination."

I am grateful indeed for my studies in the department of Mechanical Engineering at University of Thessaly. I would have to write a list of names for the private tutoring I had from many PhD students, even Professors and other faculty stuff of the department. If someone is eager to seek for knowledge and ask for it, there will always be someone willing to offer it here.

I would deeply like to thank my thesis supervisor Professor N. Aravas who entrusted me on this research work and for his guidance over the months.

This work is based on the lectures of the thesis advisor Professor N. Aravas and Professor M. Agoras, the contribution of which is gratefully acknowledged. Both can explain in a clear manner even the most challenging topics.

The author would also like to thank Dr Ioanna Papadioti for her continuous support on me for the successful outcome of this Thesis and her help in the preparation of the manuscript.

Lastly, I would like express my sincere gratitude to my parents N. Gkaintes and V. Kotsia who have offered me so much.

To my parents.

Numerical methods for porous metals with deformation-induced anisotropy

Orestis-Athanasios Gkaintes

Supervisor: Professor Nikolaos Aravas

Abstract

The present thesis is concerned with the development and numerical implementation of a non-local constitutive model for porous metals. The non-local effect is incorporated through the introduction of a non-local porosity variable, which is derived from the concurrent solution of an additional partial differential equation along with the classical equilibrium equations. The motivation for this work is twofold. First, we want to develop constitutive models that describe the mechanical behavior of structural metals that account for "material damage" and can be used in the material "softening regime" until final material failure. Second, to introduce "material lengths" that account for the material microstructure into the constitutive equations. The non-local model is based on the advanced anisotropic model presented by Aravas and Ponte Castañeda [3]. The model considers the evolution of porosity and the development of anisotropy due to changes in the shape and the orientation of the voids during plastic deformation. A methodology for the numerical integration of the constitutive equations is presented. The implementation of a non-local model in a finite element code requires a variational formulation of the problem and the development of new finite elements. Here the model is implemented in the ABAQUS general purpose finite element program via a material "user subroutine" (UMAT or VUMAT) and the coupled thermo-mechanical solution procedure. Several example problems are solved numerically. In particular, the predictions of the model are compared to unit cell finite element calculations and the problems of ductile fracture, necking and failure of a round bar, and localization in plane-strain tension are analyzed in detail.

Keywords: Porous metals; Gradient plasticity; Finite Elements;

Contents

List of Figures

List of Tables

Introduction

A well-known problem in the computational implementation of damage mechanics models is that finite element solutions depend on the mesh size (i.e., are unreliable), when the material enters the softening region that precedes material failure. The mathematical reason for the mesh dependency is that the governing equations loose ellipticity and the boundary value problem (BVP), as posed originally, becomes ill-conditioned. We are interested in the detailed analysis of metal ductile fracture, which is known to be the result of growth and coalescence of microscopic voids, which are nucleated at inclusions and second-phase particles by decohesion of the particle–matrix interface or by particle cracking.

A non-local plasticity model for porous metals that accounts for deformation-induced anisotropy is developed. The term "non-local" refers to material models in which, e.g., the deformation $\boldsymbol{\varepsilon}$ at material point A depends not only on the "local" values of the stress $\boldsymbol{\sigma}$ and the internal variables $\mathbf{s}$ at A, but it also depends on the values of $\boldsymbol{\sigma}$ and $\mathbf{s}$ in the immediate neighborhood of point A. The motivation for this work is twofold. First, we want to develop constitutive models that describe the mechanical behavior of structural metals that account for "material damage" and can be used in the material "softening regime" until final material failure. Second, to introduce "material lengths" that account for the material microstructure into the constitutive equations.

The non-local model is based on the advanced anisotropic model presented by Aravas and Ponte Castañeda [3]. The model considers the evolution of porosity and the development of anisotropy due to changes in the shape and the orientation of the voids during plastic deformation. At every material point, a "representative" ellipsoid is considered. The basic "internal variables" are the local equivalent plastic strain $\bar{\varepsilon}^p$, the local porosity f_{loc} , the aspect ratios ($w_1 = a_3/a_1, w_2 = a_3/a_2$) and the orientation of the principal axes ($\mathbf{n}^{(1)}, \mathbf{n}^{(2)}, \mathbf{n}^{(3)}$) of the ellipsoid. The material is locally orthotropic with the axes of orthotropy defined by the principal direction of the representative ellipsoid.

We developed a gradient version of the model, which is be based on a "non-local" porosity variable f and introduces a "material length" ℓ to the constitutive equations. The non-local porosity f is defined by an additional boundary value problem (BVP).

A methodology for the numerical integration of the constitutive equations is also presented. The non-local model is then implemented in the ABAQUS general purpose finite element program via a material "user subroutine" (UMAT or VUMAT) and the coupled thermo-mechanical solution procedure. Several example problems are solved numerically.

The earlier chapters of this thesis build on basic theories of continuum mechanics and plasticity so that the reader will get a better understanding on the anisotropic model for porous metals. The Thesis proceeds with Chapter 4, where the formulation of the non-local anisotropic model is presented. In Chapter 5 a methodology is presented for the numerical integration of the constitutive equations and the implementation of the non-local model in ABAQUS general purpose finite element program via a material "user subroutine" (UMAT or VUMAT) and the coupled thermo-mechanical solution procedure. Finally, in Chapter 6 several example problems are solved numerically. In particular, the predictions of the model are compared to unit cell finite element calculations and the problems of ductile fracture, necking and failure of a round bar, and localization in plane-strain tension are analyzed in detail.

Chapter 1

Notations and Nomenclatures

1.1 The Meaning of a Tensor

In continuum mechanics the term tensor is commonly used. A Cartesian tensor $\mathbf{A}$ of order N, where $N \geq 1$, is a quantity that is described by 3^N components which can be expressed in any arbitrary Cartesian coordinate system, with the property that, if $A_{ijk\dots}$ (where $i, j, k \cdots$ are N indexes taking the values 1, 2, 3) is an expression of $\mathbf{A}$ in a Cartesian frame with base vectors $\mathbf{e}_i$ and $A'_{ijk\dots}$ the corresponding expression to a Cartesian frame with base vectors $\mathbf{e}'_i$ which results from a rotation of the previous, then the components $A_{ijk\dots}$ and $A'_{ijk\dots}$ are related by

$$A'_{ijk\cdots} = Q_{ip}Q_{jq}Q_{kr}\cdots A_{pqr\cdots} \tag{1.1}$$

A common tensor in continuum mechanics is the deformation gradient second-order tensor $F_{ij} = \partial x_i/\partial X_j$ which shows how an infinitesimal fiber of length $d\mathbf{X}$ in the undeformed configuration stretches to length $d\mathbf{x}$ and rotates. The symmetric and antisymmetric parts of the tensor F_{ij} symboled as ε_{ij} and Ω_{ij} describe this stretching and rotation of the fiber respectively. Another common second-order tensor is the spatial velocity gradient tensor $L_{ij} = \partial v_i/\partial x_j$ which shows how the velocity field v_i tends to change in the deformed configuration of x_j, with its symmetric and antisymmetric part the so-called strain rate D_{ij} and strain rate W_{ij}, respectively. Lastly, it is worth mentioning the fourth-order elastic tensor $\mathcal{L}^e_{ijkl}$ which relates the stresses to strains by a constitutive relation of the form

$$\sigma_{ij} = \mathcal{L}^e_{ijkl}\varepsilon_{kl} \qquad or \qquad \varepsilon_{ij} = \mathcal{M}^e_{ijkl}\sigma_{kl} \tag{1.2}$$

where $\mathcal{M}^e_{ijkl}$ is called the elastic compliance tensor and it is the inverse of $\mathcal{L}^e_{ijkl}$.

1.2 Conventions

The summary convention (or repeated index form) will be used:

$$\mathcal{L}_{ijkl}\varepsilon_{kl} \equiv \sum_{k=1}^{3}\sum_{l=1}^{3}\mathcal{L}_{ijkl}\varepsilon_{kl}, \tag{1.3}$$

meaning that the summation symbols will be omitted for simplicity and that repeated indexes will mean summation over these indexes.

Index notation for vectors and tensors will be used throughout the text, unless mentioned otherwise. All tensor components are written with respect to a fixed Cartesian coordinate

system with base vectors $\mathbf{e}_i$ ($i = 1, 2, 3$). Whenever possible, the base letter for a vector (first-order tensor) will be a lowercase italic letter, for a second-order tensor it will be a lowercase Greek letter, and for a fourth-order tensor it will be an upper-case italic letter. For example, u_i represents a vector, ε_{ij} represents a second-order tensor, and $\mathcal{L}_{ijkl}$ represents a fourth-order tensor.

Alternately, when it is convenient, the direct (or matrix) notation of vectors and tensors will be used as well. For this purpose, boldface symbols will denote tensors the order of which are indicated by the context.

A superscript T over a second-order tensor denotes its transpose. The transpose of an arbitrary second-order tensor $\mathbf{A} = A_{ij}\mathbf{e}_i\mathbf{e}_j$ is defined as

$$\mathbf{A}^T = A_{ji}\,\mathbf{e}_i\mathbf{e}_j = A_{ij}\,\mathbf{e}_j\mathbf{e}_i\,. \tag{1.4}$$

The subscripts *sym* and *skew* denote the symmetric and antisymmetric parts of a second-order tensor. A second-order tensor $\mathbf{A}$ is called symmetric if it satisfies the condition

$$\mathbf{A}^T = \mathbf{A} \quad or \quad A_{ij} = A_{ji}\,, \tag{1.5}$$

and antisymmetric if

$$\mathbf{A}^T = -\mathbf{A} \quad or \quad A_{ij} = -A_{ji}\,. \tag{1.6}$$

Any second-order tensor $\mathbf{A}$ can be written as

$$\mathbf{A} = \frac{1}{2}(\mathbf{A} + \mathbf{A}^T) + \frac{1}{2}(\mathbf{A} - \mathbf{A}^T)\,, \tag{1.7}$$

or

$$\mathbf{A} = \mathbf{A}_{sym} + \mathbf{A}_{skew}\,, \tag{1.8}$$

with

$$\mathbf{A}_{sym} = \frac{1}{2}(\mathbf{A} + \mathbf{A}^T) \quad and \quad \mathbf{A}_{skew} = \frac{1}{2}(\mathbf{A} - \mathbf{A}^T)\,, \tag{1.9}$$

where it is readily proved that $\mathbf{A}_{sym}$ and $\mathbf{A}_{skew}$ are indeed symmetric and antisymmetric second-order tensors.

A superimposed dot denotes the material time derivative, meaning that

$$\dot{\mathbf{A}}_{ijk\cdots} = \frac{d\mathbf{A}_{ijk\cdots}}{dt} \quad or \quad \dot{A}_{ijk\cdots} = \frac{dA_{ijk\cdots}}{dt}. \tag{1.10}$$

A fourth-order tensor, $\boldsymbol{\mathcal{L}}$, is nonsingular if and only if there exists a fourth-order tensor, for example, $\boldsymbol{\mathcal{M}}$, such that

$$\boldsymbol{\mathcal{L}} \cdot \boldsymbol{\mathcal{M}} = \boldsymbol{\mathcal{M}} \cdot \boldsymbol{\mathcal{L}} = \mathbf{I}, \tag{1.11}$$

where $\mathbf{I}$ is the symmetric fourth-order identity tensor with components $I_{ijkl} = (\delta_{ik}\delta_{jl} + \delta_{il}\delta_{jk})$. In this case, it is said that $\boldsymbol{\mathcal{M}}$ is the inverse of $\boldsymbol{\mathcal{L}}$, or $\boldsymbol{\mathcal{L}}$ is the inverse of $\boldsymbol{\mathcal{M}}$, that is,

$$\boldsymbol{\mathcal{M}} = \boldsymbol{\mathcal{L}}^{-1} \quad or \quad \boldsymbol{\mathcal{L}} = \boldsymbol{\mathcal{M}}^{-1}\,. \tag{1.12}$$

The symbol δ_{ij} in the expression of $\mathbf{I}$ is called the Kronecker delta and it denotes the components of a second-order identity tensor, that is,

$$\delta_{ij} = \begin{cases} 1 & if \quad i = j, \\ 0 & if \quad i \neq j, \end{cases} \quad or \quad [\boldsymbol{\delta}] = \begin{bmatrix} 1 & 0 & 0 \\ 0 & 1 & 0 \\ 0 & 0 & 1 \end{bmatrix}. \tag{1.13}$$

1.3 Tensorial Operations

Let $\mathbf{a}, \mathbf{b}$ be vectors, $\mathbf{A}, \mathbf{B}$ second-order tensors and $\boldsymbol{\mathcal{C}}$ a fourth order tensor; then the following products are defined:

$$\begin{aligned} &Dyadic\ product: && (\mathbf{ab})_{ij} = a_i\, b_j \Leftrightarrow \mathbf{a} \otimes \mathbf{b},\ \ (\mathbf{ba})_{ij} = b_i\, a_j \Leftrightarrow \mathbf{b} \otimes \mathbf{a} \\ & && (\mathbf{AB})_{ijkl} = A_{ij}\, b_{kl} \Leftrightarrow \mathbf{A} \otimes \mathbf{B} \end{aligned} \tag{1.14}$$

$$\begin{aligned} &Dot\ product: && (\mathbf{A} \cdot \mathbf{a})_i = A_{ij}\, a_j,\ \ (\mathbf{a} \cdot \mathbf{A})_i = a_j\, A_{ji},\ \ (\mathbf{A} \cdot \mathbf{B})_{ij} = A_{ik}\, B_{kj} \\ & && \mathbf{a} \cdot \mathbf{A} \cdot \mathbf{b} = a_i\, A_{ij}\, b_j \end{aligned} \tag{1.15}$$

$$\begin{aligned} &Double-dot\ product: && (\mathbf{A} : \boldsymbol{\mathcal{C}})_{ij} = A_{kl}\, \mathcal{C}_{klij},\ \ \ (\boldsymbol{\mathcal{C}} : \mathbf{A})_{ij} = \mathcal{C}_{ijkl}\, A_{kl},\ \ \ \mathbf{A} : \mathbf{B} = A_{ij}\, B_{ij} \\ & && \mathbf{A} : \boldsymbol{\mathcal{C}} : \mathbf{B} = A_{ij}\, \mathcal{C}_{ijkl}\, B_{kl} \end{aligned} \tag{1.16}$$

1.4 The Jaumann Time Derivative

In continuum mechanics one usually requires the frame independence or *objectivity* of constitutive equations while balance laws are only Galilean-invariant[1]. If constitutive equations include time rates, then the question of building objective time derivatives is raised. The Jaumann co-rotational derivative, denoted by $\overset{\triangledown}{(\bullet)}$, is such a derivative. For the second-order stress tensor $\boldsymbol{\sigma}$, it is defined by

$$\overset{\triangledown}{\sigma} = \dot{\boldsymbol{\sigma}} - \mathbf{W} \cdot \boldsymbol{\sigma} + \boldsymbol{\sigma} \cdot \mathbf{W}, \quad with \quad W_{ij} = \frac{1}{2} \left(\mathrm{v}_{i,j} - \mathrm{v}_{j,i} \right) , \tag{1.17}$$

where $\mathbf{v}$ denotes the velocity field with v_i Cartesian components, and $\mathrm{v}_{i,j} \equiv \partial \mathrm{v}_i / \partial x_j$.

[1]Galilean invariance or Galilean relativity states that the laws of motion are the same in all inertial frames.

Chapter 2

Continuum Mechanics

2.1 Definition of Continuous Medium

[1] A continuous medium is understood as an infinite set of particles which form part of a body (solid or fluid) that will be studied macroscopically, that is, without considering the possible discontinuities existing at microscopic level (atomic or molecular level). Accordingly, one admits that there are no discontinuities between the particles and that the mathematical description of this medium and its properties can be described by continuous functions.

2.2 Configurations of the Continuous Medium

Consider the continuous medium of Fig. 2.1 at a given instant of time t_0 having an initial volume V_0 and a bounding surface Γ_0, and occupying a certain region R_0 of the physical space. When the continuum is in motion or undergoes deformation, the particles (materials points) within the continuum are displaced from one spatial position to another. At time t the body changes to volume V and boundary surface Γ, and occupies region R. A material particle, say P, in the initial configuration is characterized by a vector $\mathbf{X}$ and moves to another position denoted by $\mathbf{x}$. The equations of motion of such a particle are given by

$$\mathbf{x} = \phi(\mathbf{X}, t) \overset{not}{=} \mathbf{x}(\mathbf{X}, t) \quad or \quad x_i = x_i(X_1, X_2, X_3, t) \qquad i \in \{1, 2, 3\}.^{2} \tag{2.1}$$

The above equation provides a way to find the new location of each particle after the motion or deformation of the body. This way of description of position (and any other quantity) is called the Lagrangian description. Again vector $\mathbf{X}$ shows the position of a particle in the initial configuration R_0, and thus it can viewed as a label attached to it, while $\mathbf{x}$ indicates where the particle is located at a given time t. In contrast, when someone wants to know which particle $\mathbf{X}$ passed the spatial point $\mathbf{x}$ at a given time t, then he needs the inverse equations of (2.1) such that

$$\mathbf{X} = \phi^{-1}(\mathbf{x}, t) \overset{not}{=} \mathbf{X}(\mathbf{x}, t) \quad or \quad X_i = X_i(x_1, x_2, x_3, t) \qquad i \in \{1, 2, 3\}. \tag{2.2}$$

I.e. Eq. (2.2) keeps track of which particle happens to be at the location x_i at time t. Such a description of any quantity is called the Eulerian description. Eqs. (2.1) and (2.2) may be interpreted as a mapping between the initial configuration and the current configuration. In

[1] Big part of this chapter is based on the free notes of Xavier Oliver [31] and the lecture notes of Piaras Kelly [19].

[2] The term '*not*' over the equality sign stands for 'notation'.

order for this mapping to be one to one the Jacobian $J = |\partial x_i/\partial X_J|$ should not become zero at any time t.

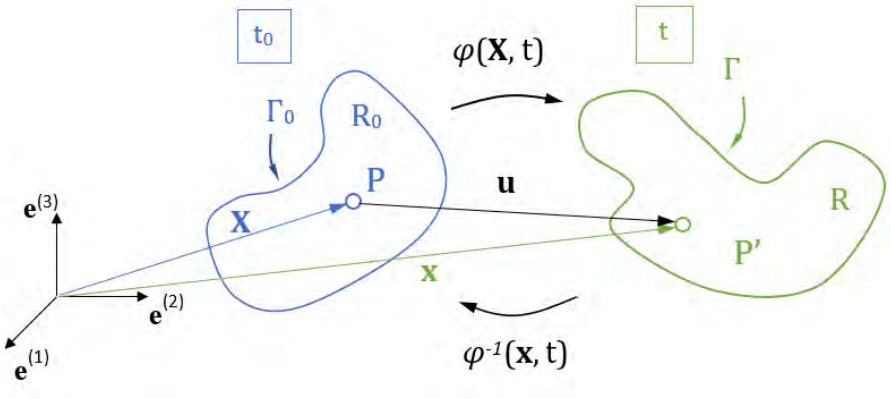

Figure 2.1: A body occupying the reference configuration R_0 at time t_0 and the configuration R at t. A particle P initially located at point $\mathbf{X}$ at time t_0 moves to point $\mathbf{x}$ at time t. The transformation taking the body from the initial configuration R_0 to the current configuration R is $\phi(\mathbf{X}, t)$, while the transformation $\phi^{-1}(\mathbf{X}, t)$ works vice versa.

The displacement field

The difference between the position vectors $\mathbf{x}$ and $\mathbf{X}$ of particle P in the current and initial configuration is called the displacement of particle P and is denoted by the vector $\mathbf{u}$. The displacement of all the particles in the continuous medium defines a displacement vector field which can be described in material form as

$$\mathbf{U}(\mathbf{X}, t) = \mathbf{x}(\mathbf{X}, t) - \mathbf{X} \quad or \quad U_i(\mathbf{X}, t) = x_i(\mathbf{X}, t) - X_i \qquad i \in \{1, 2, 3\}\,, \tag{2.3}$$

or in spatial form as

$$\mathbf{u}(\mathbf{x}, t) = \mathbf{x} - \mathbf{X}(\mathbf{x}, t) \quad or \quad u_i(\mathbf{x}, t) = x_i - X_i(\mathbf{x}, t) \qquad i \in \{1, 2, 3\}\,. \tag{2.4}$$

2.3 Deformation Gradient Tensor

Consider the continuous medium of Fig. 2.2 in rigid body motion or after deformation. A particle P in the reference configuration R_0 occupies the point P' in the present configuration R, and a particle Q situated in the differential neighborhood of P has relative positions with respect to this particle in the reference and present times $d\mathbf{X}$ and $d\mathbf{x}$, respectively.

Differentiating (2.1) with respect to the material coordinates $\mathbf{X}$ results in

$$d\mathbf{x} = \mathbf{F} \cdot d\mathbf{X} \quad or \quad dx_i = \frac{\partial x_i}{\partial X_j} dX_j = F_{ij} dX_j \qquad i,\, j \in \{1, 2, 3\}. \tag{2.5}$$

Eq. (2.5) defines the deformation gradient tensor $\mathbf{F}$ as

$$\mathbf{F} \overset{not}{=} \mathbf{x} \otimes \overline{\nabla}\,^{3} \quad or \quad F_{ij} = \frac{\partial x_i}{\partial X_j} \qquad i,\, j \in \{1, 2, 3\}, \tag{2.6}$$

[3]The bar over the Nabla operator denotes the material Nabla operator, such that $\overline{\nabla} \equiv \partial(\bullet)/\partial X_i$.

or in matrix form as

$$\mathbf{F} = \mathbf{x} \otimes \overline{\nabla} = \begin{Bmatrix} x_1 \\ x_2 \\ x_3 \end{Bmatrix} \cdot \begin{bmatrix} \frac{\partial}{\partial X_1} & \frac{\partial}{\partial X_2} & \frac{\partial}{\partial X_3} \end{bmatrix} = \begin{bmatrix} \frac{\partial x_1}{\partial X_1} & \frac{\partial x_1}{\partial X_2} & \frac{\partial x_1}{\partial X_3} \\ \frac{\partial x_2}{\partial X_1} & \frac{\partial x_2}{\partial X_2} & \frac{\partial x_2}{\partial X_3} \\ \frac{\partial x_3}{\partial X_1} & \frac{\partial x_3}{\partial X_2} & \frac{\partial x_3}{\partial X_3} \end{bmatrix} \tag{2.7}$$

Remark 2.1. The deformation gradient tensor $\mathbf{F}(\mathbf{X}, t)$ contains the information of the relative motion, along time t, of all the material particles in the differential neighborhood of a given particle, identified by its material coordinates $\mathbf{X}$. Eq. (2.5) provides the relative position vector $d\mathbf{x}$ in terms of the corresponding relative position in the reference time, $d\mathbf{X}$.

Differentiating (2.2) with respect to the spatial coordinates x_i results in

$$d\mathbf{X} = \mathbf{F}^{-1} \cdot d\mathbf{x} \quad or \quad dX_i = \frac{\partial X_i}{\partial x_j} dx_j = F^{-1}_{ij} dx_j \qquad i, j \in \{1, 2, 3\}. \tag{2.8}$$

Eq. (2.8) defines the inverse of the deformation gradient tensor $\mathbf{F}^{-1}$ as

$$\mathbf{F}^{-1} \overset{not}{=} \mathbf{X} \otimes \nabla \,^{4} \quad or \quad F^{-1}_{ij} = \frac{\partial X_i}{\partial x_j} \qquad i, j \in \{1, 2, 3\}, \tag{2.9}$$

or in matrix form as

$$\mathbf{F}^{-1} = \mathbf{X} \otimes \nabla = \begin{Bmatrix} X_1 \\ X_2 \\ X_3 \end{Bmatrix} \cdot \begin{bmatrix} \frac{\partial}{\partial x_1} & \frac{\partial}{\partial x_2} & \frac{\partial}{\partial x_3} \end{bmatrix} = \begin{bmatrix} \frac{\partial X_1}{\partial x_1} & \frac{\partial X_1}{\partial x_2} & \frac{\partial X_1}{\partial x_3} \\ \frac{\partial X_2}{\partial x_1} & \frac{\partial X_2}{\partial x_2} & \frac{\partial X_2}{\partial x_3} \\ \frac{\partial X_3}{\partial x_1} & \frac{\partial X_3}{\partial x_2} & \frac{\partial X_3}{\partial x_3} \end{bmatrix} \tag{2.10}$$

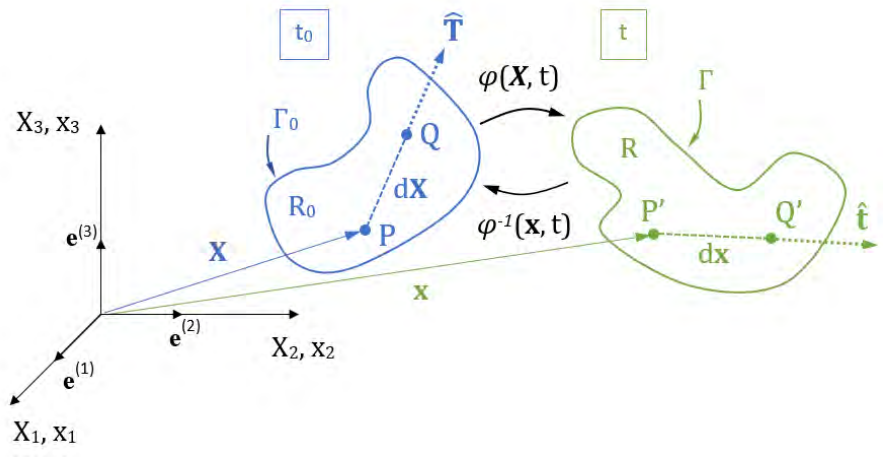

Figure 2.2: A line segment $d\mathbf{X}$ and $d\mathbf{x}$ in the initial and current configuration, respectively, emanating from point P to Q in the differential neighborhood of P.

[4]Here the symbolic form of the spatial Nabla operator, $\nabla \equiv \partial(\bullet)/\partial x_i$, is used.

Remark 2.2. *Proof* that $\mathbf{F}^{-1}$ is indeed the inverse of $\mathbf{F}$:

$$F_{ik}F^{-1}_{kj} = \frac{\partial x_i}{\partial X_k}\frac{\partial X_k}{\partial x_j} = \frac{\partial x_i}{\partial x_j} = \delta_{ij} \quad \Longleftrightarrow \quad \mathbf{F}\cdot\mathbf{F}^{-1} = \boldsymbol{\delta}\,, \tag{2.11}$$

$$F^{-1}_{ik}F_{kj} = \frac{\partial X_i}{\partial x_k}\frac{\partial x_k}{\partial X_j} = \frac{\partial X_i}{\partial X_j} = \delta_{ij} \quad \Longleftrightarrow \quad \mathbf{F}\cdot\mathbf{F}^{-1} = \boldsymbol{\delta}\,. \tag{2.12}$$

2.4 The Polar Decomposition of the Gradient Tensor

Theorem: The polar decomposition theorem of tensor analysis establishes that for any second order tensor $\mathbf{A}$ which is invertible ($det\mathbf{A} \neq 0$) there exist two positive definite [5], symmetric tensors $\mathbf{U}$, $\mathbf{V}$ and an orthogonal tensor $\mathbf{R}$ such that $\mathbf{A}$ can be written as

$$\mathbf{A} = \mathbf{R}\cdot\mathbf{U} = \mathbf{V}\cdot\mathbf{R}\,, \tag{2.13}$$

where the orthogonal[6] tensor $\mathbf{R}$ is a proper (orthogonal) tensor if ($det\mathbf{A} > 0$) and an improper (orthogonal) tensor if ($det\mathbf{A} < 0$). It is proven [1] that the polar decomposition of a tensor is unique and that the tensors $\mathbf{U}$ and $\mathbf{V}$ take the form

$$\mathbf{U} = \sqrt{\mathbf{A}^T\cdot\mathbf{A}} \quad \textit{and} \quad \mathbf{V} = \sqrt{\mathbf{A}\cdot\mathbf{A}^T}\,. \tag{2.14}$$

The product $\mathbf{A} = \mathbf{R}\cdot\mathbf{U}$ is called "right polar decomposition" and the product $\mathbf{A} = \mathbf{V}\cdot\mathbf{R}$ is called "left polar decomposition". Let λ_i and N_i be the eigenvalues and the corresponding unity eigenvectors of $\mathbf{U}$. Then, it is also proven [2] that,
i) the eigenvalues and the corresponding unity eigenvectors of $\mathbf{V}$ are λ_i and $\mathbf{n}_i$ such that

$$\mathbf{U} = \sum_{i=1}^{3}\lambda_i\mathbf{N}_i\otimes\mathbf{N}_i, \quad \textit{and} \quad \mathbf{V} = \sum_{i=1}^{3}\lambda_i\mathbf{n}_i\otimes\mathbf{n}_i\,, \quad \textit{where} \quad \mathbf{n}_i = \mathbf{R}\cdot\mathbf{N}_i\,, \tag{2.15}$$

ii) $\mathbf{A}$, $\mathbf{A}^{-1}$ and $\mathbf{R}$ can be written as

$$\mathbf{A} = \sum_{i=1}^{3}\lambda_i\,\mathbf{n}_i\otimes\mathbf{N}_i\,, \quad \mathbf{A}^{-1} = \sum_{i=1}^{3}\frac{1}{\lambda_i}\,\mathbf{N}_i\otimes\mathbf{n}_i\,, \quad \mathbf{R} = \sum_{i=1}^{3}\mathbf{n}_i\otimes\mathbf{N}_i\,. \tag{2.16}$$

Considering now the polar decomposition of the deformation gradient tensor $\mathbf{F}$ and the relation (2.5), the following is obtained,

$$d\mathbf{x} = \mathbf{F}\cdot d\mathbf{X} = (\mathbf{V}\cdot\mathbf{R})\cdot d\mathbf{X} = \overbrace{\mathbf{V}\cdot\overbrace{(\mathbf{R}\cdot d\mathbf{X})}^{\text{rotation}}}^{\text{stretching}} \tag{2.17}$$

which implies the definition of an operator $\mathbf{F}$ which acts on a tensor (when doted with it) in

[5] A second order tensor $\mathbf{A}$ is called positive definite if $\mathbf{a}\cdot\mathbf{A}\cdot\mathbf{a} = A_{ij}a_ia_j > 0$ for any vector $\mathbf{a} \neq \mathbf{0}$.

[6] A second-order tensor $\mathbf{R}$ is orthogonal if $(\mathbf{R}\cdot\mathbf{u})\cdot(\mathbf{R}\cdot\mathbf{v}) = \mathbf{u}\cdot\mathbf{v} \quad \forall\ \mathbf{u},\mathbf{v} \in \mathcal{R}^3$. Furthermore, the meaning of a proper (or improper) orthogonal second-order tensor $\mathbf{R}$ is found in chapter 1 of [2].

the following manner

$$\boxed{\mathbf{F}\cdot(\bullet)\equiv \text{stretching} \overset{\text{not}}{\circ} \text{rotation}\,(\bullet)}\,^{7}, \tag{2.18}$$

and

$$d\mathbf{x}=\mathbf{F}\cdot d\mathbf{X}=(\mathbf{R}\cdot\mathbf{U})\cdot d\mathbf{X}=\overbrace{\mathbf{R}\cdot\overbrace{(\mathbf{U}\cdot d\mathbf{X})}^{\text{stretching}}}^{\text{rotation}}, \tag{2.19}$$

so that

$$\boxed{\mathbf{F}\cdot(\bullet)\equiv \text{rotation} \overset{\text{not}}{\circ} \text{stretching}\,(\bullet)}\,. \tag{2.20}$$

A graphical representation of the polar decomposition of $\mathbf{F}$ is shown in Fig. 2.3.

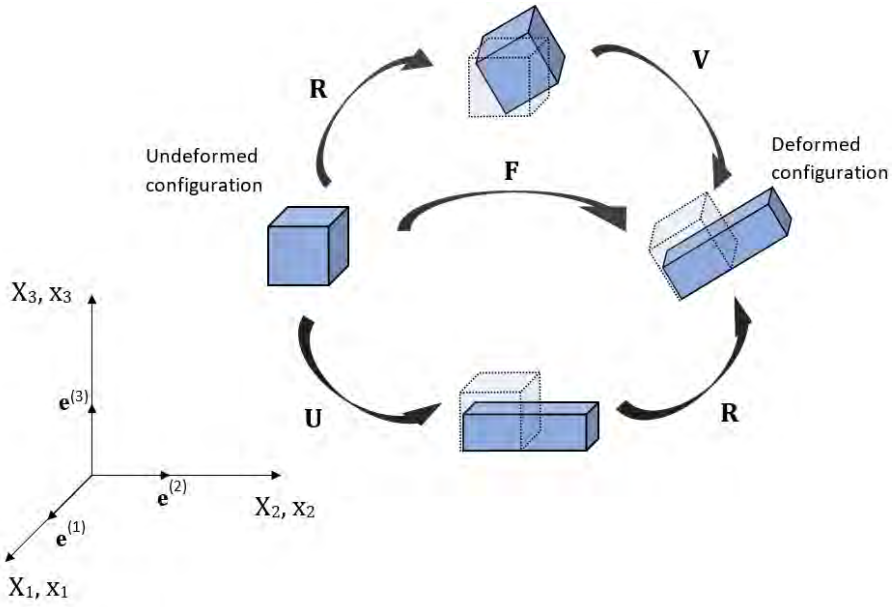

Figure 2.3: Polar decomposition of the gradient deformation tensor $\mathbf{F}$.

2.5 The Material Strain Tensor

Consider again the particle P of Fig. 2.2 and another particle Q in its differential neighborhood separated by a segment $d\mathbf{X}$ and $d\mathbf{x}$ in the initial and current configuration, respectively. Let dS be the length of segment $d\mathbf{X}$, $\hat{\mathbf{T}}$ the unit vector in the direction of $d\mathbf{X}$ and ds, $\hat{\mathbf{t}}$ be the length and unit vector, respectively, of its counterpart $d\mathbf{x}$ such that

$$\begin{cases} (ds)^2 = dx_k\,dx_k = F_{ki}\,dX_i\,F_{kj}\,dX_j = dX_i\,F_{ki}\,F_{kj}\,dX_j = dX_i\,F^T_{ik}\,F_{kj}\,dX_j \\ or \\ (ds)^2 = d\mathbf{x}\cdot d\mathbf{x} = d\mathbf{X}\cdot\mathbf{F}^T\cdot\mathbf{F}\cdot d\mathbf{X} \end{cases} \tag{2.21}$$

and

$$(dS)^2 = d\mathbf{X}\cdot d\mathbf{X}. \tag{2.22}$$

Subtracting (2.22) from (2.21) results in

$$(ds)^2-(dS)^2 = d\mathbf{X}\cdot\mathbf{F}^T\cdot\mathbf{F}\cdot d\mathbf{X}-d\mathbf{X}\cdot d\mathbf{X} = d\mathbf{X}\cdot\left(\mathbf{F}^T\cdot\mathbf{F}-\boldsymbol{\delta}\right)\cdot d\mathbf{X}\,. \tag{2.23}$$

[7] The notation $(\circ)$ is used here to indicate the composition of two operations ξ and ϕ: $z=\phi\circ\xi\,(\mathbf{x})$.

Thus, defining the material (or Green - Lagrange) strain tensor

$$\mathbf{E}(\mathbf{X},t)=\frac{1}{2}\left(\mathbf{F}^T\cdot\mathbf{F}-\boldsymbol{\delta}\right)\quad or\quad E_{ij}=\frac{1}{2}\left(F_{ki}F_{kj}-\delta_{ij}\right)\qquad i,\,j\in\{1,2,3\},\tag{2.24}$$

then (2.23) reads

$$(ds)^2-(dS)^2=2\,d\mathbf{X}\cdot\mathbf{E}\cdot d\mathbf{X}\,.\tag{2.25}$$

Remark 2.3. The material strain tensor $\mathbf{E}$ is symmetric. The proof is the following

$$\mathbf{E}^T=\frac{1}{2}\left(\mathbf{F}^T\cdot\mathbf{F}-\boldsymbol{\delta}\right)^T=\frac{1}{2}\left(\mathbf{F}^T\cdot\left(\mathbf{F}^T\right)^T-\boldsymbol{\delta}^T\right)=\frac{1}{2}\left(\mathbf{F}^T\cdot\mathbf{F}-\boldsymbol{\delta}\right)=\mathbf{E}\,.\tag{2.26}$$

The Physical Meaning of the Diagonal Components

Considering the geometric expression $d\mathbf{X}=\hat{\mathbf{T}}\,dS$ (see Fig. 2.2), then it follows from (2.25) that

$$(ds)^2-(dS)^2=2\,(dS)^2\,\hat{\mathbf{T}}\cdot\mathbf{E}\cdot\hat{\mathbf{T}}\,,\tag{2.27}$$

and by dividing both sides by $(dS)^2$, results in

$$\left(\frac{ds}{dS}\right)^2-1=\lambda_T^2-1=2\,\hat{\mathbf{T}}\cdot\mathbf{E}\cdot\hat{\mathbf{T}}\quad\Rightarrow\quad\lambda_T=\sqrt{1+2\,\hat{\mathbf{T}}\cdot\mathbf{E}\cdot\hat{\mathbf{T}}}\,,\tag{2.28}$$

where λ_T denotes the stretch of a line segment initially along the direction of the unit vector $\hat{\mathbf{T}}$ and it is equal to $\lambda_T=ds/dS$.

Let E_{ij} $i,\,j\in\{1,2,3\}$ be the components of $\mathbf{E}$ expressed in a Cartesian frame, then by making use of (2.28) the following relations are obtained in terms of the diagonal components of tensor $\mathbf{E}$

$$\begin{aligned}\varepsilon_1&=\lambda_1-1=\sqrt{1+2E_{11}}-1\,,\\ \varepsilon_2&=\lambda_2-1=\sqrt{1+2E_{22}}-1\,,\\ \varepsilon_3&=\lambda_3-1=\sqrt{1+2E_{33}}-1\,,\end{aligned}\tag{2.29}$$

where ε_T denotes the unit elongation of a line segment initially along the direction of the unit vector $\hat{\mathbf{T}}$ and it is equal to

$$\varepsilon_T=\frac{ds-dS}{dS}=\lambda_T-1\,.\tag{2.30}$$

Eq. (2.28) indicates that the material tensor $\mathbf{E}(\mathbf{X},t)$ contains information on the stretches (and unit elongations) for any direction in the differential neighborhood of a given particle. In particular, (2.29) shows that the diagonal components E_{11}, E_{22} and E_{33} of tensor $\mathbf{E}$ contain information on stretch and unit elongations of the differentials segments that were initially oriented in the directions 1, 2 and 3, respectively.

The Physical Meaning of the off-Diagonal Components

Consider a particle P and two additional particles Q and R, belonging in the differential neighborhood of P in the initial configuration, and the same particles occupying the spatial positions P',Q' and R', as shown in Fig. 2.4. Consider the line segments $d\mathbf{X}^{(1)}$ of PQ and

$d\mathbf{X}^{(2)}$ of PR with lengths $dS^{(1)}$ and $dS^{(2)}$, respectively, in the initial configuration and their counterparts $d\mathbf{x}^{(1)}$ of $P'Q'$ and $d\mathbf{x}^{(2)}$ of $P'R'$ with lengths $ds^{(1)}$ and $ds^{(2)}$ in the current configuration. Let $\hat{\mathbf{T}}^{(1)}$, $\hat{\mathbf{T}}^{(2)}$ be the unit vectors in the direction of $d\mathbf{X}_1$ and $d\mathbf{X}_2$ and $\hat{\mathbf{t}}^{(1)}$, $\hat{\mathbf{t}}^{(2)}$ be the unit vectors in the direction of $d\mathbf{x_1}$ and $d\mathbf{x_2}$, respectively.

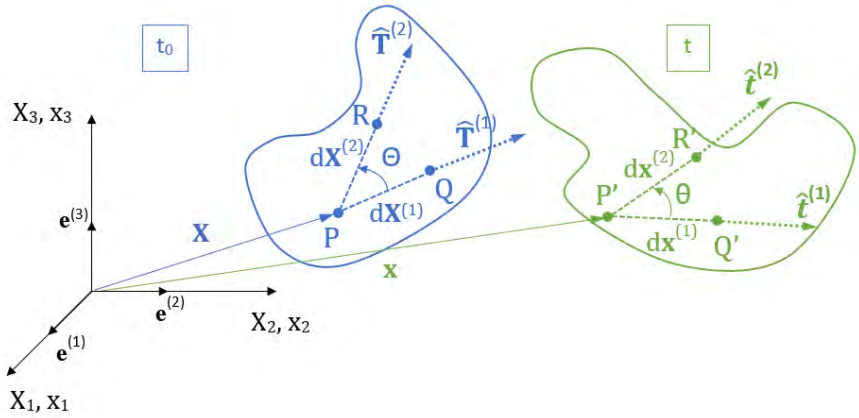

Figure 2.4: Angles between differential segments in the reference and current configuration.

Then it follows that,

$$\begin{cases} d\mathbf{X}^{(1)} = dS^{(1)}\,\hat{\mathbf{T}}^{(1)}\,, \\ d\mathbf{X}^{(2)} = dS^{(2)}\,\hat{\mathbf{T}}^{(2)}\,, \end{cases} \tag{2.31}$$

and by taking the dot product of vectors $d\mathbf{x}^{(1)}$ and $d\mathbf{x}^{(2)}$ we obtain

$$\begin{aligned} d\mathbf{x}^{(1)} \cdot d\mathbf{x}^{(2)} &= |d\mathbf{x}^{(1)}||d\mathbf{x}^{(2)}| \cos\theta = ds^{(1)} ds^{(2)} \cos\theta\,, \\ d\mathbf{x}^{(1)} \cdot d\mathbf{x}^{(2)} &= d\mathbf{X}^{(1)} \cdot \left(\mathbf{F}^T \cdot \mathbf{F}\right) \cdot d\mathbf{X}^{(2)} = \\ &= d\mathbf{X}^{(1)} \cdot (2\,\mathbf{E} + \boldsymbol{\delta}) \cdot d\mathbf{X}^{(2)} = \\ &= dS^{(1)}\,\hat{\mathbf{T}}^{(1)} \cdot (2\,\mathbf{E} + \boldsymbol{\delta}) \cdot \hat{\mathbf{T}}^{(2)}\, dS^{(2)} = \\ &= ds^{(1)}\, ds^{(2)} \frac{1}{\lambda^{(1)}\lambda^{(2)}}\, \hat{\mathbf{T}}^{(1)} \cdot (2\,\mathbf{E} + \boldsymbol{\delta}) \cdot \hat{\mathbf{T}}^{(2)}\,. \end{aligned} \tag{2.32}$$

Now by comparing the initial and final terms in (2.32) and by making use of (2.28) for the stretches $\lambda^{(1)}$ and $\lambda^{(2)}$ in the directions $\hat{\mathbf{T}}_1$ and $\hat{\mathbf{T}}_2$ we obtain

$$\cos\theta = \frac{\hat{\mathbf{T}}^{(1)} \cdot (2\,\mathbf{E} + \boldsymbol{\delta}) \cdot \hat{\mathbf{T}}^{(2)}}{\sqrt{1 + 2\,\hat{\mathbf{T}}^{(1)} \cdot \mathbf{E} \cdot \hat{\mathbf{T}}^{(1)}}\sqrt{1 + 2\,\hat{\mathbf{T}}^{(2)} \cdot \mathbf{E} \cdot \hat{\mathbf{T}}^{(2)}}} \tag{2.33}$$

In view of (2.33) it is noticed that the tensor $\mathbf{E}(\mathbf{X}, t)$ contains also information on the variation of the angles between differentials segments in the differential neighborhood of a particle at point $\mathbf{X}$ in the initial configuration.

If the line segments PQ and PR are aligned to X_i and X_j $(i \neq j)$ axis, respectively, such that $\hat{\mathbf{T}}_i \cdot \hat{\mathbf{T}}_j = 0$ and their angle $\Theta_{ij} = \pi/2$ in the initial configuration, then according to (2.33) the angle θ_{ij} in the present configuration is

$$\cos\theta_{ij} = \frac{2\,E_{ij}}{\sqrt{1 + 2\,E_{ii}}\sqrt{1 + 2\,E_{jj}}} \quad \text{(no summation over i and j)}\,, \tag{2.34}$$

which is the same as

$$\theta_{ij} = \frac{\pi}{2} - \arcsin \frac{2E_{ij}}{\sqrt{1+2E_{ii}}\sqrt{1+2E_{jj}}} \quad \text{(no summation over i and j)}\,. \tag{2.35}$$

Defining the increment of the final angle $\Delta\Theta_{ij}$ with respect to its initial value we have

$$\Delta\Theta_{ij} = \theta_{ij} - \underbrace{\Theta_{ij}}_{\pi/2} = -\arcsin \frac{2E_{ij}}{\sqrt{1+2E_{ii}}\sqrt{1+2E_{jj}}} \quad \text{(no summation over i and j)} \tag{2.36}$$

Substituting the i, j's with $(1, 2, 3)$ for $(i \neq j)$ and following a counterclockwise rotation the following relations are obtained:

$$\begin{aligned}
\Delta\Theta_{12} &= -\arcsin \frac{2E_{12}}{\sqrt{1+2E_{11}}\sqrt{1+2E_{22}}} \\
\Delta\Theta_{13} &= -\arcsin \frac{2E_{13}}{\sqrt{1+2E_{11}}\sqrt{1+2E_{33}}} \\
\Delta\Theta_{23} &= -\arcsin \frac{2E_{23}}{\sqrt{1+2E_{22}}\sqrt{1+2E_{33}}}\,.
\end{aligned} \tag{2.37}$$

Eqs. (2.37) determine the angle change of two line segments which are perpendicular to each other in the reference configuration in terms of the components of tensor **E**. It is noticed that both the off-diagonal and diagonal components contribute to this angle change, thus in finite strain theory probably there is not a direct definition for the off-diagonal components. Figure 2.5 shows a graphical depiction of Eq. (2.36).

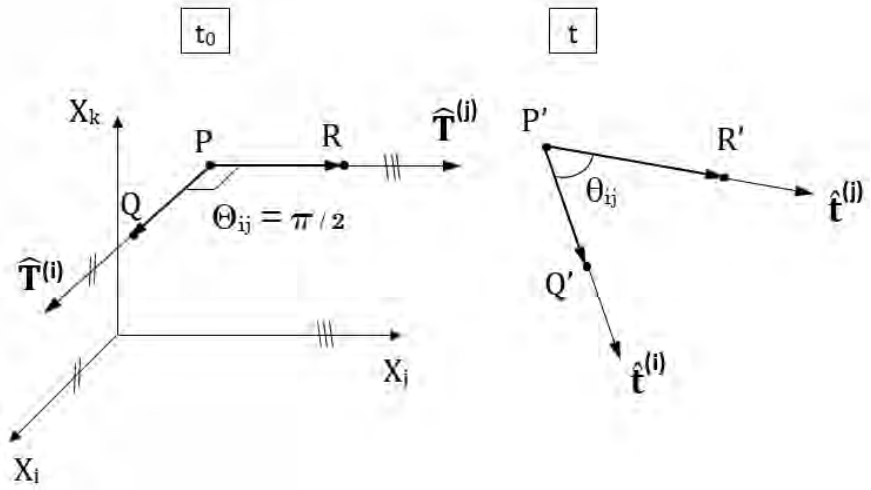

Figure 2.5: Angle variation of line segments which are perpendicular to each other in the reference configuration.

2.6 The Velocity Gradient Tensor

Consider the configuration of a body at time t and two fixed neighbouring points P' and Q', see Fig. 2.6. The velocities of the material particles at these points at time t are $\mathbf{v}(\mathbf{x})$ and $\mathbf{v}(\mathbf{x} + d\mathbf{x})$, and

$$\mathbf{v}(\mathbf{x} + d\mathbf{x}) = \mathbf{v}(\mathbf{x}) + \frac{\partial \mathbf{v}}{\partial \mathbf{x}} d\mathbf{x}\,. \tag{2.38}$$

The relative velocity between the points is

$$d\mathbf{v} = \frac{\partial \mathbf{v}}{\partial \mathbf{x}} \cdot \mathbf{x} \equiv \mathbf{L} \cdot d\mathbf{x}\,, \tag{2.39}$$

with $\mathbf{L}$ defined to be the (spatial) velocity gradient,

$$\mathbf{L} \equiv \frac{\partial \mathbf{v}(\mathbf{x}, t)}{\partial \mathbf{x}} = \mathbf{v} \otimes \nabla \quad or \quad L_{ij} = \frac{\partial \mathrm{v}_i}{\partial x_j} \quad i,\, j \in \{1, 2, 3\} \tag{2.40}$$

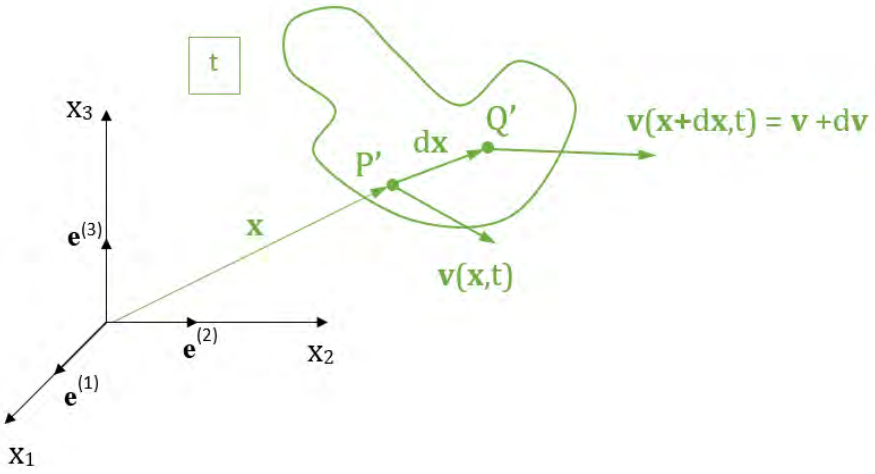

Figure 2.6: Velocities of two neighbor particles in the continuous medium at time t.

Material Derivatives of the Deformation Gradient

The spatial velocity gradient may be written in repeated index form as

$$L_{ij} = \frac{\partial \mathrm{v}_j}{\partial x_i} = \frac{\partial \mathrm{v}_j}{\partial X_k}\frac{\partial X_k}{\partial x_i} = \frac{\partial}{\partial X_k}\left(\frac{\partial x_j}{\partial t}\right)\frac{\partial X_k}{\partial x_i} = \frac{\partial}{\partial t}\left(\frac{\partial x_j}{\partial X_k}\right)\frac{\partial X_k}{\partial x_i}\,, \tag{2.41}$$

or in compact form

$$\frac{\partial \mathbf{v}}{\partial \mathbf{x}} = \frac{\partial \mathbf{v}}{\partial \mathbf{X}}\frac{\partial \mathbf{X}}{\partial \mathbf{x}} = \frac{\partial}{\partial \mathbf{X}}\left(\frac{\partial \mathbf{x}}{\partial t}\right)\frac{\partial \mathbf{X}}{\partial \mathbf{x}} = \frac{\partial}{\partial t}\left(\frac{\partial \mathbf{x}}{\partial \mathbf{X}}\right)\frac{\partial \mathbf{X}}{\partial \mathbf{x}}\,, \tag{2.42}$$

which concludes that

$$\mathbf{L} = \dot{\mathbf{F}} \cdot \mathbf{F}^{-1} \quad or \quad \dot{\mathbf{F}} = \mathbf{L} \cdot \mathbf{F}\,. \tag{2.43}$$

In a similar manner it can also be proven that

$$\dot{\mathbf{F}}^{-1} = -\mathbf{F}^{-1} \cdot \mathbf{L}\,. \tag{2.44}$$

2.7 The Strain Rate and Spin Tensors

The velocity gradient tensor can be split into a symmetric and an antisymmetric part[8],

$$\mathbf{L} = \mathbf{D} + \mathbf{W}\,, \tag{2.45}$$

where $\mathbf{D}$ is a symmetric tensor denominated *strain rate tensor*,

$$\mathbf{D} = \frac{1}{2}\left(\mathbf{L} + \mathbf{L}^T\right) = \frac{1}{2}\left(\mathbf{v}\otimes\nabla + \nabla\otimes\mathbf{v}\right)\,, \tag{2.46}$$

or

$$D_{ij} = \frac{1}{2}\left(\frac{\partial \mathrm{v}_i}{\partial x_j} + \frac{\partial \mathrm{v}_j}{\partial x_i}\right) \qquad i,j \in \{1,2,3\}, \tag{2.47}$$

and $\mathbf{W}$ is an antisymmetric tensor denominated *rotation rate tensor* or *spin tensor*, whose expression is

$$\mathbf{W} = \frac{1}{2}\left(\mathbf{L} - \mathbf{L}^T\right) = \frac{1}{2}\left(\mathbf{v}\otimes\nabla - \nabla\otimes\mathbf{v}\right)\,, \tag{2.48}$$

or

$$W_{ij} = \frac{1}{2}\left(\frac{\partial \mathrm{v}_i}{\partial x_j} - \frac{\partial \mathrm{v}_j}{\partial x_i}\right) \qquad i,j \in \{1,2,3\}. \tag{2.49}$$

Physical Interpretation of the Rate Tensor

Consider the continuous medium of Fig. 2.6. The rate at which the square of the length of the line segment $d\mathbf{x}$ changes is

$$\begin{aligned}
&\frac{d}{dt}\Big(|d\mathbf{x}|^2\Big) = 2\Big(|d\mathbf{x}|\Big)\frac{d}{dt}\Big(|d\mathbf{x}|\Big),\\
&\frac{d}{dt}\Big(|d\mathbf{x}|^2\Big) = \frac{d}{dt}\left(d\mathbf{x}\cdot d\mathbf{x}\right) = \frac{d}{dt}(d\mathbf{x})\cdot d\mathbf{x} + d\mathbf{x}\cdot\frac{d}{dt}(d\mathbf{x}) =\\
&\qquad = d\left(\frac{d\mathbf{x}}{dt}\right)\cdot d\mathbf{x} + d\mathbf{x}\cdot d\left(\frac{d\mathbf{x}}{dt}\right) = d\mathbf{v}\cdot d\mathbf{x} + d\mathbf{x}\cdot d\mathbf{v}
\end{aligned} \tag{2.50}$$

and by making use of (2.46) and (2.39), then

$$\frac{d}{dt}\Big(|d\mathbf{x}|^2\Big) = \left(d\mathbf{x}\cdot\mathbf{L}^T\right)\cdot d\mathbf{x} + d\mathbf{x}\cdot\left(\mathbf{L}\cdot d\mathbf{x}\right) = d\mathbf{x}\cdot\left(\mathbf{L}^T + \mathbf{L}\right)\cdot d\mathbf{x} = 2\,d\mathbf{x}\cdot\mathbf{D}\cdot d\mathbf{x}\,. \tag{2.51}$$

Dividing both sides of (2.51) by $2|d\mathbf{x}|^2$, then leads to

$$\frac{\dot{\lambda}}{\lambda} = \hat{\mathbf{t}}\cdot\mathbf{D}\cdot\hat{\mathbf{t}}\,, \tag{2.52}$$

where $\lambda = |d\mathbf{x}|/|d\mathbf{X}|$ is the stretch and $\hat{\mathbf{t}} = d\mathbf{x}/|d\mathbf{x}|$ is a unit vector in the direction of $d\mathbf{x}$. Eq. (2.52) computes the rate of stretching per unit of stretch in the direction $\hat{\mathbf{t}}$. Thus, the rate of deformation $\mathbf{D}$ gives the rate of stretching of line segments. The diagonal components of $\mathbf{D}$

$$D_{ii} = \mathbf{e}_i\cdot\mathbf{D}\cdot\mathbf{e}_i \quad for \quad i\in\{1,2,3\} \quad \text{(no summation over i)}\,, \tag{2.53}$$

[8] A theorem of tensorial analysis establishes that any second order $\mathbf{A}$ can be decomposed into the sum of its symmetric part and its antisymmetric or (skew-symmetric) part.

represent unit rates of extension (if positive) in the coordinate directions.

Consider now the rate of change of the angle θ between two vectors $d\mathbf{x}^{(1)}$, $d\mathbf{x}^{(2)}$. Again by making use of (2.46) and (2.39), we have

$$\begin{aligned}\frac{d}{dt}\left(d\mathbf{x}^{(1)}\cdot d\mathbf{x}^{(2)}\right) &= \frac{d}{dt}\left(d\mathbf{x}^{(1)}\right)\cdot d\mathbf{x}^{(2)} + d\mathbf{x}^{(1)}\cdot\frac{d}{dt}\left(d\mathbf{x}^{(2)}\right)\\ &= \mathbf{L}\cdot d\mathbf{x}^{(1)}\cdot d\mathbf{x}^{(2)} + d\mathbf{x}^{(1)}\cdot\mathbf{L}\cdot d\mathbf{x}^{(2)}\\ &= \left(\mathbf{L}+\mathbf{L}^T\right) d\mathbf{x}^{(1)}\cdot d\mathbf{x}^{(2)}\\ &= 2\, d\mathbf{x}^{(1)}\cdot\mathbf{D}\cdot d\mathbf{x}^{(2)}\,.\end{aligned} \tag{2.54}$$

An alternative expression for this dot product is

$$\begin{aligned}&\frac{d}{dt}\Big(|d\mathbf{x}^{(1)}||d\mathbf{x}^{(2)}|\cos\theta\Big) =\\ &\quad= \frac{d}{dt}\Big(|d\mathbf{x}^{(1)}|\Big)|d\mathbf{x}^{(2)}|\cos\theta + \frac{d}{dt}\Big(|d\mathbf{x}^{(2)}|\Big)|d\mathbf{x}^{(1)}|\cos\theta - \dot\theta\,\sin\theta|d\mathbf{x}^{(1)}||d\mathbf{x}^{(2)}|\\ &\quad= \left(\frac{\frac{d}{dt}\Big(|d\mathbf{x}^{(1)}|\Big)}{|d\mathbf{x}^{(1)}|}\cos\theta + \frac{\frac{d}{dt}\Big(|d\mathbf{x}^{(2)}|\Big)}{|d\mathbf{x}^{(2)}|}\cos\theta - \dot\theta\,\sin\theta\right)|d\mathbf{x}^{(1)}||d\mathbf{x}^{(2)}|\,.\end{aligned} \tag{2.55}$$

Equating (2.54) and (2.55) leads to

$$2\,\hat{\mathbf{t}}^{(1)}\cdot\mathbf{D}\cdot\hat{\mathbf{t}}^{(2)} = \left(\frac{\dot\lambda_1}{\lambda_1}+\frac{\dot\lambda_2}{\lambda_2}\right)\cos\theta - \dot\theta\,\sin\theta\,, \tag{2.56}$$

where $\lambda_i = |d\mathbf{x}^{(i)}|/|d\mathbf{X}^{(i)}|$ is the stretch of line segment i and $\hat{\mathbf{t}}^{(i)} = d\mathbf{x}^{(i)}/|d\mathbf{x}^{(i)}|$ is the unit normal in the direction of $d\mathbf{x}^{(i)}$.

It follows from (2.56) that the off-diagonal terms of the rate of deformation tensor represent *shear rates*; the rate of change of the right angle between line segments aligned with coordinate directions. For example, taking the base vectors $\mathbf{e}_1 = \hat{\mathbf{t}}^{(1)}$, $\mathbf{e}_2 = \hat{\mathbf{t}}^{(2)}$, then (2.56) reduces to

$$D_{12} = -\frac{1}{2}\dot\theta_{12}\,, \tag{2.57}$$

where θ_{12} is the instantaneous right angle between the axes in the current configuration.

Note that in (2.53) the D_{ii}'s are instantaneous rates of extension, in other words, they are rates of extensions of line segments in the current configuration at the current time t; they are not a measure of the rate at which a line segment in the original configuration changed into the corresponding line segment in the current configuration. Accordingly, in (2.57) the D_{ij}'s ($i \neq j$) are instantaneous rates of angle change between two line segments in the current configuration each one of which is aligned with one the of coordinate axes.

Physical Interpretation of the Spin Tensor

In view of (2.48) and (2.49) $\mathbf{W}$ is an antisymmetric tensor and in matrix form it can be written as

$$W_{ij} = \frac{1}{2}\left[\frac{\partial \mathrm{v}_i}{\partial x_j} - \frac{\partial \mathrm{v}_j}{\partial x_i}\right] \quad i,\, j\in\{1,2,3\} \quad \textit{or} \quad [\mathbf{W}] = \begin{bmatrix} 0 & W_{12} & -W_{31}\\ -W_{12} & 0 & W_{23}\\ W_{31} & -W_{23} & 0\end{bmatrix}. \tag{2.58}$$

The antisymmetric character of $\mathbf{W}$ implies that it has only three independent components and thus a vector $\boldsymbol{\omega}$,

$$\boldsymbol{\omega} = \frac{1}{2}\nabla \times \mathbf{v} = \frac{1}{2}\begin{bmatrix} -\left(\dfrac{\partial \mathrm{v}_2}{\partial x_3} - \dfrac{\partial \mathrm{v}_3}{\partial x_2}\right) \\ -\left(\dfrac{\partial \mathrm{v}_3}{\partial x_1} - \dfrac{\partial \mathrm{v}_1}{\partial x_3}\right) \\ -\left(\dfrac{\partial \mathrm{v}_1}{\partial x_2} - \dfrac{\partial \mathrm{v}_2}{\partial x_1}\right) \end{bmatrix} = \begin{bmatrix} -W_{23} \\ -W_{31} \\ -W_{12} \end{bmatrix}, \tag{2.59}$$

is extracted from $\mathbf{W}$. The vector $\boldsymbol{\omega}$ is called the *vorticity vector*. It is readily proven that

$$\boldsymbol{\omega} \times \mathbf{r} = \mathbf{W} \cdot \mathbf{r} \qquad \forall\, \mathbf{r} \in \mathcal{R}^3\,. \tag{2.60}$$

Therefore, it is possible to characterize $\boldsymbol{\omega}$ as the angular velocity of a rotation motion, and $\boldsymbol{\omega} \times \mathbf{r} = \mathbf{W} \cdot \mathbf{r}$ as the rotation velocity of the point, that has $\mathbf{r}$ as the position vector, with respect to the rotation center, as shown in Fig. 2.7.

Remark 2.4.. *Proof* of (2.60):

$$\boldsymbol{\omega} \times \mathbf{r} = det \begin{bmatrix} \mathbf{e}_1 & \mathbf{e}_2 & \mathbf{e}_3 \\ \omega_1 & \omega_2 & \omega_3 \\ r_1 & r_2 & r_3 \end{bmatrix} = \begin{bmatrix} \mathbf{e}_1 & \mathbf{e}_2 & \mathbf{e}_3 \\ -W_{23} & -W_{31} & -W_{12} \\ r_1 & r_2 & r_3 \end{bmatrix} = \begin{Bmatrix} W_{12}r_2 - W_{31}r_3 \\ W_{23}r_3 - W_{12}r_1 \\ W_{31}r_1 - W_{23}r_2 \end{Bmatrix} \tag{2.61}$$

$$\mathbf{W} \cdot \mathbf{r} = \begin{bmatrix} 0 & W_{12} & -W_{31} \\ -W_{12} & 0 & W_{23} \\ W_{31} & -W_{23} & 0 \end{bmatrix} \cdot \begin{Bmatrix} r_1 \\ r_2 \\ r_3 \end{Bmatrix} = \begin{Bmatrix} W_{12}r_2 - W_{31}r_3 \\ W_{23}r_3 - W_{12}r_1 \\ W_{31}r_1 - W_{23}r_2 \end{Bmatrix} \tag{2.62}$$

Comparing (2.61) and (2.62) it is readily seen that they are the same.

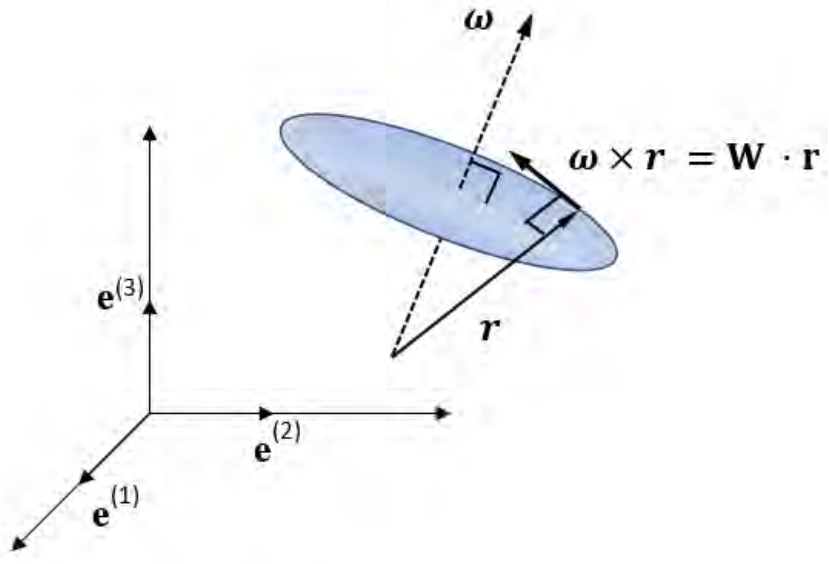

Figure 2.7: Graphical representation of the vorticity vector acting with an outer product to a vector $\mathbf{r}$.

.

Physical Interpretation of the Velocity Gradient Tensor

In view of (2.39) and (2.45) we have,

$$d\mathbf{v} = \mathbf{L} \cdot d\mathbf{x} = (\mathbf{D} + \mathbf{W}) \cdot d\mathbf{x} = \underbrace{\mathbf{D} \cdot d\mathbf{x}}_{\substack{stretch \\ velocity}} + \underbrace{\mathbf{W} \cdot d\mathbf{x}}_{\substack{rotation \\ velocity}}, \tag{2.63}$$

which allows describing the relative velocity $d\mathbf{v}$ of two neighbor particles P' and Q' of the body in the current configuration at time t as the sum of a *relative stretch velocity* (characterized by the strain rate tensor $\mathbf{D}$) and a *relative rotation velocity* (characterized by the spin tensor $\mathbf{W}$ or the vorticity vector $\boldsymbol{\omega}$), as shown in Fig. 2.8.

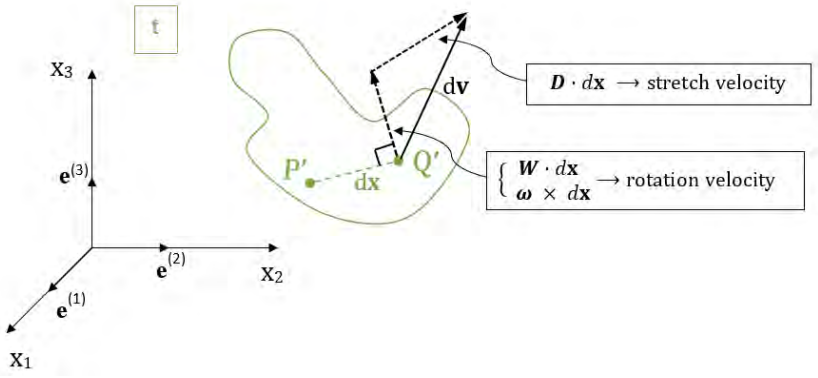

Figure 2.8: Graphical representation of the decomposition of $\mathbf{L}$.

.

Remark 2.5. Note that the theory presented in this chapter is general and it holds both for finite and infinitesimal strain theory.

Chapter 3

The constituents of General Plasticity for Rate-Independent Materials

A material enters the elastoplastic regime, when it undergoes some *permanent deformation*. Significant permanent deformations occur when the stress reaches some critical value, called the *yield stress*, σ_y, which is a material property. Plasticity theory is concerned with materials that deform elastoplastically upon reaching the yield stress.

3.1 The Yielding Mechanism

One can imagine the lattice of a metal as a structured mesh of atoms and simulate their interactive forces as that of a spring. Under the application of stresses the lattice deforms by an increase in the distance between the atoms. In the tensile test this is observed as the elastic domain. As their distance increases so does the resistance of the lattice to deformation. This resistance coming as the analogous of a spring is described by the Young's module, E. In that sense one would expect the failure of the material to be the collateral breaking of the bonds. Though, in the onset of stress yielding a new slope E^{ep} is observed in the stress-strain diagram, therefore a new mechanism must be triggered. That mechanism stems from imperfections of the lattice, where in some parts of it an extra plane of atoms is located, as shown in Fig. 3.1. This extra plane of atoms is called a *dislocation*. What is observed as elongation of the specimen after reaching the yield stress, is mainly due to the breaking of the bonds of the dislocation A (see Fig. 3.1) in the so called slip plane. This dislocation is then transferred to plane B, then C etc., up to reaching a free end. In most pure metals, only shear stresses contribute to the breaking of the bonds to the slip plane and the movement of a dislocation. Thus, the early theory of plasticity neglected the dependence of the yield stress on the normal stress components of the stress tensor [1].

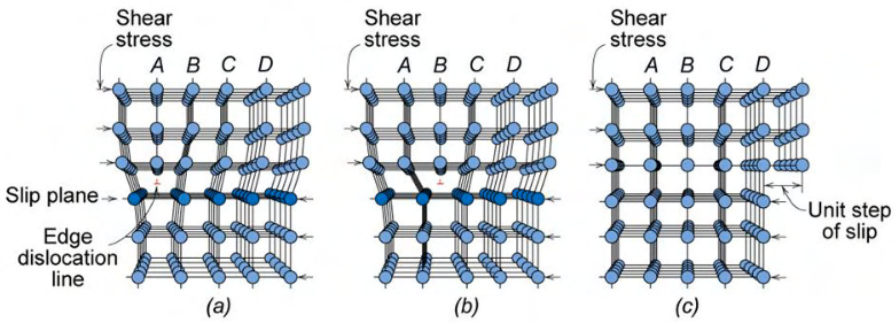

Figure 3.1: Dislocation motion [9]

[1] Which are also referred by the term hydrostatic pressure.

3.2 Assumptions of Plasticity Theory

In the formulation of general plasticity theory the following assumptions are usually made:

1. the material is incompressible in the plastic region
2. there is no Bauschinger effect
3. the yield stress is independent of hydrostatic pressure
4. the material is isotropic

Note that only the first two are usually a good approximation, while the other two may or may not be, depending on the material and the circumstances. For example, as mentioned before, a porous material satisfies orthotropic symmetry in every point of the media, and also the yield stress is dependent on the hydrostatic pressure, since the pores may act as a softening mechanism in tensile loading and as a hardening mechanism in compression.

3.3 The Principal Stress Space

Consider a a cylindrical specimen subjected to a tensile load P and a torsion load T. Focusing to an arbitrary infinitesimal cube of the specimen, i.e to a point of the material, one would observe stresses induced on its surfaces (see Fig. 3.2). In that sense it is said that the stress state to a point of a material is described by the stress tensor $\boldsymbol{\sigma}$, which happens to be symmetric and have six independent components as a consequence of the Angular Momentum Balance Principle. In a mathematical sense a tensor can be written to its principal form, which always has three non-zero components. Thus, the stress state to a point of the material corresponds to a point in the principal stress space described by a Cartesian coordinate system with each principal stress corresponding to an axis.

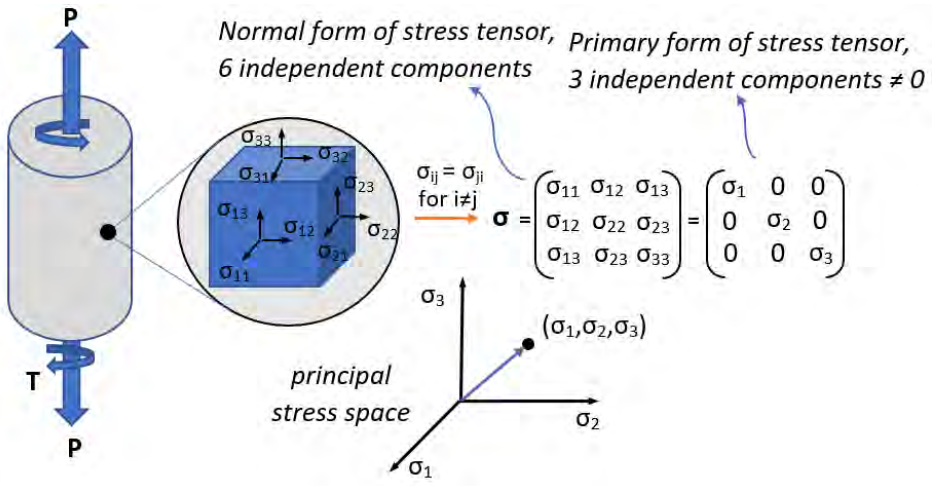

Figure 3.2: The principal stress space.

3.4 The Yield Condition

Now let $\mathbf{s} = \{s_1, s_2, ..., s_n\}$ be a set of *state or internal* variables that characterize the physical state of the material and $\boldsymbol{\sigma}$ be the tensor of stress components in each point of the media resulting from the applied loads to the material. For a given material characterized by a

vector of state variables $\mathbf{s}^*$ and subjected to a stress state $\boldsymbol{\sigma}^*$, one wishes to construct a function Φ such that

$$\Phi(\boldsymbol{\sigma}^*, \mathbf{s}^*) \begin{cases} < 0 & \Rightarrow \quad \textit{elastic response} \\ = 0 & \Rightarrow \quad \textit{elastoplastic response} \end{cases} \tag{3.1}$$

The function Φ is called the *yield function* and the condition $\Phi = 0$ defines a surface in the principal stress space which is called the *yield surface*. Note that by definition Φ can not be greater than zero, because by trying to capture the physical model, one concludes that whenever a material enters the elastoplastic zone its microstructure changes and therefore the *state* variables change. Accordingly the yield surface in the principal stress space changes. It expands and shrinks whenever the material experiences hardening and softening, respectively. In general Φ can be written in the form

$$\Phi(\boldsymbol{\sigma}, \mathbf{s}^\alpha) = \sigma_e(\boldsymbol{\sigma}, \mathbf{s}^\beta) - \sigma_y(s^\gamma)\,, \tag{3.2}$$

where $\mathbf{s}^\alpha, \mathbf{s}^\beta, \mathbf{s}^\gamma$ are three arbitrary sets of *state* variables, σ_e is a properly defined equivalent stress and σ_y is the yield stress.

3.5 The Normality Rule

Although a material may experience a large plastic deformation, the plasticity theory assumes that it reaches this amount of deformation by successive, incrementally small plastic deformations. Each one of these small plastic deformations is characterized by the plastic part of deformation-rate-tensor $\mathbf{D}^p$ which can be computed by the so called *normality rule*:

$$\mathbf{D}^p = \dot{\Lambda}\mathbf{N}\,, \quad \text{where} \quad \mathbf{N} = \frac{\partial \Phi}{\partial \sigma}\,, \;\; \dot{\Lambda} \geq 0\,, \tag{3.3}$$

i.e. Eqn. (3.3) states that $\mathbf{D}^p$ is in the same direction with $\mathbf{N}$. $\dot{\Lambda}$ is called the *plastic multiplier* and for now is just an arbitrary nonnegative number. Note that from the definition $\mathbf{N} = \partial\Phi/\partial\sigma$, $\mathbf{N}$ is a "vector" [2] which is normal to the plastic potential Φ. The reasoning to derive Eqn. (3.3) is the following. Consider for the moment the one-dimensional loading of a hardening material. Suppose that the material is initially fully elastic but has various loads, residual stresses, etc acting, so that the state of stress at a certain point is σ^*, point A in Fig. 3.3. An additional load is now applied to the material, bringing it to the current yield stress σ at point B (if σ^* is below the yield stress) and then plastically through the infinitesimal increment $d\sigma$ to point C. The additional load is then removed, bringing the stress back to σ^* and point D. The work done (per unit volume) by the additional loads during a stress cycle A-B-C-D is given by:

$$W \;\; = \int\limits_{A-B-C-D} (\sigma(\varepsilon) - \sigma^*)\, d\varepsilon\,. \tag{3.4}$$

This work is the shaded area in Fig. 3.3. Writing

$$d\varepsilon = d\varepsilon^e + d\varepsilon^p\,, \tag{3.5}$$

and noting that the elastic work is recovered, i.e. the net work due to elastic strain is zero, this work is due to the plastic strains,

[2] In reality $\mathbf{N}$ is a tensor, but we can imagine it as a vector of more than three components.

$$W = \int_{B-C} (\sigma(\varepsilon) - \sigma^*)\, d\varepsilon^p \,. \tag{3.6}$$

With $d\sigma$ infinitesimal, this equals

$$W = (\sigma - \sigma^*)\, d\varepsilon^p + \frac{1}{2} d\sigma\, d\varepsilon^p \geq 0. \tag{3.7}$$

Note that the inequality holds, because it is assumed that the net work performed by the external agency over a stress cycle is non-negative. This is a result from the laws of thermodynamics where the total work is positive (or zero) in a complete cycle.

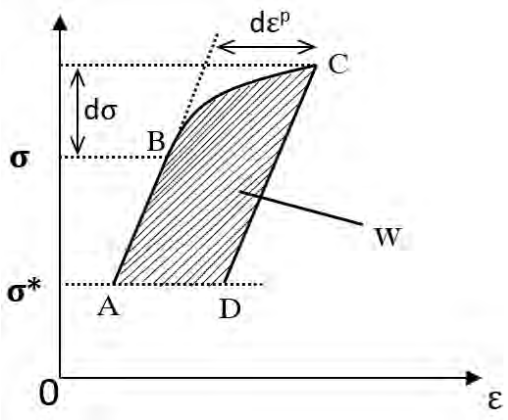

Figure 3.3: Work W done during a stress cycle of a strain-hardening material.

Assuming $(\sigma - \sigma^*) \gg d\sigma$, then Eqn. (3.7) reads

$$(\sigma - \sigma^*)\, d\varepsilon^p \geq 0 \,. \tag{3.8}$$

On the other hand, assuming $\sigma = \sigma^*$, Eqn. (3.7) reads

$$d\sigma\, d\varepsilon^p \geq 0 \,. \tag{3.9}$$

The three dimensional case is illustrated in Fig. 3.4, for which one has

$$(\sigma_{ij} - \sigma^*_{ij})\, d\varepsilon^p_{ij} \geq 0, \qquad d\sigma_{ij} d\varepsilon^p_{ij} \geq 0 \,. \tag{3.10}$$

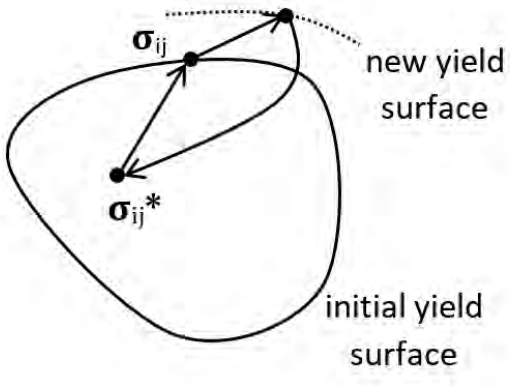

Figure 3.4: Stresses during a loading/unloading cycle.

In terms of vectors in principal stress space Eqn. (3.10) reads

$$(\boldsymbol{\sigma} - \boldsymbol{\sigma}^*) \cdot d\boldsymbol{\varepsilon}^p \geq 0\,. \tag{3.11}$$

The rate form of Eqn. (3.11) is

$$(\boldsymbol{\sigma} - \boldsymbol{\sigma}^*) \cdot \dot{\boldsymbol{\varepsilon}}^p \geq 0\,. \tag{3.12}$$

Since the dot product is non-negative, the angle between the vectors $(\boldsymbol{\sigma} - \boldsymbol{\sigma}^*)$ and $\dot{\boldsymbol{\varepsilon}}^p$ (with their starting points coincident) must be less than 90°. Recall that $\boldsymbol{\sigma}$ is the current stress state and it is always on the yield surface. The initial stress state $\boldsymbol{\sigma}^*$ is arbitrary and it can be within or on the yield surface. Let $\boldsymbol{\sigma}^*$ take the values $\boldsymbol{\sigma}_1^*$ and $\boldsymbol{\sigma}_2^*$ then Eqn. (3.12) implies that

$$\begin{aligned} &(\boldsymbol{\sigma} - \boldsymbol{\sigma}_1^*) \cdot \dot{\boldsymbol{\varepsilon}}^p \geq 0 \quad \Rightarrow \quad \dot{\boldsymbol{\varepsilon}}^p \in \mathbf{A}\,, && (a) \\ &(\boldsymbol{\sigma} - \boldsymbol{\sigma}_2^*) \cdot \dot{\boldsymbol{\varepsilon}}^p \geq 0 \quad \Rightarrow \quad \dot{\boldsymbol{\varepsilon}}^p \in \mathbf{B}\,, && (b) \end{aligned} \tag{3.13}$$

where $\mathbf{A}$ and $\mathbf{B}$ are the feasible spaces of vector $\dot{\boldsymbol{\varepsilon}}^p$ having as a starting point the one that corresponds to stress state $\boldsymbol{\sigma}$ on the yield surface, see Fig. 3.5. To satisfy both (3.13a) and (3.13b) $\dot{\boldsymbol{\varepsilon}}^p \in \mathbf{A} \cap \mathbf{B}$. In the limit case where $\boldsymbol{\sigma}_1^* \to \boldsymbol{\sigma}$ and $\boldsymbol{\sigma}_2^* \to \boldsymbol{\sigma}$, $\dot{\boldsymbol{\varepsilon}}^p$ will be outwardly normal to the yielding surface at stress state point $\boldsymbol{\sigma}$.

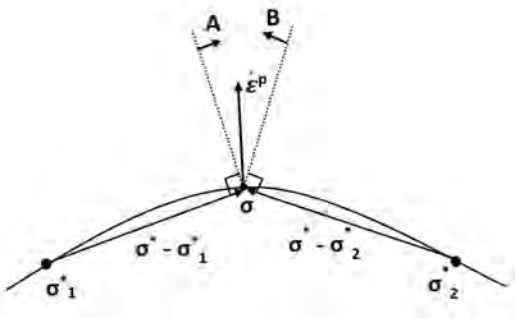

Figure 3.5: Normality of the plastic strain increment vector.

Eqn. (3.12) implies also that the yielding surface will be convex. If it was not, then there would exist an initial stress state $\boldsymbol{\sigma}^*$ on the yield surface such that the angle between the vectors $(\boldsymbol{\sigma} - \boldsymbol{\sigma}^*)$ and $\dot{\boldsymbol{\varepsilon}}^p$ would be more than 90°, as illustrated in Fig. 3.6

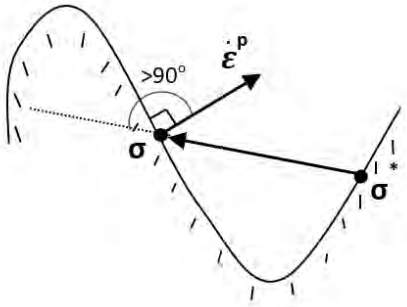

Figure 3.6: A non-convex surface.

Although Eqn. (3.12) was derived considering a hardening material, it is more general, holding also for the case of perfectly plastic and softening materials. To see this, consider a stress state σ^* which is at or below the current yield stress σ, and apply a strain $d\varepsilon > 0$. For

a perfectly plastic material, $\sigma - \sigma^* \geq 0$ and $d\varepsilon = d\varepsilon^p > 0$. For a softening material again $\sigma - \sigma^* \geq 0$ and $d\varepsilon^e < 0$, $d\varepsilon^p > d\varepsilon > 0$.

3.6 The Evolution Equations of the State Variables

When a material deforms plastically, the state variables evolve, and in turn, influence the response of the material. The general form of the evolution equations of the state variables is

$$\dot{s}^\alpha = G\left(\boldsymbol{\sigma}, \mathbf{s}^\beta, \dot{\boldsymbol{\varepsilon}}^p\right) = G(\boldsymbol{\sigma}, \mathbf{s}^\beta, \dot{\Lambda}\mathbf{N})\,, \tag{3.14}$$

where $\mathbf{s}^\beta$ is a subset of the state variables $\mathbf{s}^\alpha$. For a rate-independent material Eqn. (3.14) can be written in the form

$$\dot{s}^\alpha = \dot{\Lambda}\, G(\boldsymbol{\sigma}, \mathbf{s}^\beta, \mathbf{N})\,. \tag{3.15}$$

3.7 The Flow Rule

Consider the case of a hardening material subjected to a load causing the stress state (σ_e^A)[3] which is higher than its yield stress σ_y. In that case the material deforms plastically and σ_e^A becomes the current yield stress. The yield surface of the current state is determined by the relation

$$\Phi(\boldsymbol{\sigma}^A, \mathbf{s}^a) = 0\,, \tag{3.16}$$

as shown in Fig. 3.7. An additional infinitesimal load $d\boldsymbol{\sigma}^A$ is now applied to the material bringing it to the current yield stress $(\sigma^A + d\sigma^A)_e$, where the yield surface of the current state is determined by the relation

$$\Phi(\boldsymbol{\sigma}^A + d\boldsymbol{\sigma}^A, \mathbf{s}^a + d\mathbf{s}^a) = 0\,. \tag{3.17}$$

Since the material hardens the yield surface expands, see Fig. 3.7. Note that as the material deforms plastically its internal structure changes and that is described by the change $\mathbf{s}^a + d\mathbf{s}^a$ of the state variables.

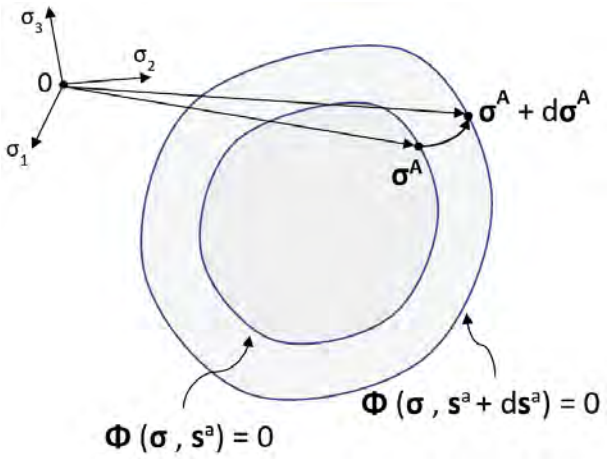

Figure 3.7: The flow rule.

[3]The subscript 'e' denotes the equivalent stress of a stress state, such that (σ_e^A) is the equivalent stress resulting from the stress state $\boldsymbol{\sigma}^A$.

Taking the difference between (3.17) and (3.16) and dividing by the infinitesimal change dt (t can be time) results in

$$\dot{\Phi} = \frac{\partial \Phi}{\partial \boldsymbol{\sigma}} : \dot{\boldsymbol{\sigma}} + \dot{\Lambda} \cdot \sum_{\alpha} \frac{\partial \Phi}{\partial s^{\alpha}} \dot{s^{\alpha}} = 0 \,. \tag{3.18}$$

Eqn. (3.18) is called the *flow rule* and one can compute $\dot{\Lambda}$ with respect to the stresses $\boldsymbol{\sigma}$ or the strains $\boldsymbol{\varepsilon}$.

In terms of the stresses, $\dot{\Lambda}$ is computed as follows. By denoting $H = -\sum_{\alpha} \frac{\partial \Phi}{\partial s^{\alpha}} \dot{s^{\alpha}}$ and recalling that $\mathbf{N} = \partial \Phi / \partial \boldsymbol{\sigma}$, then Eqn. (3.18) results in

$$\mathbf{N} : \dot{\boldsymbol{\sigma}} - \dot{\Lambda} H = 0 \Rightarrow \dot{\Lambda} = \frac{1}{H} \mathbf{N} : \dot{\boldsymbol{\sigma}} \;, \qquad H = -\sum_{\alpha} \frac{\partial \Phi}{\partial s^{\alpha}} \dot{s^{\alpha}} \,. \tag{3.19}$$

The parameter H determines the response of the material after surpassing its current σ_y, meaning that if

- $H > 0$ then the material hardens
- $H < 0$ then the material softens
- $H = 0$ then the material behaves as perfectly plastic.

Note that in the case of a perfectly plastic material Eqn. (3.19) is not defined.

With respect to the strains $\dot{\Lambda}$ is computed as follows

$$\dot{\boldsymbol{\sigma}} = \boldsymbol{\mathcal{L}}^e : \dot{\boldsymbol{\varepsilon}}^e = \boldsymbol{\mathcal{L}}^e : (\dot{\boldsymbol{\varepsilon}} - \dot{\boldsymbol{\varepsilon}}^p) = \boldsymbol{\mathcal{L}}^e : \dot{\boldsymbol{\varepsilon}} - \dot{\Lambda}\, \boldsymbol{\mathcal{L}}^e : \mathbf{N} \,, \tag{3.20}$$

where in Eqn. (3.20) we have used that $\dot{\boldsymbol{\varepsilon}} = \dot{\boldsymbol{\varepsilon}}^e + \dot{\boldsymbol{\varepsilon}}^p$ and $\dot{\boldsymbol{\varepsilon}}^p = \dot{\Lambda}\, \mathbf{N}$, and $\boldsymbol{\mathcal{L}}^e$ is the elastic modulus tensor. By substituting (3.20) to (3.18) and introducing again the vector $\mathbf{N}$ and the variable H, it follows that

$$\mathbf{N} : (\boldsymbol{\mathcal{L}}^e : \dot{\boldsymbol{\varepsilon}}) - \dot{\Lambda}\, \mathbf{N} : (\boldsymbol{\mathcal{L}}^e : \mathbf{N}) - \dot{\Lambda} H = 0 \tag{3.21}$$

and by converting everything to tensor notation it is seen that the parentheses can be omitted

$$\mathbf{N} : (\boldsymbol{\mathcal{L}}^e : \dot{\boldsymbol{\varepsilon}}) = N_{ij} (\boldsymbol{\mathcal{L}}^e : \dot{\boldsymbol{\varepsilon}})_{ij} = N_{ij} \mathcal{L}^e_{ijkl} \varepsilon^e_{kl} = \mathbf{N} : \boldsymbol{\mathcal{L}}^e : \dot{\boldsymbol{\varepsilon}} \,, \tag{3.22}$$

and

$$\mathbf{N} : (\boldsymbol{\mathcal{L}}^e : \mathbf{N}) = N_{ij} (\boldsymbol{\mathcal{L}}^e : \mathbf{N})_{ij} = N_{ij} \mathcal{L}^e_{ijkl} N_{kl} = \mathbf{N} : \boldsymbol{\mathcal{L}}^e : \mathbf{N} \,, \tag{3.23}$$

thus Eqn. (3.21) results in

$$\dot{\Lambda} = \frac{1}{L} \mathbf{N} : \boldsymbol{\mathcal{L}}^e : \dot{\boldsymbol{\varepsilon}}, \qquad L = (H + \mathbf{N} : \boldsymbol{\mathcal{L}}^e : \mathbf{N}) \,. \tag{3.24}$$

Note that the elastic modulus $\boldsymbol{\mathcal{L}}^e$ is positive definite[4], therefore $\mathbf{N} : \boldsymbol{\mathcal{L}}^e : \mathbf{N} > 0$.

[4] A forth order tensor $\boldsymbol{\mathcal{L}}$ is called positive definite if $\mathbf{A} : \boldsymbol{\mathcal{L}} : \mathbf{A} > 0$ or $A_{ij} \mathcal{L}_{ijkl} A_{kl} > 0 \quad \forall\, \mathbf{A} \neq 0,\ \mathbf{A} \in \mathcal{R}^9$.

3.8 The Rate Form of the Elastoplastic Equations

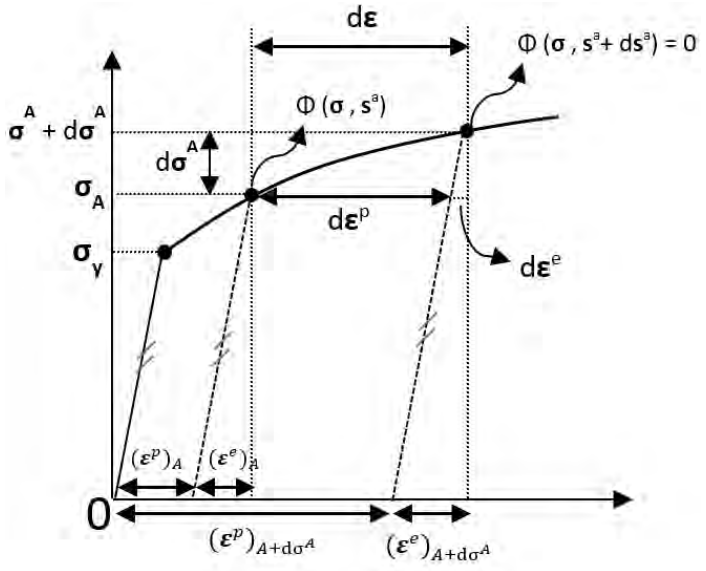

Figure 3.8: Moving along the hardening curve.

When $\Phi = 0$ and $d\Phi = 0$ one wishes to find a relation between the change $d\boldsymbol{\sigma}$ and $d\boldsymbol{\varepsilon}$ such that $d\boldsymbol{\sigma} = \boldsymbol{\mathcal{L}}^{ep} : d\boldsymbol{\varepsilon}$ or $\dot{\boldsymbol{\sigma}} = \boldsymbol{\mathcal{L}}^{ep} : \dot{\boldsymbol{\varepsilon}}$. While this is the general three dimensional case, one can view the one dimensional loading, Fig. 3.8, for simplicity. The following relations hold

$$\begin{aligned}\dot{\boldsymbol{\sigma}} = \boldsymbol{\mathcal{L}}^e : \dot{\boldsymbol{\varepsilon}}^e = \boldsymbol{\mathcal{L}}^e : (\dot{\boldsymbol{\varepsilon}} - \dot{\boldsymbol{\varepsilon}}^p) = \boldsymbol{\mathcal{L}}^e : (\dot{\boldsymbol{\varepsilon}} - \dot{\Lambda}\mathbf{N}) = \boldsymbol{\mathcal{L}}^e : \dot{\boldsymbol{\varepsilon}} - \dot{\Lambda}\,\boldsymbol{\mathcal{L}}^e : \mathbf{N} \\ = \boldsymbol{\mathcal{L}}^e : \dot{\boldsymbol{\varepsilon}} - \frac{1}{L}(\mathbf{N} : \boldsymbol{\mathcal{L}}^e : \dot{\boldsymbol{\varepsilon}})\boldsymbol{\mathcal{L}}^e : \mathbf{N}\,,\end{aligned} \tag{3.25}$$

Converting everything in notation form, Eqn. (3.25) reads

$$\begin{aligned}\dot{\sigma}_{ij} = \mathcal{L}^e_{ijkl}\dot{\varepsilon}_{kl} - \frac{1}{L}(N_{mn}\mathcal{L}^e_{mnkl}\dot{\varepsilon}_{kl})\mathcal{L}^e_{ijpq}N_{pq} \\ = (\mathcal{L}^e_{ijkl} - \frac{1}{L}N_{mn}\mathcal{L}^e_{mnkl}\mathcal{L}^e_{ijpq}N_{pq})\dot{\varepsilon}_{kl}\,,\end{aligned} \tag{3.26}$$

and by making use of the minor symmetry of $\boldsymbol{\mathcal{L}}^e$ [5], Eqn. (3.26) results in

$$\dot{\sigma}_{ij} = [\mathcal{L}^e_{ijkl} - \frac{1}{L}(\boldsymbol{\mathcal{L}}^e : \mathbf{N})_{ij}(\boldsymbol{\mathcal{L}}^e : \mathbf{N})_{kl}]\dot{\varepsilon}_{kl}\,, \tag{3.27}$$

or in compact form as

$$\dot{\boldsymbol{\sigma}} = [\boldsymbol{\mathcal{L}}^e - \frac{1}{L}(\boldsymbol{\mathcal{L}}^e : \mathbf{N})(\boldsymbol{\mathcal{L}}^e : \mathbf{N})] : \dot{\boldsymbol{\varepsilon}}\,. \tag{3.28}$$

I.e. Eqn. (3.27) reads

$$\dot{\boldsymbol{\sigma}} = \boldsymbol{\mathcal{L}}^{ep} : \dot{\boldsymbol{\varepsilon}}\,, \quad \boldsymbol{\mathcal{L}}^{ep} = \boldsymbol{\mathcal{L}}^e - \frac{1}{L}(\boldsymbol{\mathcal{L}}^e : \mathbf{N})(\boldsymbol{\mathcal{L}}^e : \mathbf{N})\,. \tag{3.29}$$

Thus, a compact equation that relates the rate of stresses with the rates of strains in the elastic or the elastoplastic regime is the following

$$\dot{\boldsymbol{\sigma}} = \boldsymbol{\mathcal{L}} : \dot{\boldsymbol{\varepsilon}}, \quad \text{where} \quad \boldsymbol{\mathcal{L}} = \begin{cases} \boldsymbol{\mathcal{L}}^e\,, & \text{if } \mathbf{N} : \boldsymbol{\mathcal{L}}^e : \dot{\boldsymbol{\varepsilon}} \le 0 \\ \boldsymbol{\mathcal{L}}^{ep}\,, & \text{if } \mathbf{N} : \boldsymbol{\mathcal{L}}^e : \dot{\boldsymbol{\varepsilon}} > 0 \end{cases} \tag{3.30}$$

[5] The minor symmetry of tensor $\boldsymbol{\mathcal{L}}^e$ is the following: $\mathcal{L}^e_{mnkl} = \mathcal{L}^e_{klmn}$.

For the reverse problem where $\dot{\boldsymbol{\varepsilon}} = \boldsymbol{\mathcal{M}}^e : \dot{\boldsymbol{\sigma}}$ or $d\boldsymbol{\varepsilon} = \boldsymbol{\mathcal{M}}^e : d\boldsymbol{\sigma}$ the following relations hold

$$\dot{\boldsymbol{\varepsilon}} = \dot{\boldsymbol{\varepsilon}}^e + \dot{\boldsymbol{\varepsilon}}^p = \boldsymbol{\mathcal{M}}^e : \dot{\boldsymbol{\sigma}} + \dot{\Lambda}\,\mathbf{N} = \boldsymbol{\mathcal{M}}^e : \dot{\boldsymbol{\sigma}} + \frac{1}{H}\,(\mathbf{N} : \dot{\boldsymbol{\sigma}})\,\mathbf{N}\,, \tag{3.31}$$

where Eqn. (3.19) has been used. Writing everything in notation form, Eqn. (3.31) reads

$$\dot{\varepsilon}_{ij} = \mathcal{M}^e_{ijkl}\,\dot{\sigma}_{kl} + \frac{1}{H} N_{kl}\,\dot{\sigma}_{kl}\,N_{ij} = (\mathcal{M}^e_{ijkl} + \frac{1}{H} N_{kl} N_{ij})\,\dot{\sigma}_{kl}\,, \tag{3.32}$$

or in compact form as

$$\dot{\boldsymbol{\varepsilon}} = (\boldsymbol{\mathcal{M}}^e + \frac{1}{H}\mathbf{N}\mathbf{N}) : \dot{\boldsymbol{\sigma}}\,. \tag{3.33}$$

Again, a compact equation that relates the rate of strains with the rate of stresses in the elastic or elastoplastic regime is the following

$$\dot{\boldsymbol{\varepsilon}} = \boldsymbol{\mathcal{M}} : \dot{\boldsymbol{\sigma}}, \quad \text{where} \quad \boldsymbol{\mathcal{M}} = \begin{cases} \boldsymbol{\mathcal{M}}^e\,, & \text{if } \mathbf{N} : \boldsymbol{\mathcal{L}}^e : \dot{\boldsymbol{\varepsilon}} \le 0 \\ \boldsymbol{\mathcal{M}}^{ep}\,, & \text{if } \mathbf{N} : \boldsymbol{\mathcal{L}}^e : \dot{\boldsymbol{\varepsilon}} > 0 \end{cases} \tag{3.34}$$

The inequalities in (3.34) and (3.30) define the "plastic loading condition" and determine whether the material is in the elastic or in the elastoplastic regime. Formulated in this way the plastic loading condition is general and it holds for hardening, softening and perfectly plastic materials. For example, if the plastic loading condition was expressed in terms of the stresses as $\mathbf{N} : \dot{\boldsymbol{\sigma}}$, then for a softening material the condition $\mathbf{N} : \dot{\boldsymbol{\sigma}} \le 0$ would not necessarily imply that the material is in the elastic regime.

Summary

Summarizing, the constituents of plasticity theory for rate-independent materials are the following:

▷ Yield condition: $\Phi(\boldsymbol{\sigma}, \mathbf{s}^\alpha) \le 0$

▷ The normality rule: $\mathbf{D}^p = \dot{\Lambda}\mathbf{N}(\boldsymbol{\sigma}, \mathbf{s}^\alpha) = \dot{\Lambda}\,\dfrac{\partial \Phi}{\partial \sigma}\,,\ \dot{\Lambda} \ge 0$

▷ Evolution of state variables: $\mathbf{s}^\alpha = \dot{\Lambda}\,G(\boldsymbol{\sigma}, \mathbf{s}^\beta, \mathbf{N})$

▷ The flow rule: $\dot{\Phi} = 0 \Rightarrow \dot{\Lambda} = \dfrac{1}{H}\,\mathbf{N} : \dot{\boldsymbol{\sigma}} = \dfrac{1}{L}\,\mathbf{N} : \boldsymbol{\mathcal{L}}^e : \dot{\boldsymbol{\varepsilon}}\,,$

where $H = -\displaystyle\sum_\alpha \frac{\partial \Phi}{\partial s^\alpha}\,\dot{s^\alpha}$ and $L = H + \mathbf{N} : \boldsymbol{\mathcal{L}}^e : \mathbf{N}$

▷ Rate form of elastoplastic equations:

- stresses with respect to strains: $\dot{\boldsymbol{\sigma}} = \boldsymbol{\mathcal{L}} : \dot{\boldsymbol{\varepsilon}}$, where $\boldsymbol{\mathcal{L}} = \begin{cases} \boldsymbol{\mathcal{L}}^e\,, & \text{if } \mathbf{N} : \boldsymbol{\mathcal{L}}^e : \dot{\boldsymbol{\varepsilon}} \le 0 \\ \boldsymbol{\mathcal{L}}^{ep}\,, & \text{if } \mathbf{N} : \boldsymbol{\mathcal{L}}^e : \dot{\boldsymbol{\varepsilon}} > 0 \end{cases}$

  with $\boldsymbol{\mathcal{L}}^{ep} = \boldsymbol{\mathcal{L}}^e - \dfrac{1}{L}(\boldsymbol{\mathcal{L}}^e : \mathbf{N})(\boldsymbol{\mathcal{L}}^e : \mathbf{N})$

- strains with respect to stresses: $\dot{\boldsymbol{\varepsilon}} = \boldsymbol{\mathcal{M}} : \dot{\boldsymbol{\sigma}}$, where $\boldsymbol{\mathcal{M}} = \begin{cases} \boldsymbol{\mathcal{M}}^e\,, & \text{if } \mathbf{N} : \boldsymbol{\mathcal{L}}^e : \dot{\boldsymbol{\varepsilon}} \le 0 \\ \boldsymbol{\mathcal{M}}^{ep}\,, & \text{if } \mathbf{N} : \boldsymbol{\mathcal{L}}^e : \dot{\boldsymbol{\varepsilon}} > 0 \end{cases}$

  with $\boldsymbol{\mathcal{M}}^{ep} = (\boldsymbol{\mathcal{M}}^e + \dfrac{1}{H}\mathbf{N}\mathbf{N})\,.$

Chapter 4

The Constitutive Model for Porous Materials

Description of the Model

In this chapter a gradient anisotropic model for porous materials is presented. The non-local model builds on the work of [3]. The porous material is composed of two phases. The matrix phase consists of an isotropic, incompressible, rate-independent material which behaves with an elasto-plastic response after reaching its yield stress σ_y. In addition, it is assumed to exhibit isotropic hardening and hence σ_y is taken to be a function of the equivalent plastic strain $\bar{\varepsilon}^p$. The inclusion phase is vacuous and comprises of ellipsoidal voids of the same shape and orientation distributed uniformly over the representative volume element[1]. It is assumed [22, 29, 30] that the centers of the voids are distributed with ellipsoidal symmetry, i.e. the distribution (or two-point correlation) function of the centers voids has also ellipsoidal shape. Under finite deformations the voids evolve into ellipsoidal shapes and hence the porous medium becomes at every material point locally orthotropic, with the local axes of orthotropy coinciding with the principal axes of the representative local ellipsoid. The orientation of the principal axes is defined by the unit vectors $\mathbf{n}^{(i)}$, $i = \{1, 2, 3\}$ and the corresponding lengths are $2a_1$, $2a_2$ and $2a_3$, as shown in Fig. 4.1. During finite deformations, the micro-structure of the material changes inducing anisotropy to the material. A set of *state* variables describes the evolution of the microstructure at every deformation state.

In the original formulation of the classical (local) anisotropy theory, the relevant state variables describing the state of the micro-structure are:

$$\mathbf{s} = \{\bar{\varepsilon}^p, f_{loc}, w_1, w_2, \mathbf{n}^{(1)}, \mathbf{n}^{(2)}, \mathbf{n}^{(3)} = \mathbf{n}^{(1)} \times \mathbf{n}^{(2)}\}, \tag{4.1}$$

where $\bar{\varepsilon}^p$ is the local equivalent plastic strain in the matrix phase, f_{loc} is the local porosity (i.e. volume fraction of the voids), $w_1 = a_3/a_1$ and $w_2 = a_3/a_2$ are two aspect ratios characterizing the shape of the voids and their distribution functions, and the vectors $\mathbf{n}^{(i)}$ (with $i = 1, 2, 3$), as mentioned earlier, denote the orientation of the principal axes of the voids. Note that if V_v is the total volume of the voids and V is the total material volume, then the local volume fraction or *local porosity* f_{loc} is defined as

$$f_{loc} = \frac{V_v}{V}\,. \tag{4.2}$$

[1]Since the material consists of two phases it is a heterogeneous material. However, the heterogeneity of the material can only be identified below a certain scale with characteristic length d. For a microscopically length scale D, such that $d/D << 1$ the material can be conceived as a homogeneous material by observing its mean (or effective) properties. A volume element with characteristic dimensions of D is called a representative volume element (RVE) because the overall properties on any RVE would be the same, i.e. the overall properties of the RVE represent the overall properties of the heterogeneous material. In that sense the heterogeneous material can be conceived as the summation of the RVEs in the volume of the medium.

Moreover, the effective yield function Φ depends on the aforementioned internal variables

$$\Phi = \Phi(\boldsymbol{\sigma}, \mathbf{s}) = \Phi(\boldsymbol{\sigma}, \bar{\varepsilon}^p, f_{loc}, w_1, w_2, \mathbf{n}^{(1)}, \mathbf{n}^{(2)}, \mathbf{n}^{(3)}). \tag{4.3}$$

In the context of the gradient anisotropic constitutive model proposed in this thesis, a *nonlocal porosity* variable f is introduced for the regularization of the aforementioned local model. The nonlocal porosity f is determined from the solution of a boundary value problem (BVP for short) of the form [32]:

$$\begin{aligned} &f - \ell^2 \nabla^2 f = f_{loc} \quad in \quad V \\ &B.C. : \frac{\partial f}{\partial n} = 0 \quad on \quad \partial V \end{aligned} \tag{4.4}$$

where ∂V is the boundary of the domain V, with outward-pointing vector $\mathbf{n}$, and ℓ is a characteristic length scale of interest of the material. It is now assumed that the yield function Φ depends on the nonlocal porosity f instead of f_{loc} :

$$\Phi = \Phi(\boldsymbol{\sigma}, \mathbf{s}) = \Phi(\boldsymbol{\sigma}, \bar{\varepsilon}^p, f, w_1, w_2, \mathbf{n}^{(1)}, \mathbf{n}^{(2)}, \mathbf{n}^{(3)}) \tag{4.5}$$

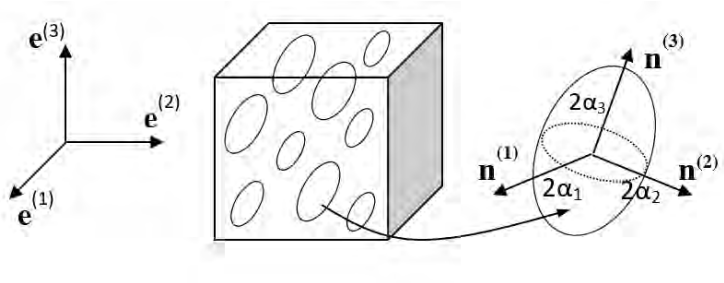

Figure 4.1: Graphical presentation of the microstructure in a RVE showing a representative ellipsoidal void with the local orientation axes $\mathbf{n}^{(i)}$ $(i = 1, 2, 3)$ and corresponding lengths $(2a_1, 2a_2, 2a_3)$.

4.1 Instantaneous Constitutive Relations

The rate-of-deformation tensor $D_{ij} = (\mathrm{v}_{i,j} + \mathrm{v}_{j,i})/2$ (with v_i denoting the Cartesian components of the overall applied velocity) can be written as

$$\mathbf{D} = \mathbf{D}^e + \mathbf{D}^p \quad or \quad D_{ij} = D^e_{ij} + D^p_{ij}, \tag{4.6}$$

where $\mathbf{D}^e$ and $\mathbf{D}^p$ are the elastic and plastic parts. In other words the elastic and plastic response are treated independently, and combined later to obtain the full elastic-plastic response. This treatment is reasonably accurate, unless the material is subjected to cyclic loading.

Note that due to the presence of voids the overall material behavior is compressible implying that the plastic strain-rate tensor is not deviatoric (i.e. $D^p_{kk} \neq 0$).

4.1.1 Elasticity

A hypoelastic[2] form is assumed for the elastic part of the rate-deformation tensor. The elastic response of the porous material is described in terms of an effective compliance tensor

[2]Materials considered hypoelastic are such that the work during a closed loading cycle is not zero even in the absence of inelastic deformation and so, a stress-strain relationship cannot be derived from a potential function.

$\mathcal{M}^{\mathbf{e}}$ via

$$\mathbf{D}^e = \boldsymbol{\mathcal{M}}^e : \overset{\circ}{\boldsymbol{\sigma}}, \tag{4.7}$$

where $\overset{\circ}{\boldsymbol{\sigma}}$ is a rate of the Cauchy stress which is co-rotational with the spin of the voids,

$$\overset{\circ}{\boldsymbol{\sigma}} = \dot{\boldsymbol{\sigma}} - \boldsymbol{\omega}\cdot\boldsymbol{\sigma} + \boldsymbol{\sigma}\cdot\boldsymbol{\omega}, \tag{4.8}$$

$\boldsymbol{\omega}$ being the spin of the voids relative to a stationary frame. The antisymmetric tensor $\boldsymbol{\omega}$ which is called the "microstructural spin", is calculated in section 4.2.2

The compliance tensor of the composite is written as [28]

$$\boldsymbol{\mathcal{M}}^e = \boldsymbol{\mathcal{M}} + \frac{f}{1-f}\mathbf{Q}^{-1}, \tag{4.9}$$

where $\mathbf{Q}$ is a fourth-order tensor that describes the microstructure of the material and depends on $(\mu, \nu, w_1, w_2, \mathbf{n}^{(1)}, \mathbf{n}^{(2)}, \mathbf{n}^{(3)})$. $\mathbf{Q}$ [28] is linked to the Eshelby tensor $\boldsymbol{\mathcal{S}}$ [10] via

$$\mathbf{Q} = \boldsymbol{\mathcal{L}} : (\boldsymbol{\mathcal{I}} - \boldsymbol{\mathcal{S}}). \tag{4.10}$$

Note that the Eshelby tensor has the minor symmetries ($\mathcal{S}_{ijkl} = \mathcal{S}_{jikl} = \mathcal{S}_{ijlk}$), whereas $\mathbf{Q}$ has both the major ($Q_{ijkl} = Q_{klij}$) and minor symmetries of the elasticity tensor. Expressions for the tensors $\boldsymbol{\mathcal{S}}$ and $\mathbf{Q}$ are given in Appendix A.

In (4.9), $\boldsymbol{\mathcal{M}}$ is the elastic compliance tensor of the matrix material, which is the inverse of the elastic modulus tensor $\boldsymbol{\mathcal{L}}$. Since the matrix phase is assumed to be isotropic both $\boldsymbol{\mathcal{L}}$ and $\boldsymbol{\mathcal{M}}$ depend only on two variables, and can be written as

$$\boldsymbol{\mathcal{L}} = 2\mu\boldsymbol{\mathcal{K}} + 3\kappa\boldsymbol{\mathcal{J}}, \quad \boldsymbol{\mathcal{M}} = \boldsymbol{\mathcal{L}}^{-1} = \frac{1}{2\mu}\boldsymbol{\mathcal{K}} + \frac{1}{3\kappa}\boldsymbol{\mathcal{J}} = \frac{1}{2\mu}(\boldsymbol{\mathcal{K}} + \frac{1-2\nu}{1+\nu}\boldsymbol{\mathcal{J}}), \tag{4.11}$$

with

$$\mathcal{J}_{ijkl} = \frac{1}{3}\delta_{ij}\delta_{kl}, \quad \mathcal{K}_{ijkl} = \mathcal{I}_{ijkl} - \mathcal{J}_{ijkl}, \quad \mathcal{I}_{ijkl} = \frac{1}{2}\left(\delta_{ik}\delta_{jl} + \delta_{il}\delta_{jk}\right), \tag{4.12}$$

where μ and κ denote the elastic shear and bulk moduli of the matrix, ν is the Poisson's ratio of the matrix, δ is the Kronecker delta.

4.1.2 Plasticity

Although the present study focuses on rate-independent materials, in order to derive the rate-independent constitutive relations one has to construct a general homogenized dissipation (rate-dependent) potential $U(\sigma_{ij})$ and consider an appropriate limit to account for rate-independence. Such a potential is explained in more detail in [20, 7] and takes the form

$$U(\boldsymbol{\sigma}, \mathbf{s}) = (1-f)\frac{\dot{\varepsilon}_0\,\sigma_y}{n+1}\left[\frac{\hat{\sigma}_e}{\sigma_y\left(\bar{\varepsilon}^p\right)}\right]^{n+1}, \tag{4.13}$$

where $\hat{\sigma}_e(\boldsymbol{\sigma}, \mathbf{s})$ is the equivalent stress containing all the information about the micro-structure and it is detailed later in this section, σ_y is the yield stress of the matrix in tension, $\dot{\varepsilon}_0$ denotes a reference strain rate, and n is the creep exponent ($1 \leq n \leq \infty$). The value $n = 1$ corresponds to a linearly viscous material, whereby the limit $n \to \infty$ leads to a rate-independent material response.

Thus, by considering the limit $n \to \infty$ in (4.13), one can obtain

$$U(\boldsymbol{\sigma}, \mathbf{s}) = \begin{cases} 0, & \hat{\sigma}_e \leq \sigma_y(\bar{\varepsilon}^p), \\ \infty, & otherwise, \end{cases} \tag{4.14}$$

which directly gives the yield function as

$$\Phi(\boldsymbol{\sigma}, \mathbf{s}) = \hat{\sigma}_e - \sigma_y\left(\bar{\varepsilon}^p\right), \tag{4.15}$$

such that the yield condition is defined by $\Phi(\boldsymbol{\sigma}, \mathbf{s}) = 0$.

The original Variational formulae (VAR)

In the original variational method, the effective stress measure $\hat{\sigma}_e$ is given by the explicit expression [23, 13]

$$\hat{\sigma}_e = \sqrt{\frac{\sigma_{ij}\, m_{ijkl}\, \sigma_{kl}}{1-f}} \quad or \quad \hat{\sigma}_e = \sqrt{\frac{\sigma : \mathbf{m} : \sigma}{1-f}}. \tag{4.16}$$

The fourth order tensor $\mathbf{m}$ corresponds to an appropriately normalized effective viscous compliance tensor for the fictitious linear comparison porous material and is defined as

$$\mathbf{m}^{var} = \mathbf{m}^{var}(f, w_1, w_2, \mathbf{n}^{(1)}, \mathbf{n}^{(2)}, \mathbf{n}^{(3)}) = 3\mu \boldsymbol{\mathcal{M}}^e|_{\nu=1/2} = \frac{3}{2}\boldsymbol{\mathcal{K}} + \frac{3f}{1-f}\mu\, \mathbf{Q}^{-1}|_{\nu=1/2}\,, \tag{4.17}$$

where $\boldsymbol{\mathcal{M}}^e$ is exactly the same as in (4.9), computed in the limit $\nu \to 1/2$ to account for the incompressibility of the matrix. The subscript "var" has been used to denote the original result of Ponte Castañeda [20], which is a rigorous upper bound of the effective response of the porous material. In the limit $\nu \to 1/2$ in (4.17), the tensor $\mathbf{Q}$ becomes a homogeneous function of degree one in μ and hence the tensor $\mathbf{m}$ is independent of μ. In addition, $\mathbf{Q}$ and consequently $\mathbf{m}$ are functions of the microstructural variables $\mathbf{s}$ and for a non-zero porosity f are both compressible. Note further that when the voids become non-spherical, i.e., when the aspect ratios, defined in (4.5), take values other than unity, $\mathbf{m}$ becomes anisotropic.

The modified variational or modified secant formulae (MVAR)

The original variational formulation of Ponte Castañeda [20], discussed previously, has been found to be sufficiently accurate at low stress triaxialities but tends to overestimate the effective response of the porous material at high stress triaxialities, especially at low porosities. In this connection, Aravas N. and Danas K. [8] following the earlier work of Ponte Castañeda [21] and Michel and Suquet [17], corrected expression (4.17) by modifying the hydrostatic part of $\mathbf{m}$, such that

$$\mathbf{m}^{mvar} = \mathbf{m}^{var} + (q_J^2 - 1)\, \boldsymbol{\mathcal{J}} : \mathbf{m}^{var} : \boldsymbol{\mathcal{J}}, \quad q_J = \frac{1-f}{\sqrt{f}\ln(1/f)}. \tag{4.18}$$

The scalar factor q_J brings the yield function (4.15) into alignment with the spherical shell (or equivalently the "composite sphere assemblage") and the cylindrical shell (or equivalently the "composite cylinder assemblage") solutions when subjected to purely hydrostatic loadings, while preserving standard requirements, such as convexity and smoothness of the yield surface for the entire range of microstructural configurations. Note, however, that the new modified variational model in (4.18) is not an upper bound but an estimate for the effective behavior of porous materials. Nonetheless, it still reproduces the Gurson model in the special case of spherical voids and purely hydrostatic loading.

Therefore, the effective yield function of the composite can be written in the form

$$\Phi(\boldsymbol{\sigma}, \mathbf{s}) = \frac{1}{1-f}\,\boldsymbol{\sigma} : \mathbf{m} : \boldsymbol{\sigma} - \sigma_y^2(\bar{\varepsilon}^{\mathbf{p}}), \tag{4.19}$$

where $\mathbf{m}$ is computed either from (4.17) or (4.18). In the most general case Φ exhibits orthotropic symmetry with symmetry axes aligned with the axes of the voids, i.e. aligned with the vectors $\mathbf{n}^{(i)}\,(i = 1, 2, 3)$. Note that if perfect plasticity was assumed then $\sigma_y = \textit{constant}$; however, here the metal matrix is assumed to harden isotropically and σ_y is a function of the equivalent plastic strain $\bar{\varepsilon}^{\mathbf{p}}$.

The matrix material, with Young's modulus E and Poisson's ratio v, exhibits isotropic hardening with

$$\sigma_y(\bar{\varepsilon}^p) = \sigma_0 \left(1 + \frac{\bar{\varepsilon}^p}{\varepsilon_0}\right)^{1/n}, \tag{4.20}$$

where σ_0 is the yield stress in tension, $n \geq 1$ is the hardening exponent, and $\varepsilon_0 = \sigma_0/E$.

The plastic rate-of-deformation tensor $\mathbf{D}^p$ is obtained in terms of Φ from the normality rule

$$\mathbf{D}^p = \dot{\Lambda}\mathbf{N}, \quad \mathbf{N} = \frac{\partial \Phi}{\partial \sigma} = \frac{2}{1-f}\,\mathbf{m} : \boldsymbol{\sigma}, \tag{4.21}$$

where $\dot{\Lambda} \geq 0$ is the plastic multiplier, which is determined from the flow rule as discussed in chapter 3.

4.2 Evolution of the Microstructure

When the porous material deforms plastically, its microstructure changes. The microstructure evolution, in turn affects the elasto-plastic response of the material since the yield condition and the plastic flow rule depend on the current state of the microstructure. Thus, evolution laws for the microstructural state variables $\mathbf{s}$ have to be prescribed. These evolution laws are obtained by considering appropriate kinematic relations as discussed in this section. In this theory of porous materials, it is assumed that all changes in the microstructure occur only due to the plastic deformation of the matrix, which changes the volume, the shape and the orientation of the voids. This is expected to be reasonable, since the elastic strains here are relatively small compared to the plastic strains. A final note is that the purpose of homogenization models is the description of the effective behaviour in average terms. The model discussed here suggests that under applied deformation the ellipsoidal voids evolve-on average- to ellipsoidal voids with different size and orientation. This in turn, implies that average change in size and orientation of the voids depends only upon the average strain rate $\mathbf{D}^v$ and the average spin $\mathbf{W}^v$ in the vacuous phase.

4.2.1 Evolution of the equivalent plastic strain $\bar{\varepsilon}^p$ and local porosity f_{loc}

The evolution of $\bar{\varepsilon}^p$ is determined from the condition that the local macroscopic plastic work $\boldsymbol{\sigma} : \mathbf{D}^p = \dot{\Lambda}\,\boldsymbol{\sigma} : \mathbf{N}$ equals the corresponding microscopic work $(1-f)\,\sigma_y\,\dot{\bar{\varepsilon}}^p$, which implies that

$$\dot{\bar{\varepsilon}}^p = \dot{\Lambda}\,\frac{\boldsymbol{\sigma} : \mathbf{N}}{(1-f)\sigma_y(\bar{\varepsilon}^p)} \equiv \dot{\Lambda}\,g_1(\boldsymbol{\sigma}, \mathbf{s}). \tag{4.22}$$

Since the presence of porosity in a metal can be viewed as some kind of "damage" in the material and any changes in porosity due to elastic deformations are small and fully recoverable, it is assumed that changes in f_{loc} are due to volumetric plastic deformation rates D^p_{kk} only (as opposed to the total D_{kk}). In view of the plastic incompressibility of the matrix phase, the evolution equation for the local porosity f_{loc} follows from the continuity equation and is given by

$$\dot{f}_{loc} = (1-f)D^p_{kk} = \dot{\Lambda}(1-f)N_{kk} \equiv \dot{\Lambda}\, g_2(\boldsymbol{\sigma}, \mathbf{s}). \tag{4.23}$$

4.2.2 Evolution of the local aspect ratios and the local axes of orthotropy

The average deformation rate and the average spin of the local ellipsoid are determined in terms of the macroscopic plastic deformation rate $\mathbf{D}^p$ and the macroscopic continuum spin $\mathbf{W}$. In particular, the average deformation rate $\mathbf{D}^v$ and the average spin $\mathbf{W}^v$ in the local representative ellipsoidal void are

$$\mathbf{D}^v = \boldsymbol{\mathcal{A}} : \mathbf{D}^p \quad \text{and} \quad \mathbf{W}^v = \mathbf{W} - \boldsymbol{\mathcal{C}} : \mathbf{D}^p, \tag{4.24}$$

where $\boldsymbol{\mathcal{A}}$ and $\boldsymbol{\mathcal{C}}$ are the relevant fourth-order "concentration tensors" defined as

$$\boldsymbol{\mathcal{A}} = [\boldsymbol{\mathcal{I}} - (1-f)\boldsymbol{\mathcal{S}}|_{\nu=1/2}]^{-1} \quad \text{and} \quad \boldsymbol{\mathcal{C}} = -(1-f)\boldsymbol{\Pi} : \boldsymbol{\mathcal{A}}. \tag{4.25}$$

The derivation of (4.24) and (4.25) can be found in [15, 23, 20]. Here $\boldsymbol{\Pi}$ is the fourth-order Eshelby [10, 11] rotation tensor that determines the spin of an isolated void in infinite linear viscous matrix and depends on $(w_1, w_2, \mathbf{n}^{(1)}, \mathbf{n}^{(2)}, \mathbf{n}^{(3)})$. An expression for the evaluation of $\boldsymbol{\Pi}$ is given in Appendix A. The "concentration tensors" $\boldsymbol{\mathcal{A}}$ and $\boldsymbol{\mathcal{C}}$ both depend on $(f, w_1, w_2, \mathbf{n}^{(1)}, \mathbf{n}^{(2)}, \mathbf{n}^{(3)})$. In the limit as $f \to 0$ the expressions for $\boldsymbol{\mathcal{A}}$ and $\boldsymbol{\mathcal{C}}$ reduce to the corresponding formulae of the Eshelby [10, 11] for the case of an isolated void in an infinite incompressible matrix.

The evolution of the aspect rations (w_1, w_2) is determined, by starting from their definition $w_1 = a_3/a_1$, as follows

$$\begin{aligned} \dot{w}_1 = \frac{\dot{\alpha}_3}{\alpha_1} - \alpha_3 \frac{\dot{\alpha}_1}{\alpha_1^2} = w_1 \left(\frac{\dot{\alpha}_3}{\alpha_3} - \frac{\dot{\alpha}_1}{\alpha_1} \right) &= w_1 \left(\mathbf{n}^{(3)} \cdot \mathbf{D}^v \cdot \mathbf{n}^{(3)} - \mathbf{n}^{(1)} \cdot \mathbf{D}^v \cdot \mathbf{n}^{(1)} \right) \\ &= w_1 \left(\mathbf{n}^{(3)}\mathbf{n}^{(\mathbf{3})} - \mathbf{n}^{(\mathbf{1})}\mathbf{n}^{(\mathbf{1})} \right) : \mathbf{D}^v, \end{aligned} \tag{4.26}$$

where $2\alpha_i$ is the length of the $i-th$ principal axis of the local representative ellipsoid. Taking into account that $\mathbf{D}^v = \boldsymbol{\mathcal{A}} : \mathbf{D}^p$ and $\mathbf{D}^p = \dot{\Lambda}\mathbf{N}$, then (4.26) is written as

$$\dot{w}_1 = \dot{\Lambda} w_1 \left(\mathbf{n}^{(3)}\mathbf{n}^{(3)} - \mathbf{n}^{(1)}\mathbf{n}^{(1)} \right) : \boldsymbol{\mathcal{A}} : \mathbf{N} \equiv \dot{\Lambda}\, g_3(\boldsymbol{\sigma}, \mathbf{s}). \tag{4.27}$$

Similarly,

$$\dot{w}_2 = \dot{\Lambda} w_2 \left(\mathbf{n}^{(3)}\mathbf{n}^{(3)} - \mathbf{n}^{(2)}\mathbf{n}^{(2)} \right) : \boldsymbol{\mathcal{A}} : \mathbf{N} \equiv \dot{\Lambda}\, g_4(\boldsymbol{\sigma}, \mathbf{s}). \tag{4.28}$$

Next the evolution equations for the orientation vectors $\mathbf{n}^{(i)}$ are defined. Since the $\mathbf{n}^{(i)}$'s are the unit vectors, their time derivative can be written in the form

$$\dot{\mathbf{n}}^{(i)} = \boldsymbol{\omega} \cdot \mathbf{n}^{(i)}, \tag{4.29}$$

where $\boldsymbol{\omega}$ is an antisymmetric tensor.

The local representative ellipsoid can be thought as developing during plastic flow from a "reference spherical void" of radius α_0. The deformation gradient of the ellipsoidal void $\mathbf{F}^v(t)$ relative to the reference spherical void can be written as

$$\mathbf{F}^v(t) = \bar{\mathbf{F}}^v(t) \cdot \bar{\mathbf{F}}^v_0, \tag{4.30}$$

where $\bar{\mathbf{F}}^v_0$ is the deformation gradient of the initial representative void relative to the reference spherical void, and $\bar{\mathbf{F}}^v(t)$ the deformation gradient of the evolving ellipsoidal void relative to its initial shape. Making use of a common identity in linear algebra[3], it can be derived from (4.30) that

$$(\mathbf{F}^v(t))^{-1} = (\bar{\mathbf{F}}^v_0)^{-1} \cdot (\bar{\mathbf{F}}^v(t))^{-1}, \tag{4.31}$$

and by making use of (2.43) and (2.45), then the average velocity gradient of the voids $\mathbf{L}^v$ can be written as

$$\mathbf{L}^v = \mathbf{D}^v + \mathbf{W}^v = \dot{\mathbf{F}}^v \cdot (\mathbf{F}^v)^{-1} = \dot{\bar{\mathbf{F}}}^v \cdot \mathbf{F}^v_0 \cdot (\mathbf{F}^v_0)^{-1} \cdot (\bar{\mathbf{F}}^v)^{-1} = \dot{\bar{\mathbf{F}}}^v \cdot (\bar{\mathbf{F}}^v)^{-1}. \tag{4.32}$$

Remark 4.1 Taking into account (4.24), then (4.32) can be written as

$$\dot{\mathbf{F}}^v \cdot (\mathbf{F}^v)^{-1} = \dot{\Lambda}\,(\boldsymbol{\mathcal{A}} - \boldsymbol{\mathcal{C}}) : \mathbf{N} + \mathbf{W}\,, \tag{4.33}$$

which is the differential equation that together with the initial condition $\mathbf{F}^v(0) = \mathbf{F}^v_0$ defines the deformation gradient of the local representative ellipsoid $\mathbf{F}^v(t)$.

The orientation of the unit vectors $\mathbf{n}^{(i)}$ along the principal axes of the local representative ellipsoid coincide with the Eulerian axes of $\mathbf{F}^v$. Therefore, the spin $\boldsymbol{\omega}$ in (4.29) is determined by the kinematical relationship (the derivation of which is found in Appendix B)

$$\omega'_{ij} = W^{v\prime}_{ij} - \frac{\lambda_i^2 + \lambda_j^2}{\lambda_i^2 - \lambda_j^2} D'^v_{ij}, \quad i \neq j, \quad w_i \neq w_j, \quad \text{(no sum over i)}, \tag{4.34}$$

where λ_i are the stretch ratios of $\mathbf{F}^v$, i.e.,

$$\lambda_i = \frac{\alpha_i}{\alpha_0} = \frac{\alpha_3/\alpha_0}{\alpha_3/\alpha_i} = \frac{\lambda_3}{w_i}, \quad i = 1,2,3 \quad \text{with} \quad w_3 = 1. \tag{4.35}$$

Therefore, (4.34) can be written as

$$\omega'_{ij} = W^{v\prime}_{ij} + \frac{w_i^2 + w_j^2}{w_i^2 - w_j^2} D'^v_{ij}, \quad i \neq j, \quad w_i \neq w_j, \quad \text{(no sum over i)}. \tag{4.36}$$

Note that in relations (4.34) and (4.36), and for the rest of this section, primed quantities indicate components in a coordinate frame that coincides instantaneously with the principal axes of the local representative ellipsoid, as determined by the vectors $\mathbf{n}^{(i)}$ (e.g. $\mathbf{D}^p = D'^p_{ij}\mathbf{n}^{(i)}\mathbf{n}^{(j)}$, etc.).

In finite element computations it is convenient to refer to all tensor components with respect to a fixed Cartesian coordinate system. Therefore, it is useful to state (4.36) in "direct notation"

[3]Let $\mathbf{A}$, $\mathbf{B}$ be two invertible matrices then $(\mathbf{A} \cdot \mathbf{B})^{-1} = \mathbf{B}^{-1} \cdot \mathbf{A}^{-1}$.

(for $i \neq j$, $w_i \neq w_j$)

$$\mathbf{n}^{(i)} \cdot \omega \cdot \mathbf{n}^{(j)} = \mathbf{n}^{(i)} \cdot \mathbf{W}^v \cdot \mathbf{n}^{(j)} + \frac{w_i^2 + w_j^2}{w_i^2 - w_j^2} \mathbf{n}^{(i)} \cdot \mathbf{D}^v \cdot \mathbf{n}^{(j)} \quad \text{(no sum over i)}. \tag{4.37}$$

Also, since $\mathbf{D}^v$ is symmetric, then

$$\mathbf{n}^{(i)} \cdot \mathbf{D}^v \cdot \mathbf{n}^{(j)} = (\mathbf{n}^{(i)}\mathbf{n}^{(j)}) : \mathbf{D}^v = \frac{1}{2}(\mathbf{n}^{(i)}\mathbf{n}^{(j)} + \mathbf{n}^{(j)}\mathbf{n}^{(i)}) : \mathbf{D}^v. \tag{4.38}$$

Therefore, the microstructural spin $\boldsymbol{\omega} = (\mathbf{n}^{(i)} \cdot \boldsymbol{\omega} \cdot \mathbf{n}^{(j)})\mathbf{n}^{(i)}\mathbf{n}^{(j)}$ can be written in direct notation as

$$\boldsymbol{\omega} = \mathbf{W}^v + \frac{1}{2} \sum_{\substack{i,j=1 \\ i\neq j \\ w_i \neq w_j}}^{3} \frac{w_i^2 + w_j^2}{w_i^2 - w_j^2} [(\mathbf{n}^{(i)}\mathbf{n}^{(j)} + \mathbf{n}^{(j)}\mathbf{n}^{(i)}) : \mathbf{D}^v]\mathbf{n}^{(i)}\mathbf{n}^{(j)} \quad (w_3 = 1), \tag{4.39}$$

where $\mathbf{W}^v = (\mathbf{n}^{(i)} \cdot \mathbf{W}^v \cdot \mathbf{n}^{(j)})\mathbf{n}^{(i)}\mathbf{n}^{(j)}$ as well as (4.37) and (4.38) have been taken into account.

Taking into account that $\mathbf{D}^v = \boldsymbol{\mathcal{A}} : \mathbf{D}^p$, $\mathbf{W}^v = \mathbf{W} - \boldsymbol{\mathcal{C}} : \mathbf{D}^p$, and $\mathbf{D}^p = \dot{\Lambda}\,\mathbf{N}$ then (4.39) can be written as

$$\boldsymbol{\omega} = \mathbf{W} - \dot{\Lambda}\left[\boldsymbol{\mathcal{C}} : \mathbf{N} - \frac{1}{2} \sum_{\substack{i,j=1 \\ i\neq j \\ w_i \neq w_j}}^{3} \frac{w_i^2 + w_j^2}{w_i^2 - w_j^2} \Big[(\mathbf{n}^{(i)}\mathbf{n}^{(j)} + \mathbf{n}^{(j)}\mathbf{n}^{(i)}) : \boldsymbol{\mathcal{A}} : \mathbf{N}\Big]\mathbf{n}^{(i)}\mathbf{n}^{(j)}\right]. \tag{4.40}$$

Finally, introducing the so-called plastic spin $\mathbf{W}^p = \mathbf{W} - \boldsymbol{\omega}$, then (4.40) can be written as

$$\mathbf{W}^p = \dot{\Lambda}\boldsymbol{\Omega}^p, \tag{4.41}$$

where

$$\boldsymbol{\Omega}^p = \left[\boldsymbol{\mathcal{C}} : \mathbf{N} - \frac{1}{2} \sum_{\substack{i,j=1 \\ i\neq j \\ w_i \neq w_j}}^{3} \frac{w_i^2 + w_j^2}{w_i^2 - w_j^2} \Big[(\mathbf{n}^{(i)}\mathbf{n}^{(j)} + \mathbf{n}^{(j)}\mathbf{n}^{(i)}) : \boldsymbol{\mathcal{A}} : \mathbf{N}\Big]\mathbf{n}^{(i)}\mathbf{n}^{(j)}\right], \quad (w_3 = 1) \tag{4.42}$$

Taking the definition of $\overset{\circ}{\mathbf{n}}{}^{(i)}$ which is the rate of $\mathbf{n}^{(i)}$ corotational with the spin of the voids, i.e., $\overset{\circ}{\mathbf{n}}{}^{(i)} = \dot{\mathbf{n}}^{(i)} - \boldsymbol{\omega} \cdot \mathbf{n}^{(i)}$ then (4.29) takes the form

$$\overset{\circ}{\mathbf{n}}{}^{(i)} = \mathbf{0}. \tag{4.43}$$

Taking into account that $\mathbf{W} = \boldsymbol{\omega} + \mathbf{W}^p$ and (4.41), (4.43) then the Jaumann derivative of $\mathbf{n}^{(i)}$, $\overset{\triangledown}{\mathbf{n}}{}^{(i)} = \dot{\mathbf{n}}^{(i)} - \mathbf{W} \cdot \mathbf{n}^{(i)}$ can be written as

$$\overset{\triangledown}{\mathbf{n}}{}^{(i)} = \overset{\circ}{\mathbf{n}}{}^{(i)} - \mathbf{W}^p \cdot \mathbf{n}^{(i)} = -\mathbf{W}^p \cdot \mathbf{n}^{(i)} = -\dot{\Lambda}\,\boldsymbol{\Omega}^p \cdot \mathbf{n}^{(i)}. \tag{4.44}$$

Remark 4.2 The evolution equations for all the microstructural $\mathbf{s}$, as given by the relations

(4.22), (4.23), (4.27), (4.28) and (4.44) can be written in compact form as

$$\overset{\triangledown}{\mathbf{s}} = \dot{\Lambda}\mathbf{G}(\boldsymbol{\sigma}, \mathbf{s})\,. \tag{4.45}$$

where $\overset{\triangledown}{\mathbf{s}} = \{\dot{\bar{\varepsilon}}^p, \dot{f}, \dot{w}_1, \dot{w}_2, \overset{\triangledown}{\mathbf{n}}^{(1)}, \overset{\triangledown}{\mathbf{n}}^{(2)}, \overset{\triangledown}{\mathbf{n}}^{(3)}\}$ and $\mathbf{G}$ is a collection of suitable isotropic functions. The plastic multiplier $\dot{\Lambda}$ will be computed from the flow rule in the next section.

Remark 4.3 The constitutive functions $\Phi, \mathbf{N}, g_1, g_2, g_3, g_4$, and $\boldsymbol{\Omega}^p$ are isotropic functions of their arguments, i.e., they are such that

$$\Phi\big(\mathbf{R}\cdot\boldsymbol{\sigma}\cdot\mathbf{R}^T, f, w_1, w_2, \mathbf{R}\cdot\mathbf{n}^{(i)}\big) = \Phi\big(\boldsymbol{\sigma}, f, w_1, w_2, \mathbf{n}^{(i)}\big), \tag{4.46}$$

$$\mathbf{N}\big(\mathbf{R}\cdot\boldsymbol{\sigma}\cdot\mathbf{R}^T, f, w_1, w_2, \mathbf{R}\cdot\mathbf{n}^{(i)}\big) = \mathbf{R}\cdot\mathbf{N}\big(\boldsymbol{\sigma}, f, w_1, w_2, \mathbf{n}^{(i)}\big)\cdot\mathbf{R}^T\,, \tag{4.47}$$

for all proper orthogonal tensors $\mathbf{R}$. The mathematical isotropy of the aforementioned functions guarantees the invariance of the constitutive equations under superposed rigid body rotations. It should be empasized, however, that the material is *anisotropic*, due to the tensorial character of the $\mathbf{n}^{(i)}$'s.

In summary, constitutive laws have now been developed to describe the behaviour of a porous material. In the elastic regime the behaviour is characterized by Eqs. (4.7)-(4.11) and in the plastic regime by Eqs.(4.19)-(4.21). The evolution of the microstructural variables $\mathbf{s}$ is characterized by Eqs. (4.22), (4.23), (4.27), (4.28) and (4.44).

4.3 Rate Form of the Elastoplastic Equations

The procedure is the same as in chapter 3, though now we want to derive the relation between the Jaumann derivative of the stress tensor $\overset{\triangledown}{\boldsymbol{\sigma}}$ and the total deformation rate $\mathbf{D}$. The derivation is as follows.

Assuming plastic loading ($\dot{\Lambda} > 0$), substitution of $\mathbf{D}^e = \mathbf{D} - \mathbf{D}^p = \mathbf{D} - \dot{\Lambda}\,\mathbf{N}$ into (4.7) yields

$$\overset{\circ}{\boldsymbol{\sigma}} = \boldsymbol{\mathcal{L}}^e : \mathbf{D} - \dot{\Lambda}\,\boldsymbol{\mathcal{L}}^e : \mathbf{N}, \tag{4.48}$$

where $\boldsymbol{\mathcal{L}}^e = \boldsymbol{\mathcal{M}}^{e-1}$. Since Φ is an isotropic function, the flow rule $\dot{\Phi} = 0$ can be written in the form [6]

$$\dot{\Phi} = \frac{\partial\Phi}{\partial\sigma} : \overset{\circ}{\boldsymbol{\sigma}} + \frac{\partial\Phi}{\partial\mathbf{s}}\cdot\overset{\circ}{\mathbf{s}} = 0\,, \tag{4.49}$$

where $\overset{\circ}{\mathbf{s}} = (\dot{\bar{\varepsilon}}^p, \dot{f}, \dot{w}_1, \dot{w}_2, \overset{\circ}{\mathbf{n}}^{(1)}, \overset{\circ}{\mathbf{n}}^{(2)}, \overset{\circ}{\mathbf{n}}^{(3)})$. In view of the fact that $\overset{\circ}{\mathbf{n}}^{(i)} = \mathbf{0}$ (Eq.(4.43)), then (4.49) can be written as

$$\mathbf{N} : \overset{\circ}{\boldsymbol{\sigma}} + \frac{\partial\Phi}{\partial\bar{\varepsilon}^p}\,\dot{\bar{\varepsilon}}^p + \frac{\partial\Phi}{\partial f}\,\dot{f} + \frac{\partial\Phi}{\partial w_1}\,\dot{w}_1 + \frac{\partial\Phi}{\partial w_2}\,\dot{w}_2 = 0. \tag{4.50}$$

Substitution of $\dot{\bar{\varepsilon}}^p$, $\dot{w}_1$ and $\dot{w}_2$ from (4.22), (4.27) and (4.28) into (4.50) yields

$$\mathbf{N} : \overset{\circ}{\boldsymbol{\sigma}} + \frac{\partial\Phi}{\partial f}\,\dot{f} - \dot{\Lambda}H = 0 \quad \text{or} \quad \dot{\Lambda} = \frac{1}{H}\,(\mathbf{N} : \overset{\circ}{\boldsymbol{\sigma}} + \frac{\partial\Phi}{\partial f}\,\dot{f}) \quad (\text{for H} \neq 0), \tag{4.51}$$

where

$$H = -\left(\frac{\partial \Phi}{\partial \bar{\varepsilon}^p}\, g_1 + \frac{\partial \Phi}{\partial w_1}\, g_3 + \frac{\partial \Phi}{\partial w_2}\, g_4 \right). \tag{4.52}$$

An alternative expression for $\dot{\Lambda}$ is obtained if one substitutes $\overset{\circ}{\boldsymbol{\sigma}}$ from (4.48) in (4.51):

$$\mathbf{N} : \boldsymbol{\mathcal{L}}^e : \mathbf{D} + \frac{\partial \Phi}{\partial f}\, \dot{f} - \dot{\Lambda}(\mathbf{N} : \boldsymbol{\mathcal{L}}^e : \mathbf{N} + H) = 0 \quad \text{or} \quad \dot{\Lambda} = \frac{1}{L}(\mathbf{N} : \boldsymbol{\mathcal{L}}^e : \mathbf{D} + \frac{\partial \Phi}{\partial f}\, \dot{f}), \tag{4.53}$$

where $L = H + \mathbf{N} : \boldsymbol{\mathcal{L}}^e : \mathbf{N}$.

Remark 4.4 Note that H is of order (flow stress)^3 and can be positive or negative; on the other hand, the term $\mathbf{N} : \boldsymbol{\mathcal{L}}^e : \mathbf{N}$ is positive, since $\boldsymbol{\mathcal{L}}^e$ is positive definite. In metals, the elastic modulus is several orders of magnitude larger than the flow stress; therefore, the term $\mathbf{N} : \boldsymbol{\mathcal{L}}^e : \mathbf{N}$ dominates and $L = H + \mathbf{N} : \boldsymbol{\mathcal{L}}^e : \mathbf{N}$ is always positive.

For a stress state on the yield surface (i.e., such that $\Phi(\boldsymbol{\sigma}, \mathbf{s}) = 0$, the requirement $\dot{\Lambda} \geq 0$ defines the "plastic loading condition"

$$\mathbf{N} : \boldsymbol{\mathcal{L}}^e : \mathbf{D} > 0, \tag{4.54}$$

whereas $\mathbf{N} : \boldsymbol{\mathcal{L}}^e : \mathbf{D} = 0$ corresponds to "neutral loading" ($\dot{\Lambda} = 0$), and $\mathbf{N} : \boldsymbol{\mathcal{L}}^e : \mathbf{D} < 0$ to "elastic unloading" ($\dot{\Lambda} = 0$ as well).

Substitution of $\dot{\Lambda}$ from (4.53) into (4.48) yields

$$\overset{\circ}{\boldsymbol{\sigma}} = \left(\boldsymbol{\mathcal{L}}^e - \frac{1}{L} \boldsymbol{\mathcal{L}}^e : \mathbf{N}\, \mathbf{N} : \boldsymbol{\mathcal{L}}^e \right) : \mathbf{D} - \frac{1}{L} \left(\boldsymbol{\mathcal{L}}^e : \mathbf{N} \right) \frac{\partial \Phi}{\partial f}\, \dot{f}. \tag{4.55}$$

The Jaumann derivative $\overset{\triangledown}{\sigma}$ is related to $\overset{\circ}{\boldsymbol{\sigma}}$ by the following expression

$$\overset{\triangledown}{\sigma} = \overset{\circ}{\boldsymbol{\sigma}} + \boldsymbol{\sigma} \cdot \mathbf{W}^p - \mathbf{W}^p \cdot \boldsymbol{\sigma} = \overset{\circ}{\boldsymbol{\sigma}} + \dot{\Lambda}(\boldsymbol{\sigma} \cdot \boldsymbol{\Omega}^p - \boldsymbol{\Omega}^p \cdot \boldsymbol{\sigma}). \tag{4.56}$$

Finally, substitution of $\overset{\circ}{\boldsymbol{\sigma}}$ from (4.55) into (4.56) yields the desired equation

$$\boxed{\overset{\triangledown}{\sigma} = \boldsymbol{\mathcal{L}}^{ep} : \mathbf{D} + \mathbf{A}\, \dot{f}}, \tag{4.57}$$

where

$$\boldsymbol{\mathcal{L}}^{ep} = \boldsymbol{\mathcal{L}}^e - \frac{1}{L}(\boldsymbol{\mathcal{L}}^e : \mathbf{N} - \boldsymbol{\sigma} \cdot \boldsymbol{\Omega}^p + \boldsymbol{\Omega}^p \cdot \boldsymbol{\sigma})(\boldsymbol{\mathcal{L}}^e : \mathbf{N}), \quad \mathbf{A} = -\frac{1}{L}(\boldsymbol{\mathcal{L}}^e : \mathbf{N} - \boldsymbol{\sigma} \cdot \boldsymbol{\Omega}^p + \boldsymbol{\Omega}^p \cdot \boldsymbol{\sigma}) \frac{\partial \Phi}{\partial f}$$

provided that $\mathbf{N} : \boldsymbol{\mathcal{L}}^e : \mathbf{D} > 0$ (plastic loading).

When $\mathbf{N} : \boldsymbol{\mathcal{L}}^e : \mathbf{D} \leq 0$ (neutral loading or elastic unloading), the corresponding equation is

$$\overset{\triangledown}{\sigma} = \boldsymbol{\mathcal{L}}^e : \mathbf{D}. \tag{4.58}$$

Also, substitution of the value of $\dot{\Lambda}$ from (4.53) in (4.23), leads to the expression

$$\boxed{\dot{f}_{loc} = \mathbf{B} : \mathbf{D} + K\, \dot{f}}, \qquad \text{where} \qquad \mathbf{B} = \frac{g_2}{L}\, \boldsymbol{\mathcal{L}}^e : \mathbf{N}, \qquad K = \frac{g_2}{L}\, \frac{\partial \Phi}{\partial f}. \tag{4.59}$$

Chapter 5

Numerical Implementation

5.1 Numerical Integration of the Constitutive Equations

The solution of the problem is developed incrementally and the constitutive equations are integrated at the element Gauss points. Let $\mathbf{F}$ denote the deformation gradient tensor. At a given Gauss point, the solution $(\mathbf{F}_n, \boldsymbol{\sigma}_n, \mathbf{s}_n)$ at time t_n as well as the deformation gradient $\mathbf{F}_{n+1}$ at time t_{n+1} are known, and the problem is to determine $(\boldsymbol{\sigma}_{n+1}, \mathbf{s}_{n+1})$. The time variation of the deformation gradient $\mathbf{F}$ during the time increment $[t_n, t_{n+1}]$ can be written as

$$\mathbf{F}(t) = \Delta\mathbf{F}(t) \cdot \mathbf{F}_n = \mathbf{R}(t) \cdot \mathbf{U}(t) \cdot \mathbf{F}_n, \quad t_n \le t \le t_{n+1}\,, \tag{5.1}$$

where $\mathbf{R}(t)$ and $\mathbf{U}(t)$ are the rotation and right stretch tensors associated with $\Delta\mathbf{F}(t)$. The corresponding deformation rate $\mathbf{D}(t)$ and spin $\mathbf{W}(t)$ tensors are given by

$$\mathbf{D}(t) = [\mathbf{L}(t)]_{sym} = [\dot{\mathbf{F}}(t) \cdot \mathbf{F}^{-1}(t)]_{sym} = [\Delta\dot{\mathbf{F}}(t) \cdot \Delta\mathbf{F}^{-1}(t)]_{sym} \tag{5.2}$$

and

$$\mathbf{W}(t) = [\mathbf{L}(t)]_{skew} = [\dot{\mathbf{F}}(t) \cdot \mathbf{F}^{-1}(t)]_{skew} = [\Delta\dot{\mathbf{F}}(t) \cdot \Delta\mathbf{F}^{-1}(t)]_{skew}\,, \tag{5.3}$$

where the subscripts 'sym' and 'skew' denote the symmetric and anti-symmetric parts, respectively of a tensor.

If it assumed that the Lagrangian triad associated with $\Delta\mathbf{F}(t)$ (i.e. the eigenvectors of $\mathbf{U}(t)$) remains fixed in the time interval $[t_n, t_{n+1}]$, then it can be shown that

$$\mathbf{D}(t) = \mathbf{R}(t) \cdot \dot{\mathbf{E}}(t) \cdot \mathbf{R}^T(t), \quad \mathbf{W}(t) = \dot{\mathbf{R}}(t) \cdot \dot{\mathbf{R}}^T(t) \tag{5.4}$$

and

$$\overset{\triangledown}{\boldsymbol{\sigma}} = \mathbf{R}(t) \cdot \dot{\hat{\boldsymbol{\sigma}}} \cdot \dot{\mathbf{R}}^T(t), \quad \overset{\triangledown}{\mathbf{n}}{}^{(i)}(t) = \mathbf{R}(t) \cdot \dot{\hat{\mathbf{n}}}(t)\,, \tag{5.5}$$

where $\mathbf{E}(\mathrm{t}) = \ln \mathbf{U}(t)$ is the logarithmic strain relative to the configuration at t_n, $\hat{\boldsymbol{\sigma}}(t) = \mathbf{R}^T(t) \cdot \boldsymbol{\sigma} \cdot \mathbf{R}(t)$, and $\hat{\mathbf{n}}^{(i)}(t) = \mathbf{R}^T(t) \cdot \mathbf{n}^{(i)}(t)$.

It is noted that at the start of the increment $(t = t_n)$

$$\mathbf{F}_n = \mathbf{R}_n = \mathbf{U}_n = \boldsymbol{\delta}, \quad \hat{\boldsymbol{\sigma}}_n = \boldsymbol{\sigma}, \quad \hat{\mathbf{n}}_n^{(i)} = \hat{\mathbf{n}}_n \quad \mathbf{E}_n = \mathbf{0}\,, \tag{5.6}$$

whereas at the end of the increment $(t = t_{n+1})$

$$\Delta\mathbf{F}_{n+1} = \mathbf{F}_{n+1} \cdot \mathbf{F}_n^{-1} = \mathbf{R}_{n+1} \cdot \mathbf{U}_{n+1} = \text{known}, \quad \text{and} \quad \mathbf{E}_{n+1} = \ln \mathbf{U}_{n+1} = \text{known}. \tag{5.7}$$

Taking into account that $\Phi, \mathbf{N}$, g_1, g_2, g_3, g_4 and $\boldsymbol{\Omega}^p$ are isotropic functions of their arguments, the elastoplastic equations can be written in the form

$$\dot{\mathbf{E}} = \dot{\mathbf{E}}^e + \dot{\mathbf{E}}^p \,, \tag{5.8}$$

$$\dot{\hat{\boldsymbol{\sigma}}} = \hat{\boldsymbol{\mathcal{L}}}^e : \dot{\mathbf{E}}^e + \dot{\Lambda} \left[\hat{\boldsymbol{\sigma}} \cdot \boldsymbol{\Omega}^p(\hat{\boldsymbol{\sigma}}, \hat{\mathbf{s}}) - \boldsymbol{\Omega}^p(\hat{\boldsymbol{\sigma}}, \hat{\mathbf{s}}) \cdot \hat{\boldsymbol{\sigma}} \right] , \tag{5.9}$$

$$\Phi(\hat{\boldsymbol{\sigma}}, \hat{\mathbf{s}}) = 0 \,, \tag{5.10}$$

$$\dot{\mathbf{E}}^p = \dot{\Lambda} \mathbf{N}(\hat{\boldsymbol{\sigma}}, \hat{\mathbf{s}}) \,, \tag{5.11}$$

$$\dot{\bar{\varepsilon}}^p = \dot{\Lambda}\, g_1(\hat{\boldsymbol{\sigma}}, \hat{\mathbf{s}}) = \frac{\hat{\boldsymbol{\sigma}} : \dot{\mathbf{E}}^p}{(1-f)\sigma_y(\bar{\varepsilon}^p)} \,, \tag{5.12}$$

$$\dot{f}_{loc} = \dot{\Lambda}\, g_2(\hat{\boldsymbol{\sigma}}, \hat{\mathbf{s}}) = (1-f)\dot{E}^p_{kk} \,, \tag{5.13}$$

$$\dot{w}_1 = \dot{\Lambda}\, g_3(\hat{\boldsymbol{\sigma}}, \hat{\mathbf{s}}) = w_1(\hat{\mathbf{n}}^{(3)}\hat{\mathbf{n}}^{(3)} - \hat{\mathbf{n}}^{(1)}\hat{\mathbf{n}}^{(1)}) : \hat{\boldsymbol{\mathcal{A}}} : \dot{\mathbf{E}}^p \,, \tag{5.14}$$

$$\dot{w}_2 = \dot{\Lambda}\, g_4(\hat{\boldsymbol{\sigma}}, \hat{\mathbf{s}}) = w_2(\hat{\mathbf{n}}^{(3)}\hat{\mathbf{n}}^{(3)} - \hat{\mathbf{n}}^{(2)}\hat{\mathbf{n}}^{(2)}) : \hat{\boldsymbol{\mathcal{A}}} : \dot{\mathbf{E}}^p \,, \tag{5.15}$$

$$\dot{\hat{\mathbf{n}}}^{(i)} = -\dot{\Lambda} \boldsymbol{\Omega}^p(\hat{\boldsymbol{\sigma}}, \hat{\mathbf{s}}) \cdot \hat{\mathbf{n}}^{(i)} \,, \tag{5.16}$$

where $\hat{\mathcal{L}}^e_{ijkl} = R_{mi} R_{nj} R_{pk} R_{ql} \hat{\mathcal{L}}^e_{mnpq}$, $\hat{\mathbf{s}} = \left(\bar{\varepsilon}^p, f, w_1, w_2, \hat{\mathbf{n}}^{(1)}, \hat{\mathbf{n}}^{(2)}, \hat{\mathbf{n}}^{(3)}\right)$ and $\hat{\boldsymbol{\mathcal{A}}} = \boldsymbol{\mathcal{A}}\left(\bar{\varepsilon}^p, f, w_1, w_2, \hat{\mathbf{n}}^{(1)}, \hat{\mathbf{n}}^{(2)}, \hat{\mathbf{n}}^{(3)}\right)$.

Remark 5.1 The corotational rates $\overset{\triangledown}{\boldsymbol{\sigma}}$ and $\overset{\triangledown}{\mathbf{n}}{}^{(i)}$ in the original equations $\overset{\triangledown}{\boldsymbol{\sigma}} = \boldsymbol{\mathcal{L}}^e : \mathbf{D}^e + \dot{\Lambda}\,(\boldsymbol{\sigma} \cdot \boldsymbol{\Omega}^p - \boldsymbol{\Omega}^p \cdot \boldsymbol{\sigma})$ and $\overset{\triangledown}{\mathbf{n}}{}^{(i)} = -\dot{\Lambda}\, \boldsymbol{\Omega}^p \cdot \mathbf{n}^{(i)}$ are now replaced to (5.9) and (5.16) by the usual time derivatives $\dot{\hat{\boldsymbol{\sigma}}}$ and $\dot{\hat{\mathbf{n}}}^{(i)}$. This is a consequence of the assumption that the Lagrangian triad associated with $\Delta\mathbf{F}(t)$ remains fixed in the time interval $[t_n, t_{n+1}]$ so that $\mathbf{W} = \dot{\mathbf{R}} \cdot \mathbf{R}^T$, which implies in turn that $\overset{\triangledown}{\boldsymbol{\sigma}} = \mathbf{R} \cdot \dot{\hat{\boldsymbol{\sigma}}} \cdot \mathbf{R}^T$ and $\overset{\triangledown}{\mathbf{n}}{}^{(i)} = \mathbf{R} \cdot \dot{\hat{\mathbf{n}}}^{(i)}$.

When in the elastic regime a forward Euler scheme of (5.9) will determine the evolution of the stresses

$$\boldsymbol{\sigma}_{n+1} = \boldsymbol{\sigma}_n + \boldsymbol{\mathcal{L}}^e : \Delta\mathbf{E} \,, \tag{5.17}$$

where $\Delta\mathbf{E} = \Delta\mathbf{E}^e$, since $\Delta\mathbf{E}^p = 0$ and there are no substantially rotations to account for. Just before entering the elastoplastic regime one part of the strains will account only for pure elasticity, while after entering the elastoplastic regime the strain increment will have an elastic and a plastic part. Therefore, there is the need to compute the elastic fraction, r, for the stresses such that

$$\Delta\mathbf{E} = r\,\Delta\mathbf{E} + (1-r)\,\Delta\mathbf{E}, \quad \textit{with } r < 1, \tag{5.18}$$

and $r\,\Delta\mathbf{E} = r\,\Delta\mathbf{E}^e$, since it is purely elastic in the elastic regime, thus just before reaching the yield stress the new value of stress is determined as

$$\boldsymbol{\sigma}_{n+1} = \boldsymbol{\sigma}_n + r\,\boldsymbol{\mathcal{L}}^e : \Delta\mathbf{E}^e = \boldsymbol{\sigma}_n + r\,\Delta\boldsymbol{\sigma}^e \,, \tag{5.19}$$

where the value of r is determined by replacing (5.19) to the yield criterion (4.19), resulting

$$\begin{aligned} &\Phi(\boldsymbol{\sigma}_n + r\,\Delta\boldsymbol{\sigma}^e, \mathbf{s}_0) = 0 \\ &\Rightarrow \frac{1}{1-f}\,(\boldsymbol{\sigma}_n + r\,\Delta\boldsymbol{\sigma}^e) : \mathbf{m} : (\boldsymbol{\sigma}_n + r\,\Delta\boldsymbol{\sigma}^e) - \sigma_y^2 = 0 \\ &\Rightarrow A^2 \cdot r^2 + 2B \cdot r + C = 0 \quad with \quad r = \frac{-B + \sqrt{B^2 - A \cdot C}}{A}\,, \end{aligned} \tag{5.20}$$

where

$$A = \Delta\boldsymbol{\sigma}^e : \mathbf{m}(\mathbf{s}) : \Delta\boldsymbol{\sigma}^e, \quad B = \boldsymbol{\sigma}_n : \mathbf{m}(\mathbf{s}) : \Delta\boldsymbol{\sigma}^e, \quad C = (1 - f_n)\,\Phi(\boldsymbol{\sigma}_n, \mathbf{s})\,. \tag{5.21}$$

The fraction $(1 - r)$ of the strain increment will have an elastic part and a plastic part and result to stresses that will be computed from the solution of Eqs.(5.8)-(5.16).

When in the elastoplastic regime, if forward Euler scheme is used in order to integrate numerically the above set of equations, then the magnitude of the stain increment has to be small relative to the yield strain, so that the results are accurate. An alternative method is the following. A backward Euler scheme is used for the numerical integration of the flow rule (5.11):

$$\mathbf{G} = \Delta\mathbf{E}^p - \Delta\Lambda\hat{\mathbf{N}}_{n+1} = \mathbf{0}, \quad \hat{\mathbf{N}}_{n+1} = \mathbf{N}(\hat{\boldsymbol{\sigma}}_{n+1}\,, f_{n+1}\,, w_a|_{n+1}, \hat{\mathbf{n}}^{(i)}_{n+1})\,. \tag{5.22}$$

The quantities $\Delta\Lambda$ and $\Delta\mathbf{E}^p$ are chosen as the primary unknowns and the flow rule (5.22) and the yield condition:

$$\Phi\big(\hat{\boldsymbol{\sigma}}_{n+1}(\Delta\Lambda, \Delta\mathbf{E}^p), \hat{\mathbf{s}}_{n+1}\big(\Delta\Lambda, \Delta\mathbf{E}^p\big)\big) = 0\,, \tag{5.23}$$

are treated as the basic equations.

A backward Euler scheme is also implemented for the numerical integration of the evolution equations for $\bar{\varepsilon}^p$ and f_{loc}:

$$\bar{\varepsilon}^p_{n+1}(\Delta\mathbf{E}^p) = \bar{\varepsilon}^p_n + \frac{\hat{\boldsymbol{\sigma}}_{n+1} : \Delta\mathbf{E}^p}{(1 - f_{n+1})\sigma_y(\bar{\varepsilon}^p_n)} \equiv \bar{\varepsilon}^p_n + \mathbf{R}_2 : \Delta\mathbf{E}^p\,, \tag{5.24}$$

$$f_{loc}|_{n+1} = f_{loc}|_n + (1 - f_{n+1})\,\Delta E^p_{kk}\,, \tag{5.25}$$

$\hat{\boldsymbol{\sigma}}_{n+1}$, $w_1|_{n+1}$, $w_2|_{n+1}$, and $\hat{\mathbf{n}}^{(i)}_{n+1}$ are defined by the following equations:

$$\begin{aligned} \hat{\boldsymbol{\sigma}}_{n+1}(\Delta\Lambda,\, \Delta\mathbf{E}^p) &= \hat{\boldsymbol{\sigma}}^e - \boldsymbol{\mathcal{L}}^e_n : \Delta\mathbf{E}^p + \Delta\Lambda\,(\boldsymbol{\sigma}_n \cdot \boldsymbol{\Omega}^p - \boldsymbol{\Omega}^p \cdot \boldsymbol{\sigma}_n) \\ &\equiv \hat{\boldsymbol{\sigma}}^e - \boldsymbol{\mathcal{L}}^e_n : \Delta\mathbf{E}^p + \Delta\Lambda\,\mathbf{R}_1\,, \end{aligned} \tag{5.26}$$

$$w_1|_{n+1}(\Delta\mathbf{E}^p) = w_1|_n + w_1|_n(\mathbf{n}^{(3)}_n\mathbf{n}^{(3)}_n - \mathbf{n}^{(1)}_n\mathbf{n}^{(1)}_n) : \hat{\boldsymbol{\mathcal{A}}}_n : \Delta\mathbf{E}^p \equiv w_1|_n + \mathbf{R}_{31} : \Delta\mathbf{E}^p\,, \tag{5.27}$$

$$w_2|_{n+1}(\Delta\mathbf{E}^p) = w_2|_n + w_2|_n(\mathbf{n}^{(3)}_n\mathbf{n}^{(3)}_n - \mathbf{n}^{(2)}_n\mathbf{n}^{(2)}_n) : \hat{\boldsymbol{\mathcal{A}}}_n : \Delta\mathbf{E}^p \equiv w_2|_n + \mathbf{R}_{32} : \Delta\mathbf{E}^p\,, \tag{5.28}$$

$$\hat{\mathbf{n}}^{(i)}_{n+1}(\Delta\Lambda) = \exp(-\Delta\Lambda\,\boldsymbol{\Omega}^p_n) \cdot \mathbf{n}^{(i)}_n\,, \tag{5.29}$$

where $\hat{\boldsymbol{\sigma}}^e = \boldsymbol{\sigma}_n + \boldsymbol{\mathcal{L}}^e_n : \Delta\mathbf{E} =$ known is the "elastic predictor", and use has been made of the fact that $\hat{\boldsymbol{\sigma}}_n = \boldsymbol{\sigma}_n$, $\hat{\mathbf{n}}^{(i)}_n = \mathbf{n}^{(i)}_n$ and $\hat{\boldsymbol{\mathcal{L}}}^e_n = \boldsymbol{\mathcal{L}}^e_n$. The symbols $\mathbf{R}$'s are introduced here to write simpler formulas later, and their values are defined by the context. The notation $\Delta(\bullet) = (\bullet)_{n+1} - (\bullet)_n$ is used, and $\Delta\mathbf{E} = \mathbf{E}_{n+1} - \mathbf{E}_n =$ known. Eqs. (5.26) - (5.28) derive from (5.9), (5.14), and (5.15) by implementing a forward Euler scheme for their numerical integration.

Remark 5.2 Note that (5.29) requires the evaluation of the exponential of the antisymmetric second order tensor $-\Delta\Lambda\,\boldsymbol{\Omega}_n^p$. The exponential of the antisymmetric second-order tensor $\mathbf{A}$ ($\mathbf{A}^T = -\mathbf{A}$) is an orthogonal tensor that can be determined from the following formula, attributed to Gibbs [4]

$$\exp(\mathbf{A}) = \boldsymbol{\delta} + \frac{sin\,a}{a}\mathbf{A} + \frac{1 - cos\,a}{a^2}\mathbf{A}^2 \tag{5.30}$$

where $a = \sqrt{\mathbf{A} : \mathbf{A}/2}$ is the magnitude of the axial vector of $\mathbf{A}$.

Eqs. (5.22) and (5.23) are solved for $\Delta\Lambda$ and $\Delta\mathbf{E}^p$ by using Newton's method. First estimates for starting the Newton iterations are obtained for $(\Delta\Lambda, \Delta\mathbf{E}^p)$ by using equations (4.53) and (5.11)

$$\Delta\Lambda_{est} = \frac{1}{L_n}(\mathbf{N}_n : \boldsymbol{\mathcal{L}}_n{}^e : \Delta\mathbf{E} + \left.\frac{\partial\Phi}{\partial f}\right|_n (f_{n+1} - f_n)), \quad \Delta\mathbf{E}^p_{est} = \Delta\Lambda_{est}\,\mathbf{N}_n. \tag{5.31}$$

Renewed values for $\Delta\mathbf{E}^p$ and $\Delta\Lambda$ are computed as follows:

$$(\Delta\Lambda)^{(k+1)} = (\Delta\Lambda)^{(k)} + \delta(\Delta\Lambda) \tag{5.32}$$

and

$$(\Delta\mathbf{E}^p)^{(k+1)} = (\Delta\mathbf{E}^p)^{(k)} + \delta(\Delta\mathbf{E}^p)\,, \tag{5.33}$$

where the superscript '(k)' denotes the k-*th* iteration in the Newton's method, $\delta(\bullet)$ denotes the correction of its argument during the Newton's method iterations. According to the Newton's method the values of $\delta(\Delta\Lambda)$ and $\delta(\Delta\mathbf{E}^p)$ are determined from the solution of the linear system

$$\begin{bmatrix} \frac{\partial\Phi}{\partial\Delta\Lambda} & \frac{\partial\Phi}{\partial\Delta\mathbf{E}^p} \\ \frac{\partial\Delta\mathbf{G}}{\partial\Delta\Lambda} & \frac{\partial\Delta\mathbf{G}}{\partial\Delta\mathbf{E}^p} \end{bmatrix} \cdot \begin{Bmatrix} \delta(\Delta\Lambda) \\ \delta(\Delta\mathbf{E}^p) \end{Bmatrix} = \begin{Bmatrix} \Phi \\ \mathbf{G} \end{Bmatrix} \tag{5.34}$$

Explicit expressions for the quantities $\frac{\partial\Phi}{\partial\Delta\Lambda}$, $\frac{\partial\Phi}{\partial\Delta\mathbf{E}^p}$, $\frac{\partial\Delta\mathbf{G}}{\partial\Delta\Lambda}$, and $\frac{\partial\Delta\mathbf{G}}{\partial\Delta\mathbf{E}^p}$ that appear in the calculation of the Jacobian in (5.34) can be derived by taking into account the analytical expressions for all involved quantities and by using the chain rule on Φ and $\mathbf{G}$ as follows:

$$\frac{\partial\Phi}{\partial\Delta\Lambda} = \frac{\partial\Phi}{\partial\hat{\boldsymbol{\sigma}}} : \frac{\partial\hat{\sigma}}{\partial\Delta\Lambda} + \frac{\partial\Phi}{\partial\hat{\mathbf{n}}^{(i)}} \cdot \frac{\partial\hat{\mathbf{n}}^{(i)}}{\partial\Delta\Lambda} \simeq \mathbf{N} : \mathbf{R}_1\,, \tag{5.35}$$

$$\begin{aligned} \frac{\partial\Phi}{\partial\Delta\mathbf{E}^p} &= \frac{\partial\Phi}{\partial\hat{\boldsymbol{\sigma}}} : \frac{\partial\hat{\sigma}}{\partial\Delta\mathbf{E}^p} + \frac{\partial\Phi}{\partial\bar{\varepsilon}^p} \cdot \frac{\partial\bar{\varepsilon}^p}{\partial\Delta\mathbf{E}^p} + \frac{\partial\Phi}{\partial w_a}\frac{\partial w_a}{\partial\Delta\mathbf{E}^p} = \\ &= -\mathbf{N} : \boldsymbol{\mathcal{L}}_n^e + \frac{\partial\Phi}{\partial\bar{\varepsilon}^p}\mathbf{R}_2 + \frac{\partial\Phi}{\partial w_a}\mathbf{R}_{3a}\,, \qquad \alpha = 1, 2\,, \end{aligned} \tag{5.36}$$

$$\frac{\partial\mathbf{G}}{\partial\Delta\Lambda} = -\mathbf{N} - \Delta\Lambda\left(\frac{\partial\mathbf{N}}{\partial\hat{\boldsymbol{\sigma}}} : \frac{\partial\hat{\sigma}}{\partial\Delta\Lambda} + \frac{\partial\mathbf{N}}{\partial\hat{\mathbf{n}}^{(i)}} \cdot \frac{\partial\hat{\mathbf{n}}^{(i)}}{\partial\Delta\Lambda}\right) \simeq -\mathbf{N} - \Delta\Lambda\frac{\partial\mathbf{N}}{\partial\hat{\boldsymbol{\sigma}}} : \mathbf{R}_1\,, \tag{5.37}$$

$$\begin{aligned}\frac{\partial \mathbf{G}}{\partial \Delta \mathbf{E}^p} &= \mathbf{I} - \Delta\Lambda \left(\frac{\partial \mathbf{N}}{\partial \hat{\boldsymbol{\sigma}}} : \frac{\partial \hat{\boldsymbol{\sigma}}}{\partial \Delta \mathbf{E}^p} + \frac{\partial \mathbf{N}}{\partial w_a} \frac{\partial w_a}{\partial \Delta \mathbf{E}^p} \right) \\ &= \mathbf{I} - \Delta\Lambda \left(-\frac{\partial \mathbf{N}}{\partial \hat{\boldsymbol{\sigma}}} : \boldsymbol{\mathcal{L}}^e + \frac{\partial \mathbf{N}}{\partial w_a} \mathbf{R}_{3a} \right) ,\end{aligned} \tag{5.38}$$

where $\partial\Phi/\partial\hat{\mathbf{n}}^{(i)}$ and $\partial\mathbf{N}/\partial\hat{\mathbf{n}}^{(i)}$ are assumed to be relatively small, thus neglected. In addition, by taking into consideration (4.21) the following relations are obtained:

$$\frac{\partial \Phi}{\partial \hat{\boldsymbol{\sigma}}} = \frac{\partial \Phi}{\partial \boldsymbol{\sigma}} = \mathbf{N} , \tag{5.39}$$

$$\frac{\partial \mathbf{N}}{\partial \hat{\boldsymbol{\sigma}}} = \frac{\partial \mathbf{N}}{\partial \boldsymbol{\sigma}} = \frac{2}{1-f} \mathbf{m} , \tag{5.40}$$

$$\frac{\partial \mathbf{N}}{\partial w_a} = \frac{2}{1-f} \frac{\partial \mathbf{m}}{\partial w_a} : \hat{\boldsymbol{\sigma}}, \quad \alpha = 1, 2 . \tag{5.41}$$

Note that it is difficult to find an analytic expression for $\partial\mathbf{m}/\partial w_a$, thus it is computed numerically.

Finally, recalling the $\mathbf{R}'s$ introduced to Eqs.(5.24)-(5.28) the following differentials take the form:

$$\frac{\partial \hat{\boldsymbol{\sigma}}}{\partial \Delta\Lambda} = \mathbf{R}_1, \quad \frac{\partial \hat{\boldsymbol{\sigma}}}{\partial \Delta \mathbf{E}^p} = -\boldsymbol{\mathcal{L}}^e, \quad \frac{\partial \bar{\varepsilon}^p}{\partial \Delta \mathbf{E}^p} = \mathbf{R}_2, \quad \frac{\partial w_a}{\partial \Delta \mathbf{E}^p} = \mathbf{R}_{3a} \tag{5.42}$$

When the values of the five unknowns $\Delta\Lambda$ and $\Delta\mathbf{E}^p$ converge from the Newton's method, which means that (5.22) and (5.23) are satisfied, then $\hat{\boldsymbol{\sigma}}_{n+1}$, $\bar{\varepsilon}^p_{n+1}$, $w_1|_{n+1}$, $w_2|_{n+1}$, $f_{loc}|_{n+1}$ and $\hat{\mathbf{n}}^{(i)}_n$ are determined from Eqs.(5.24) - (5.29). Finally, $\boldsymbol{\sigma}_{n+1}$ and $\mathbf{n}^{(i)}_{n+1}$ are computed from

$$\boldsymbol{\sigma}_{n+1} = \mathbf{R}_{n+1} \cdot \hat{\boldsymbol{\sigma}}_{n+1} \cdot \mathbf{R}^T_{n+1}, \qquad \mathbf{n}^{(i)}_{n+1} = \mathbf{R}_{n+1} \cdot \hat{\mathbf{n}}^{(i)}_{n+1} , \tag{5.43}$$

which completes the integration process.

5.2 Non-local problems in ABAQUS/Standard via "UMAT"

The constitutive model described above is implemented into the ABAQUS general purpose finite element code. Non-local constitutive models cannot be handled by the commercial finite element codes, that are commonly used for the solution of structural mechanics problems. To overcome this difficulty, we take advantage of the similarities between the BVP that defines the non-local variable f and the steady-state heat transfer problem in an isotropic material, and use the available elements in commercial codes for coupled thermo-mechanical analysis of structures.

One version of the steady-state heat transfer problem in an isotropic material is :

$$\begin{aligned} & k\,\nabla^2 T + r\,(\Delta\boldsymbol{\varepsilon}, T) = 0 \quad in \quad V \\ & k\,\mathbf{n} \cdot \nabla T = \hat{q} \qquad on \quad \partial V, \end{aligned} \tag{5.44}$$

where T is the temperature, k the thermal conductivity, r the heat supply per unit of volume, $\hat{q}$ the prescribed boundary heat flux vector and $\Delta\boldsymbol{\varepsilon}$ a strain increment properly defined in terms of nodal displacements.

As it was previously mentioned in Chapter 4 the BVP problem for the non-local porosity f is

$$\begin{aligned} & f - \ell^2 \nabla^2 f = f_{loc} \quad in \quad V \\ & B.C. : \frac{\partial f}{\partial n} = 0 \quad on \quad \partial V \,. \end{aligned} \tag{5.45}$$

Comparing the BVP (5.44) and (5.45), we conclude that the non-local variable f can be identified with the temperature field T provided the following correspondence is used

$$T \longleftrightarrow f, \quad k \longleftrightarrow \ell^2, \quad r\,(\Delta\boldsymbol{\varepsilon}, T) \longleftrightarrow f_{loc}(\Delta\boldsymbol{\varepsilon}, f) - f\,, \quad \hat{q} \to 0\,. \tag{5.46}$$

It should be also noted that the coupled temperature - displacement in ABAQUS/Standard can be used for the solution of quasi-static implicit strain-gradient plasticity problems, but it cannot be used for dynamic problems, in which inertia effects become important.

So, in the special case of quasi-static problems, the solution can be obtained using user material subroutine UMAT in ABAQUS/Standard together with a *COUPLED TEMPERATURE DISPLACEMENT, STEADY STATE analysis option.

With a User Material (UMAT) subroutine, a new constitutive model can be introduced into the ABAQUS finite element program. It is an out-source piece of code written in FORTRAN. The UMAT subroutine is called by ABAQUS at every integration point for all elements where user-defined material behaviour is specified. UMAT has a twofold role. First, it provides ABAQUS the material Jacobian matrix $\partial(\Delta\boldsymbol{\sigma})/\partial(\Delta\boldsymbol{\varepsilon})$ corresponding to the mechanical constitutive model under consideration. Secondly, in the case of a mechanical problem UMAT takes as input at the start of the integration increment the values $\mathbf{F}_n$, $\boldsymbol{\sigma}_n$, and $\mathbf{F}_{n+1}$ and calculates $\boldsymbol{\sigma}_{n+1}$, as well as a set of solution-dependent state variables at the end of the increment.

The constitutive equations are integrated numerically in user subroutine UMAT. In UMAT, the value of f is provided as "temperature", f_{loc} is determined from the numerical integration of the constitutive equations using the algorithm described in section 5.1, and r (variable RPL in UMAT) is identified with the difference $f_{loc} - f$. The derivatives $\partial\boldsymbol{\sigma}/\partial\boldsymbol{\varepsilon}$ (DDSDDE), $\partial\boldsymbol{\sigma}/\partial\theta$ (DDSDDT), $\partial r/\partial\Delta\boldsymbol{\varepsilon}$ (DRPLDE), and $\partial r/\partial\theta$ (DRPLDT) are also evaluated in UMAT.

In view of (4.57) and (4.59), i.e.,

$$\overset{\triangledown}{\boldsymbol{\sigma}} = \boldsymbol{\mathcal{L}}^{ep} : \mathbf{D} + \mathbf{A}\,\dot{f} \qquad \text{and} \qquad \dot{f}_{loc} = \mathbf{B} : \mathbf{D} + K\,\dot{f}\,, \tag{5.47}$$

$\partial\boldsymbol{\sigma}/\partial\Delta\boldsymbol{\varepsilon}$, $\partial\boldsymbol{\sigma}/\partial\theta$, $\partial r/\partial\Delta\boldsymbol{\varepsilon}$ and $\partial r/\partial\theta$ are approximated as follows

$$\frac{\partial\boldsymbol{\sigma}}{\partial\Delta\boldsymbol{\varepsilon}} = \boldsymbol{\mathcal{L}}^{ep}, \qquad \frac{\partial\boldsymbol{\sigma}}{\partial\theta} = \frac{\partial\boldsymbol{\sigma}}{\partial f} \simeq \mathbf{A}, \tag{5.48}$$

and

$$\frac{\partial r}{\partial\Delta\boldsymbol{\varepsilon}} = \frac{\partial f_{loc}}{\partial\Delta\boldsymbol{\varepsilon}} \simeq \mathbf{B}, \qquad \frac{\partial r}{\partial\theta} = \frac{\partial f_{loc}}{\partial f} - 1 \simeq K - 1. \tag{5.49}$$

where

$$\boldsymbol{\mathcal{L}}^{ep} = \boldsymbol{\mathcal{L}}^{e} - \frac{1}{L}(\boldsymbol{\mathcal{L}}^{e} : \mathbf{N} - \boldsymbol{\sigma}\cdot\boldsymbol{\Omega}^{p} + \boldsymbol{\Omega}^{p}\cdot\boldsymbol{\sigma})(\boldsymbol{\mathcal{L}}^{e} : \mathbf{N}), \quad \mathbf{A} = -\frac{1}{L}(\boldsymbol{\mathcal{L}}^{e} : \mathbf{N} - \boldsymbol{\sigma}\cdot\boldsymbol{\Omega}^{p} + \boldsymbol{\Omega}^{p}\cdot\boldsymbol{\sigma})\frac{\partial\Phi}{\partial f},$$

$$\mathbf{B} = \frac{g_2}{L}\,\boldsymbol{\mathcal{L}}^{e} : \mathbf{N}, \qquad K = \frac{g_2}{L}\,\frac{\partial\Phi}{\partial f}.$$

Such an approximation of the Jacobian is first-order accurate as the size of the increment

$\Delta t \to 0$. It should be emphasized, however, that the aforementioned approximation influences only the rate of the convergence of the loop and not the accuracy of the results.

A typical UMAT code interface is presented below:

```
SUBROUTINE UMAT(STRESS, STATEV, DDSDDE, SSE, SPD, SCD,
+ RPL, DDSDDT, DRPLDE, DRPLDT,
+ STRAN, DSTRAN, TIME, DTIME, TEMP, DTEMP, PREDEF, DPRED, CMNAME,
+ NDI, NSHR, NTENS, NSTATV, PROPS, NPROPS, COORDS, DROT, PNEWDT,
+ CELENT, DFGRD0, DFGRD1, NOEL, NPT, LAYER, KSPT, JSTEP, KINC)

INCLUDE 'ABAPARAM. INC '

CHARACTER*80 CMNAME
DIMENSION STRESS(NTENS), STATEV(NSTATV),
DDSDDE(NTENS,NTENS), DDSDDT(NTENS), DRPLDE(NTENS),
+ STRAN(NTENS), DSTRAN(NTENS), TIME(2), PREDEF(1), DPRED(1),
+ PROPS(NPROPS), COORDS(3), DROT(3,3), DFGRD0(3,3), DFGRD1(3,3),
+ JSTEP(4)

user coding to define DDSDDE, STRESS, STATEV, SSE, SPD, SCD and , if necessary ,
RPL, DDSDDT, DRPLDE, DRPLDT, PNEWDT

RETURN
END
```

The basic variables predefined in a general UMAT subroutine are summarized in Table 5.1.

Table 5.1: Description of the predefined variables in a UMAT subroutine.

Variable	Description
NDI	Number of direct stress components.
NSHR	Number of engineering shear stress components.
NTENS	Size of the stress or strain component array (NDI + NSHR).
NSTATV	Number of solution-dependent state variables that are associated with this material type.
NPROPS	User-defined number of material constants associated with this user material.
STRESS(NTENS)	An array with the components of the stress tensor.
DDSDDE(NTENS,NTENS)	The Jacobian matrix of the constitutive model, i.e. $\partial\Delta\boldsymbol{\sigma}/\partial\Delta\boldsymbol{\varepsilon}$.
STATEV(NSTATV)	An array containing the solution-dependent state variables.
SSE	The specific elastic strain energy.
SPD	The plastic dissipation energy.
SCD	The creep dissipation energy.
RPL	Volumetric heat generation per unit of time due to mechanical working of the material
DRPLDT	Variation of RPL with respect to the temperature.
DRPLDE(NTENS)	Variation of RPL with respect to the strain increments.
DDSDDT(NTENS)	Variation of the stress increments with respect to the temperature.

TEMP	Temperature at the start of the increment.
DTEMP	Increment of temperature.
DFGRD0(3,3)	Array containing the deformation gradient at the beginning of the increment.
DFGRD1(3,3)	Array containing the deformation gradient at the end of the increment.
STRAN(NTENS)	An array containing the total strains. It contains only the mechanical strains.
DSTRAN(NTENS)	Array of strain increments (only the mechanical strain increments).
DROT(3,3)	Rotation increment matrix.
TIME(1)	Value of step time at the beginning of the current increment or frequency.
TIME(2)	Value of total time at the beginning of the current increment.
DTIME	Time increment.
PREDEF	An array of interpolated values of predefined field variables at a point at the start of the increment.
DPRED	An array of increments of predefined field variables.
CMNAME	User-defined material name.
COORDS	An array containing the coordinates of a point.
CELENT	Characteristic element length.
NOEL	Element number.
NPT	Integration point number.
JSTEP(1)	Step number.
KINC	Increment number.

Chapter 6

Applications

The non-local model is implemented in the ABAQUS general purpose finite element program via a material "user subroutine" (UMAT or VUMAT) and the coupled thermo-mechanical solution procedure, in which temperature and displacements are the nodal degrees of freedom, and temperature is identified with the non-local porosity. Several example problems are solved numerically. In particular, the predictions of the model are compared to unit cell finite element calculations and the problems of ductile fracture, necking and failure of a round bar, and localization in plane-strain tension are analyzed in detail.

6.1 Unit Cell Finite Element Calculations

The scope of the present section is to validate the anisotropic model for porous metals which was previously presented, using periodic three-dimensional unit cell calculations comprising a large number of spherical pores distributed randomly in a matrix phase. The Mises plasticity model is used in the finite element calculations.

The periodic unit cell is a cube with edge size L and is constructed using the method presented by Segurado and Llorca [26]. The virtual microstructure contains a dispersion of a sufficiently large number of non-overlapping spherical pores of uniform (monodisperse) size. The inclusions are randomly located within the cell and are generated using the Random Sequential Adsorption Algorithm (RSA) [24]. In these analyses the number of pores in the unit cell was selected to be thirty. In addition, the unit cell is periodic, i.e., it can be repeated in all three directions to represent a 3-D periodic structure.

According to the RSA algorithm, the center positions of the pores are generated randomly and sequentially. The sequential addition of pores is constrained so that the distance between the pores with other pores and with the boundaries of the cubic unit cell take a minimum value that guaranties adequate spatial discretization(see, e.g., Segurado and Llorca, [26]; Fritzen *et al.*, [12]). In particular:

- The center-to-center distance between a new pore i in the sequential algorithm and any previously accepted pore $j = 1, 2, \cdots, i-1$ has to be greater than the minimum value $s_1 = 2R_m(1 + d_1)$, where d_1 is an offset distance. Mathematically this can be written as

$$\|\mathbf{X}^i - \mathbf{X}^j - \mathbf{h}\| \geq s_1, \tag{6.1}$$

  where $\mathbf{X}^i$, $\mathbf{X}^j$ denote the location of the center of the pores i, j and $\mathbf{h}$ is a vector with entries 0, L or -L for each of its three Cartesian components with respect to the principal axes of the cubic unit cell.

- The pores should be considerably distant from the boundaries of the unit cell as imposed by the following inequalities

$$\|X_k^i - R_m\| \geq s_2 \quad \text{and} \quad \|X_k^i + R_m - L\| \geq s_2 \quad (k = 1, 2, 3), \tag{6.2}$$

  where $s_2 = d_2 R_m$ with d_2 being an another offset value.

In (6.2) R_m represents the radius of the pores and it is equal to

$$R_m = L \left(\frac{3f}{4\pi N} \right)^{1/3}, \tag{6.3}$$

where N is the number of particles in the cell and f is the porosity.

Meshing

Finite element discretizations of the cubic unit cell were created using the mesh generator code NETGEN [25], which has the capability to create periodic meshes as required. All calculations were carried out using the ABAQUS general purpose finite element code. Three dimensional 10-node quadratic tetrahedral elements with a constant pressure interpolation were used (C3D10H in ABAQUS); all analyses were carried out incrementally and accounted for geometry changes due to deformation (finite strain solutions).
Figure 6.1 illustrates (a) a representative unit cell generated by the above algorithm for $N = 30$ and porosity $f = 3\%$ and (b) the finite element mesh created using the mesh generator code NETGEN.

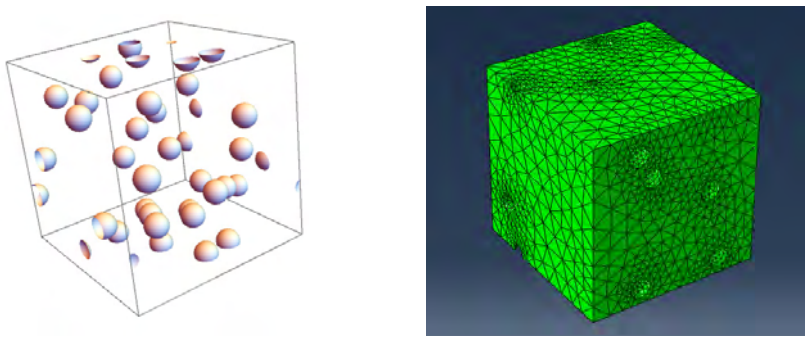

(a) (b)

Figure 6.1: (a) Representative unit cell of unit volume $L^3 = 1$ and porosity $f = 3\%$,containing $N = 30$ randomly distributed spherical pores (b) the finite element mesh in the undeformed configuration creared by NETGEN

Material

The matrix material, with Young's modulus E and Poisson's ratio v, exhibits isotropic hardening following Eq. (4.20). The values $E = 300\,\sigma_0$, $\nu = 0.3$ and $n = 10$ are used in the calculations. The voids are assumed to be initially spherical and uniformly distributed in the isotropic metal matrix with an initial porosity $f_0 = \{1, 2, 3, 4, 5\}\%$.

Loading Cases

In order to validate the anisotropic model for porous metals, multiple loading cases and initial porosities f_0 are examined. In addition, one-element finite element calculations are carried out, in which the element is subjected to the same deformation gradient as the unit cell and the corresponding uniform stress state in the element is calculated by using the algorithm described in chapter 5 for the porous material. It should be noted that the same calculations are conducted with two versions of the anisotropic costitutive model for porous metals. The

first version is the original variational formulation (VAR) of Ponte Castañeda [20] and the second is the modified variational method (MVAR) proposed by Aravas N. and Danas K. [8]. The original variational formulation has been found to be sufficiently accurate at low stress triaxialities but tends to overestimate the effective response of the porous material at high stress triaxialities. The modified variational method is in alignment with the spherical shell and the cylindrical shell solutions. By examining multiple loading cases we will be able to conclude how efficient this modification is.

We identify the coordinate axes of the unit cell with the principal directions of the stress tensor and write the principal stresses in the form

$$\left\{ \begin{array}{c} \sigma_1 \\ \sigma_2 \\ \sigma_3 \end{array} \right\} = \sigma_e \left(X_\Sigma \left\{ \begin{array}{c} 1 \\ 1 \\ 1 \end{array} \right\} + \frac{2}{3} \left\{ \begin{array}{c} \cos\left(\theta + \frac{\pi}{6}\right) \\ \sin\theta \\ -\cos\left(\theta - \frac{\pi}{6}\right) \end{array} \right\} \right), \tag{6.4}$$

where $X_\Sigma = p/\sigma_e$ is the stress triaxiality and θ is the "Lode angle", so that

$$J_3 = \det\mathbf{s} = -\frac{2}{27}\,\sigma_e^3\,\sin 3\theta. \tag{6.5}$$

Angle θ takes values in the range $-30^\circ \leq \theta \leq 30^\circ$, where, to within a hydrostatic stress, $\theta = -30^\circ$ corresponds to uniaxial tension, $\theta = 0$ to pure shear, and $\theta = 30^\circ$ to uniaxial compression.
We studied the following cases:
For $\theta = -30^\circ$ and $\theta = 0^\circ$

- Initial porosity $f_0 = 1\%$ and triaxialities $X_\Sigma = 1/3$, $X_\Sigma = 1$, $X_\Sigma = 3$.
- Initial porosity $f_0 = 2\%$ and triaxialities $X_\Sigma = 1/3$, $X_\Sigma = 1$, $X_\Sigma = 3$.
- Initial porosity $f_0 = 3\%$ and triaxialities $X_\Sigma = 1/3$, $X_\Sigma = 1$, $X_\Sigma = 3$.
- Initial porosity $f_0 = 4\%$ and triaxialities $X_\Sigma = 1/3$, $X_\Sigma = 1$, $X_\Sigma = 3$.
- Initial porosity $f_0 = 5\%$ and triaxialities $X_\Sigma = 1/3$, $X_\Sigma = 1$, $X_\Sigma = 3$.

In the following, we present the most representative cases in order to be able to reach some conclusions.

6.1.1 $\theta = -30^\circ$ (uniaxial tension)

Figure 6.2 shows the (a) $\sigma - logE$, (b) $f - logE$, (c) $\bar{\varepsilon}^p - logE$, and (d) $w - logE$ curves for $f_0 = 0.01$ and $X_\Sigma = 1/3$. Recall that the label (VAR) stands for the original variational formulae, on which the fourth order tensor $\mathbf{m}$ takes its value from (4.17), while (MVAR) stands for the modified variational formulae where the tensor $\mathbf{m}$ takes its value from (4.18).

It is evident that, regarding the stress-strain curves both versions of the constitutive model agree with the unit cell calculations. However, the modified variational method seems to overestimate the evolution of the porosity whereas the variational method agrees very well with the unit cell calculations. As far as the equivalent plastic strain there seems to be a perfect match between the two versions of the constitutive model and the unit cell calculations. Regarding the aspect ratio there is a general good agreement between the results, but the original variational method seems to perform better.

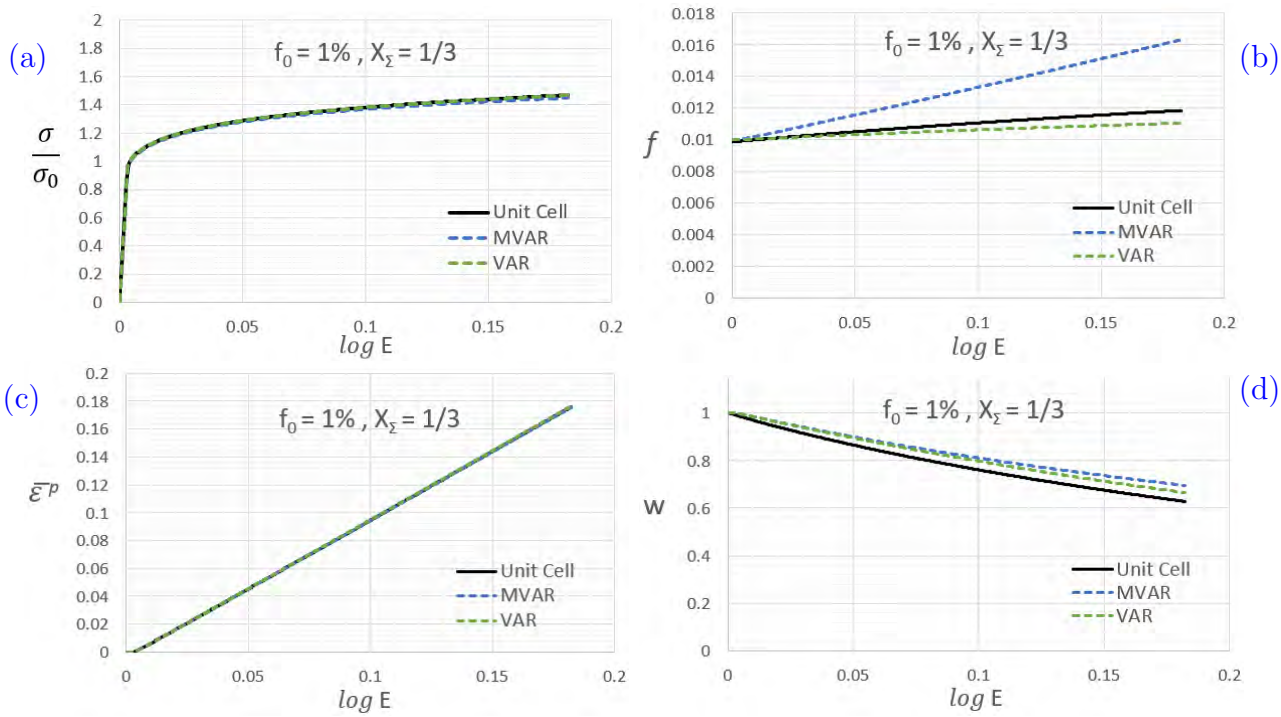

Figure 6.2: (a) $\sigma - logE$, (b) $f - logE$, (c) $\bar{\varepsilon}^p - logE$, and (d) $w - logE$ curves for $\theta = -30°$, $f_0 = 0.01$ and $X_\Sigma = 1/3$.

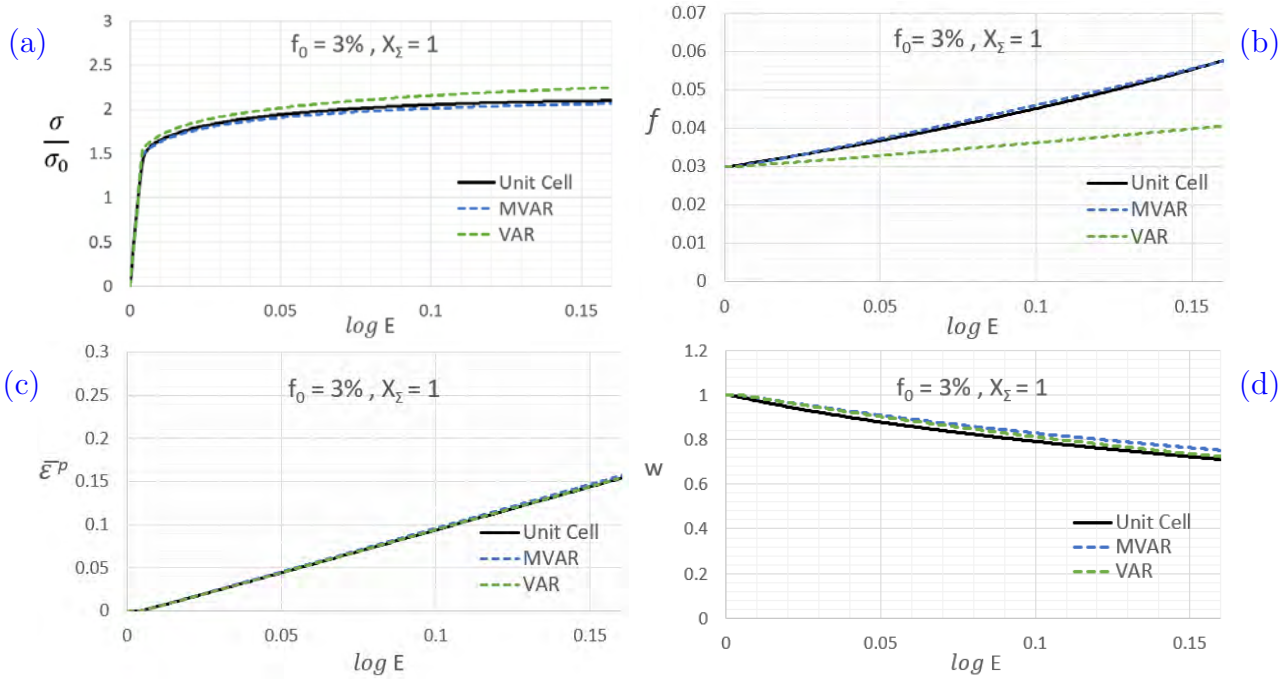

Figure 6.3: (a) $\sigma - logE$, (b) $f - logE$, (c) $\bar{\varepsilon}^p - logE$, and (d) $w - logE$ curves for $\theta = -30°$, $f_0 = 0.03$ and $X_\Sigma = 1$.

Figure 6.3 shows the (a) $\sigma - logE$, (b) $f - logE$, (c) $\bar{\varepsilon}^p - logE$, and (d) $w - logE$ curves for $f_0 = 0.03$ and $X_\Sigma = 1$.

Regarding the stress-strain curves there seems to be a slight mismatch with between the results of the variational method and the other two methods. The porosity graph is quite interesting because now we observe a very good agreement between the modified variational method and the unit cell calculations. The original variational method seems to underestimate

the porosity. As far as the equivalent plastic strain there seems to be a perfect match between the two versions of the constitutive model and the unit cell calculations. Regarding the aspect ratio there is a general good agrement between the results, but the original variational method seems to perform better.

Finally, Fig. 6.4 shows the (a) $\sigma - logE$, (b) $f - logE$, (c) $\bar{\varepsilon}^p - logE$, and (d) $w - logE$ curves for $f_0 = 0.05$ and $X_\Sigma = 3$.

As we can see from the graphs below, the modified variational method predicts more accurately the stress-strain curves, the porosity evolution and the equivalent plastic strain. As far as the aspect ratio both versions of the constitutive model agree with the unit cell calculations.

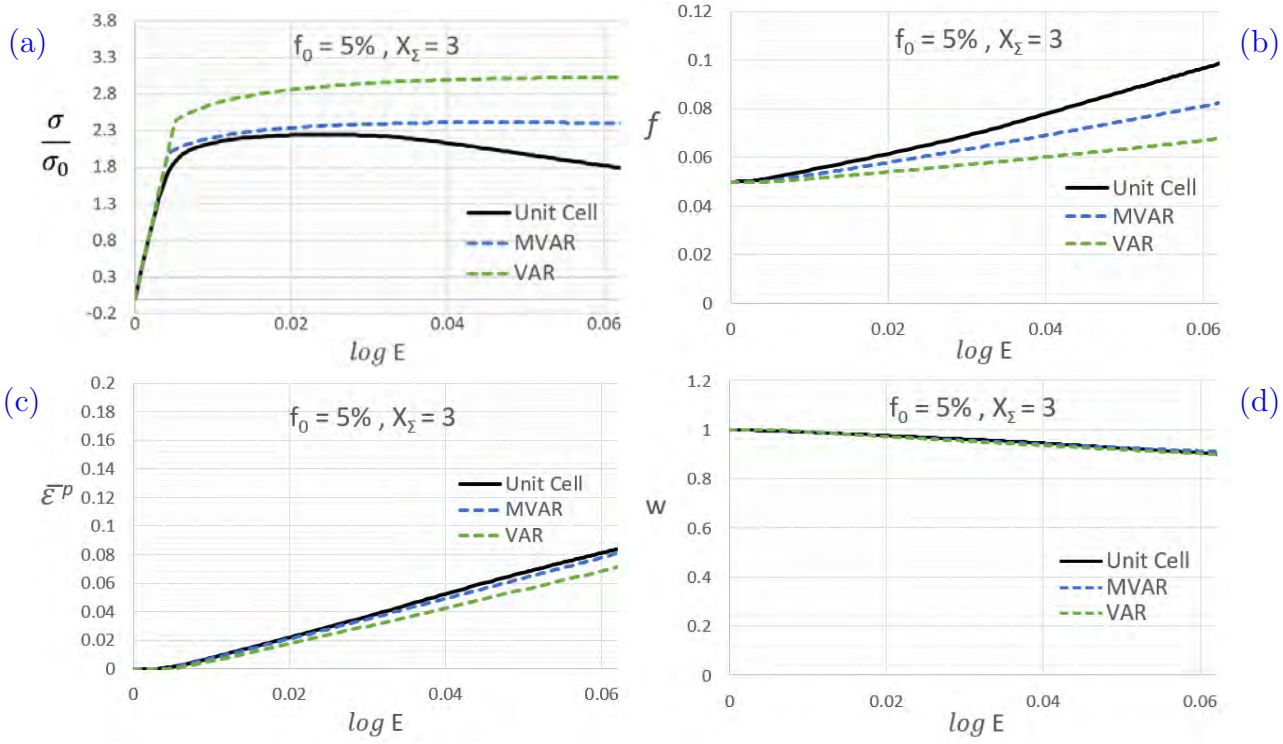

Figure 6.4: (a) $\sigma - logE$, (b) $f - logE$, (c) $\bar{\varepsilon}^p - logE$, and (d) $w - logE$ curves for $\theta = -30°$, $f_0 = 0.05$ and $X_\Sigma = 3$.

6.1.2 $\theta = 0°$ (simple shear)

Figure 6.5 shows the (a) $\sigma - logE$, (b) $f - logE$, (c) $\bar{\varepsilon}^p - logE$, and (d) $w - logE$ curves for $f_0 = 0.01$ and $X_\Sigma = 1/3$. Recall that the label (VAR) stands for the original variational formulae, while (MVAR) stands for the modified variational formulae.

It is evident that, regarding the stress-strain curves both versions of the constitutive model agree with the unit cell calculations. However, the modified variational method seems to overestimate the evolution of the porosity whereas the variational method agrees very well with the unit cell calculations. As far as the equivalent plastic strain there seems to be a perfect match between the two versions of the constitutive model and the unit cell calculations. Regarding the aspect ratio both the original and the modified variational method deviate from the unit cell calculations.

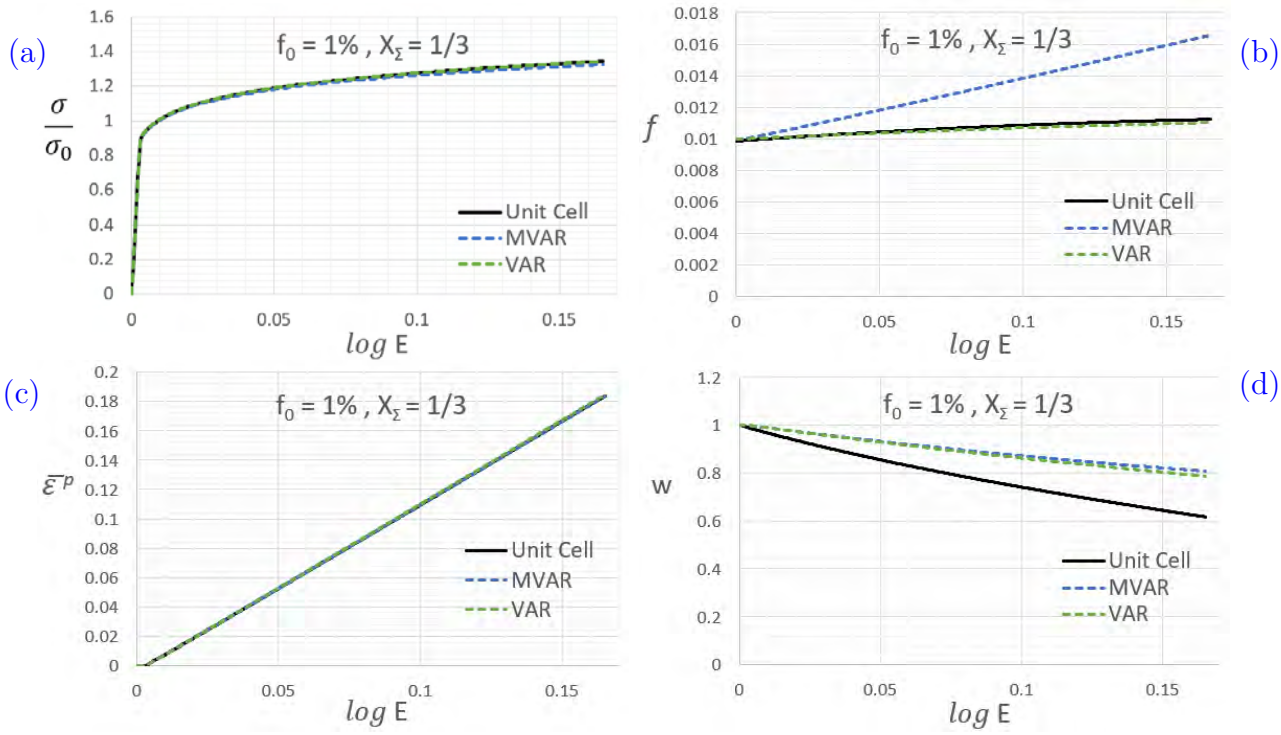

Figure 6.5: (a) $\sigma - logE$, (b) $f - logE$, (c) $\bar{\varepsilon}^p - logE$, and (d) $w - logE$ curves for $\theta = 0°$, $f_0 = 0.01$ and $X_\Sigma = 1/3$.

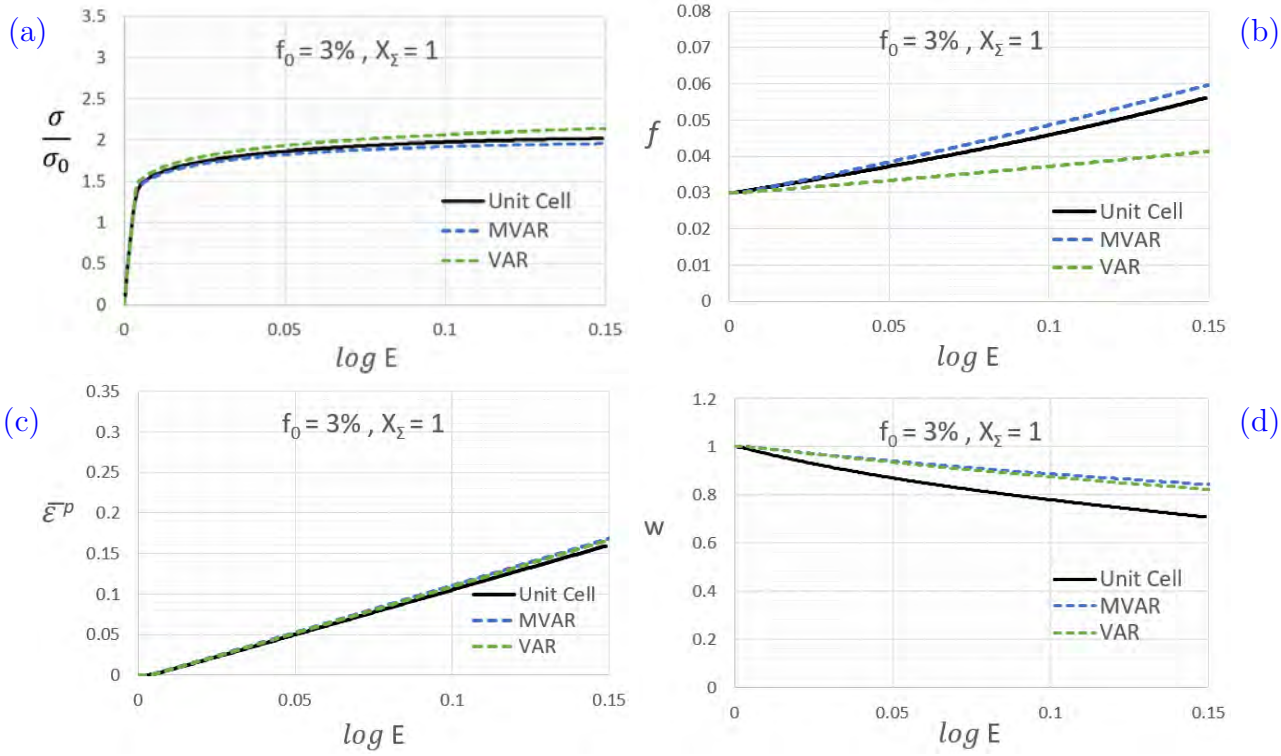

Figure 6.6: (a) $\sigma - logE$, (b) $f - logE$, (c) $\bar{\varepsilon}^p - logE$, and (d) $w - logE$ curves for $\theta = 0°$, $f_0 = 0.03$ and $X_\Sigma = 1$.

Figure 6.6 shows the (a) $\sigma - logE$, (b) $f - logE$, (c) $\bar{\varepsilon}^p - logE$, and (d) $w - logE$ curves for $f_0 = 0.03$ and $X_\Sigma = 1$.

Regarding the stress-strain curves there seems to be a slight mismatch with between the results of the variational method and the other two methods. The porosity graph is quite

interesting because now we observe a very good agreement between the modified variational method and the unit cell calculations. The original variational method seems to underestimate the porosity. As far as the equivalent plastic strain there seems to be a perfect match between the two versions of the constitutive model and the unit cell calculations. Regarding the aspect ratio neither the original nor the modified variational method seems to agree with the unit cell calculations, but the original variational method seems to perform better.

Finally, Fig. 6.7 shows the (a) $\sigma - logE$, (b) $f - logE$, (c) $\bar{\varepsilon}^p - logE$, and (d) $w - logE$ curves for $f_0 = 0.05$ and $X_\Sigma = 3$.

As we can see from the graphs below, the modified variational method predicts more accurately the stress-strain curves, the porosity evolution and the equivalent plastic strain. As far as the aspect ratio both versions of the constitutive model agree with the unit cell calculations.

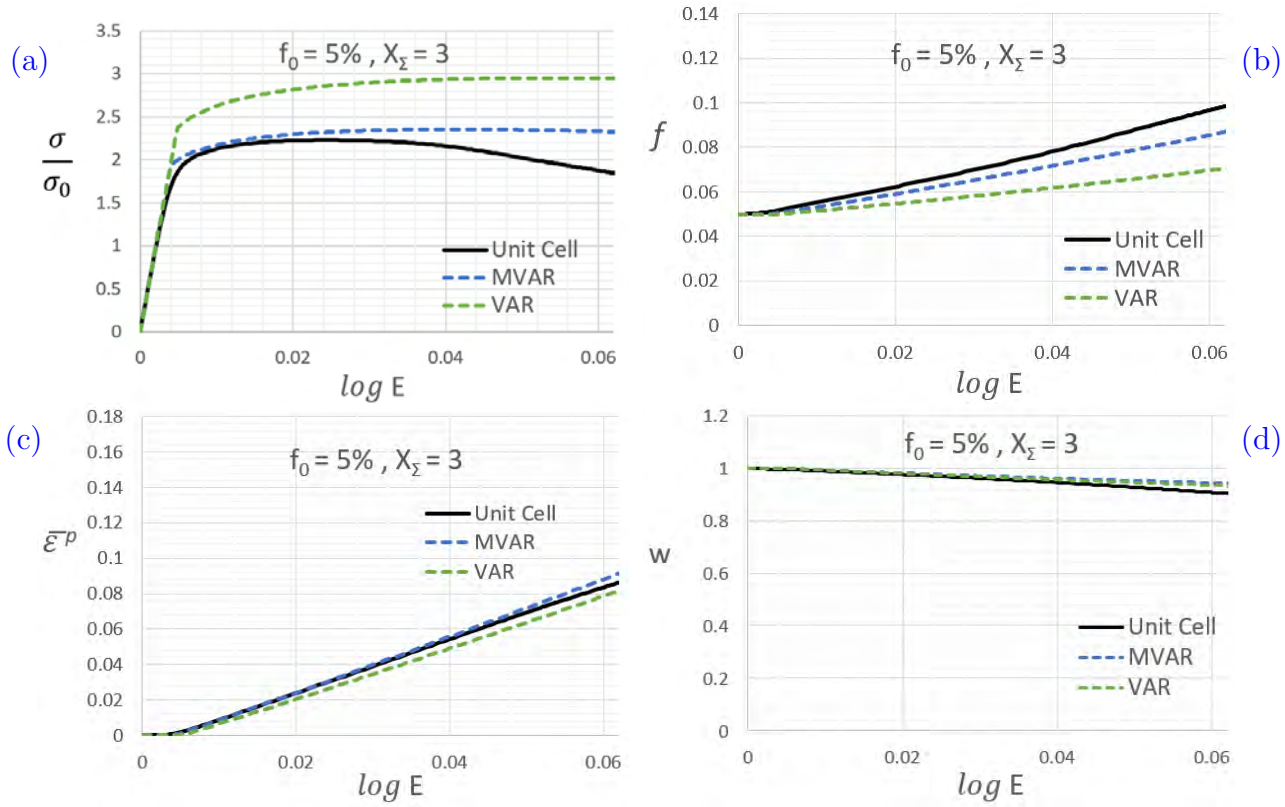

Figure 6.7: (a) $\sigma - logE$, (b) $f - logE$, (c) $\bar{\varepsilon}^p - logE$, and (d) $w - logE$ curves for $\theta = 0°$, $f_0 = 0.05$ and $X_\Sigma = 3$.

6.1.3 Remarks

In this section we examined the accuracy of the MVAR model by studying multiple loading cases with the initial porosity in the range $1\% \leq f_0 \leq 5\%$. The same calculations were conducted by using the MVAR and the VAR model and the predictions of the models were compared to unit cell calculations.

For both $\theta = -30°$ and $\theta = 0°$, it was observed that the MVAR model works quite well under high triaxiality loading conditions but in cases where both the porosity and the triaxiality levels are low the results generated are not accurate enough. In conclusion, an alternate modification needs to be implemented in the model in order to make it perform better for low values of X_Σ and f_0.

6.2 Ductile Fracture

Description of the Problem

Consider the problem of a plane-strain mode-I crack in a homogeneous porous elastoplastic material under small scale yielding conditions. Because of symmetry, only half of the region (*i.e.*, $0 \leq \theta \leq \pi$) is analyzed. The outermost radius of the mesh is $R \cong 1.2 \times 10^3\, b_0$, where b_0 is the initial radius of the semicircular notch at the tip of the blunt crack. Note that near the crack tip the field of displacements and stresses is difficult to be determined, and thus a larger number of elements is used close to that region.

Calculations are carried out for the local and the non-local versions of the model. The ABAQUS elements used are CPE4H for the local model and CPE4HT in the coupled temperature-displacement calculations for the non-local model. Two different meshes were used in the calculations:

- **mesh A**: nodes = 1742 , elements = 1658
- **mesh B**: nodes = 3861 , elements = 3704

Figures 6.8a and 6.8b show the finite element meshes A and B of the model respectively, while figures 6.8c and 6.8d show the meshes A and B in the region near the crack tip.

The purpose of this application is to conduct a convergence study, i.e., to compare the results from the solutions obtained for the two different meshes.

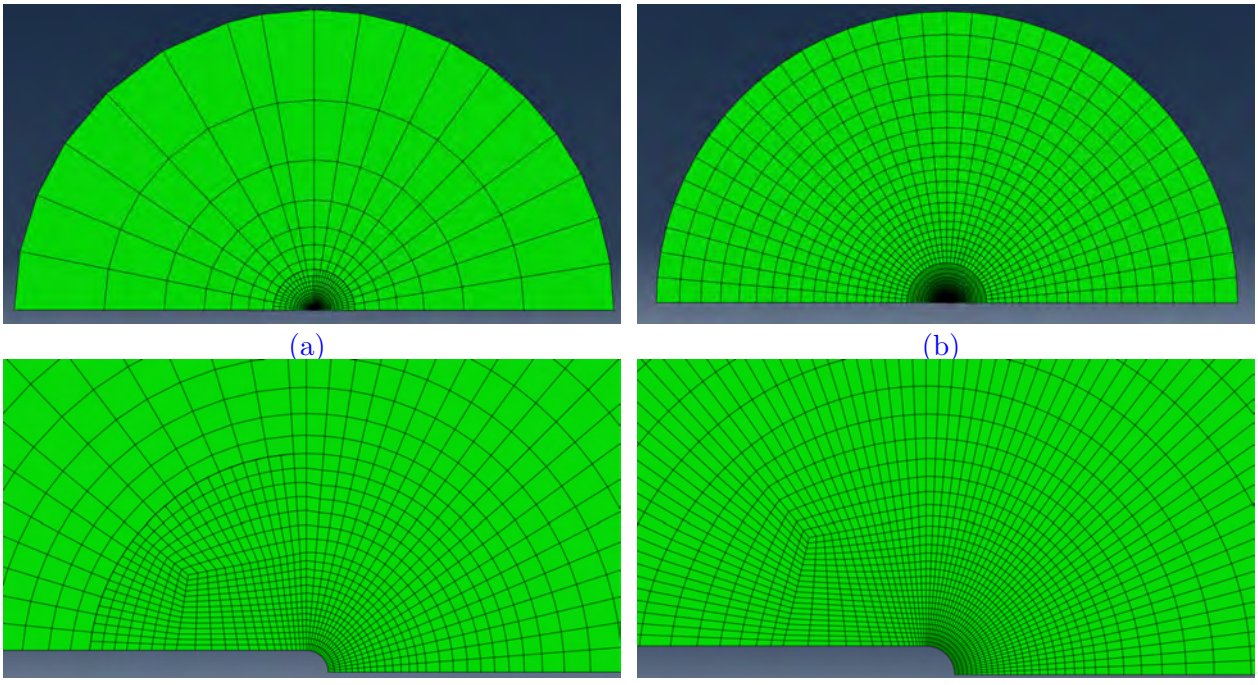

(a) (b) (c) (d)

Figure 6.8: Mesh of the model, (a) mesh A; (b) mesh B; (c) near the crack tip of mesh A; (d) near the crack tip of mesh B

Boundary Conditions

The following displacement boundary conditions are imposed to the nodes along the circumference of the disc (as shown in red in Fig. 6.9)

$$\begin{Bmatrix} u_1 \\ u_2 \end{Bmatrix} = \frac{K_I}{2\,\mu}\sqrt{\frac{r}{2\,\pi}}\,(3 - 4\nu\cos\theta) \begin{Bmatrix} \cos\dfrac{\theta}{2} \\ \sin\dfrac{\theta}{2} \end{Bmatrix}, \tag{6.6}$$

where u_i are the displacement components, K_I is the mode-I intensity factor, x_1 and x_2 are crack-tip Cartesian coordinates with x_1 being the axis of symmetry and x_2 the direction of the mode-I loading, and (r, θ) are crack-tip polar coordinates.

On the lower, right side of the disc the nodes are fixed, while on the lower, left side of the disc traction free boundary conditions are used.

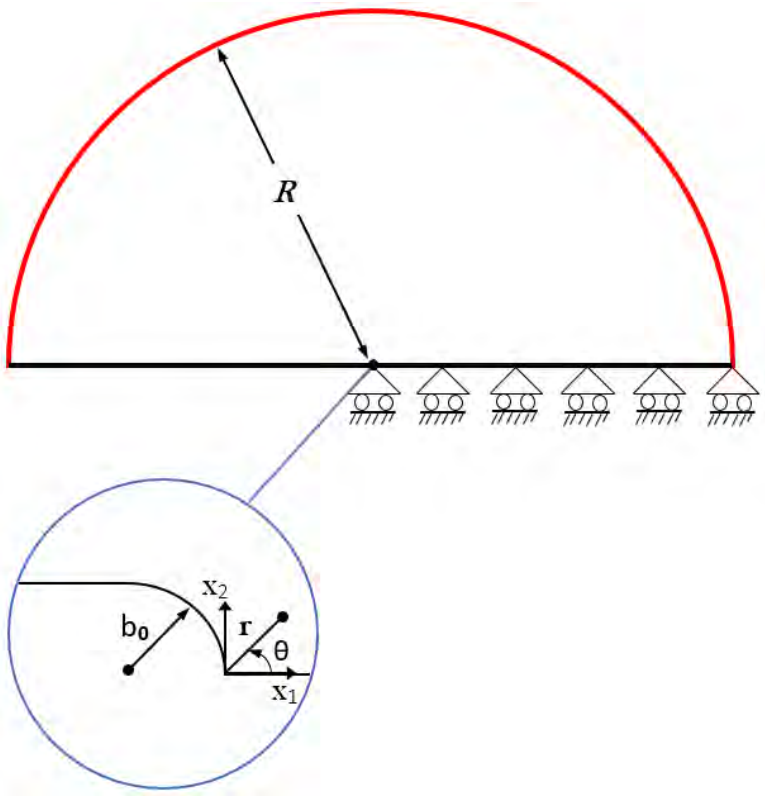

Figure 6.9: Schematic representation of the boundary conditions on the semicircular disc of radius $R \cong 1.2 \times 10^3\, b_0$ with the notch of radius b_0.

Material

The matrix is an elastoplastic material with Young's modulus $E = 300\sigma_0$ and Poisson's ratio $\nu = 0.3$ that hardens according to the relation (4.20). The value $n = 10$ for the hardening exponent of the matrix is used in the calculations. The initial porosity is assumed to be $f_0 = 0.01$. In the non-local model, a material length $\ell = 0.3\, b_0$ is used.

In this set of calculations the nucleation of new voids in the material by cracking or interfacial decohesion of inclusion or precipitate particles is taken into account. The evolution equation of local porosity f_{loc} is now written as

$$\dot{f}_{loc} = \dot{f}_{growth} + \dot{f}_{nucleation}\,, \tag{6.7}$$

where the terms $\dot{f}_{growth}$ and $\dot{f}_{nucleation}$ are determined from the following relations:

$$\dot{f}_{growth} = (1 - f) D^p_{kk}\,, \tag{6.8}$$

and

$$\dot{f}_{nucleation} = \mathcal{A}\, \dot{\bar{\varepsilon}}^p\,, \tag{6.9}$$

where the $\mathcal{A}$-term accounts for the aforementioned void nucleation. The parameter $\mathcal{A}$ is chosen so that the nucleation strain follows a normal distribution with mean value ε_N and

standard deviation s_N [5]:

$$\mathcal{A}(\bar{\varepsilon}^p) = \frac{f_N}{s_N\sqrt{2\pi}} \exp\left[-\frac{1}{2}\left(\frac{\bar{\varepsilon}^p - \varepsilon_N}{s_N}\right)^2\right], \tag{6.10}$$

where f_N is the volume fraction of void nucleating particles. The values $f_N = 0.04$, $\varepsilon_N = 0.4$ and $s_N = 0.1$ are used in the computations. Eq. (5.25) is now replaced by

$$f_{loc}|_{n+1}(\Delta\mathbf{E}^p) = f_{loc}|_n + (1 - f_{n+1})\Delta E^p_{kk} + \mathcal{A}(\bar{\varepsilon}^p_n)\,\Delta\bar{\varepsilon}^p(\Delta\mathbf{E}^p)\,, \tag{6.11}$$

where $\Delta\bar{\varepsilon}^p(\Delta\mathbf{E}^p)$ is determined from (5.24).

Results

Figures 6.10-6.13 show the variation of the opening stress σ_{22}, the hydrostatic stress $p = \sigma_{kk}/3$, the porosity f, and the equivalent plastic strain $\bar{\varepsilon}^p$, ahead of the crack tip at different load levels $K1 = K_I/(\sigma_0\sqrt{b_0})$ for both the local and the non-local anisotropic model. Note that x is the distance of a material point in the undeformed configuration ahead from the crack tip.

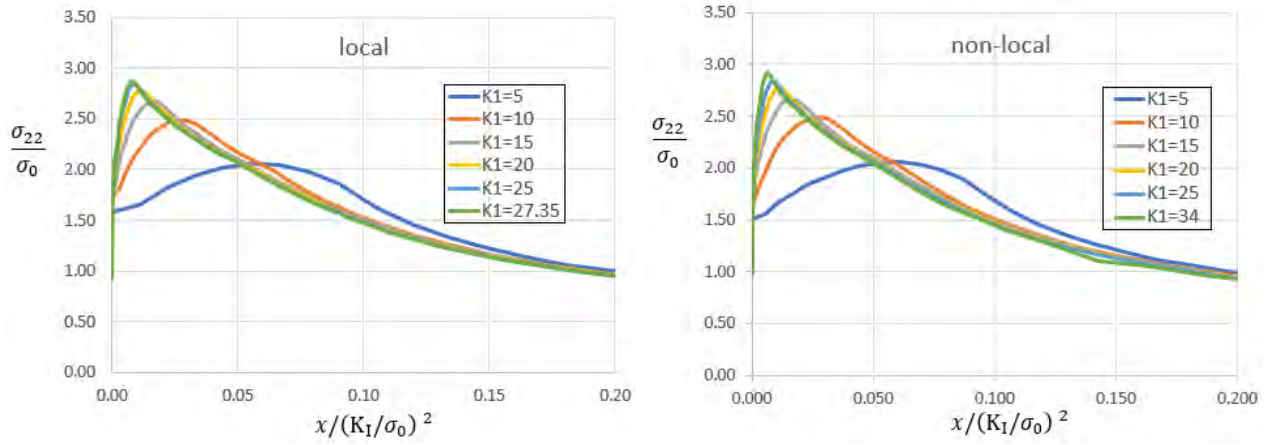

Figure 6.10: Normal stress distribution ahead of the crack tip at different load levels.

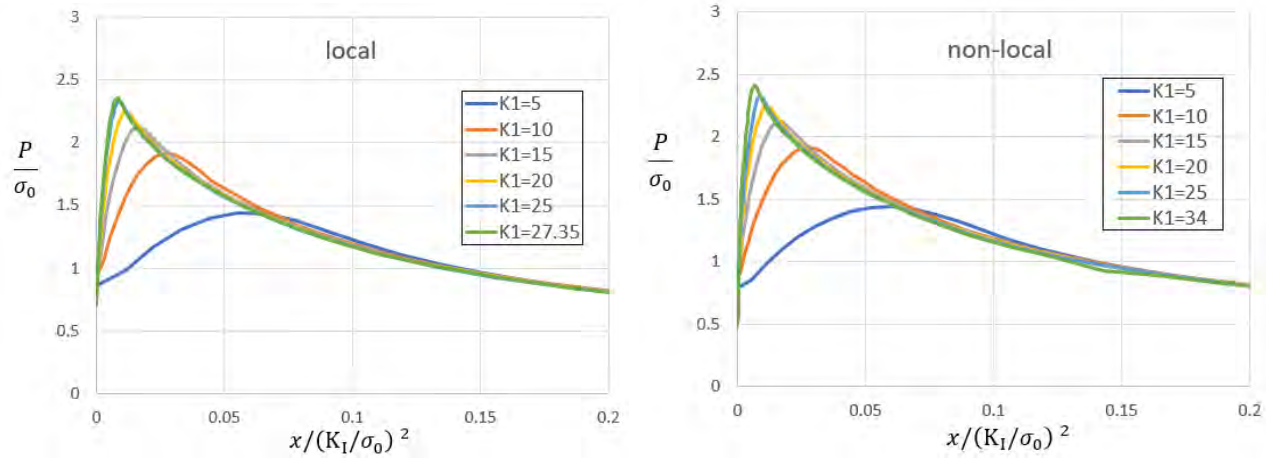

Figure 6.11: Distribution of hydrostatic stress ahead of the crack tip at different load levels.

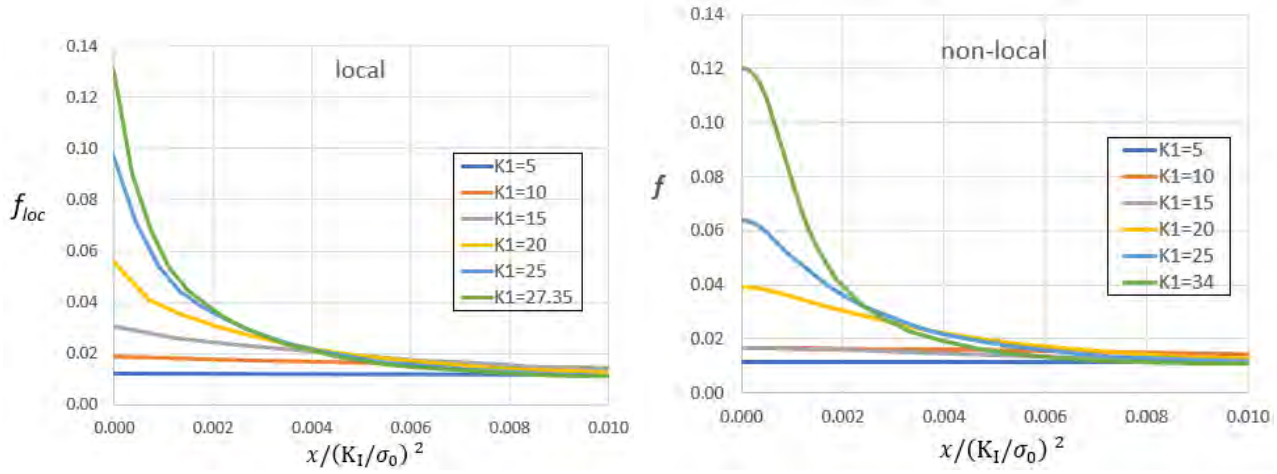

Figure 6.12: Porosity distribution ahead of the crack tip at different load levels.

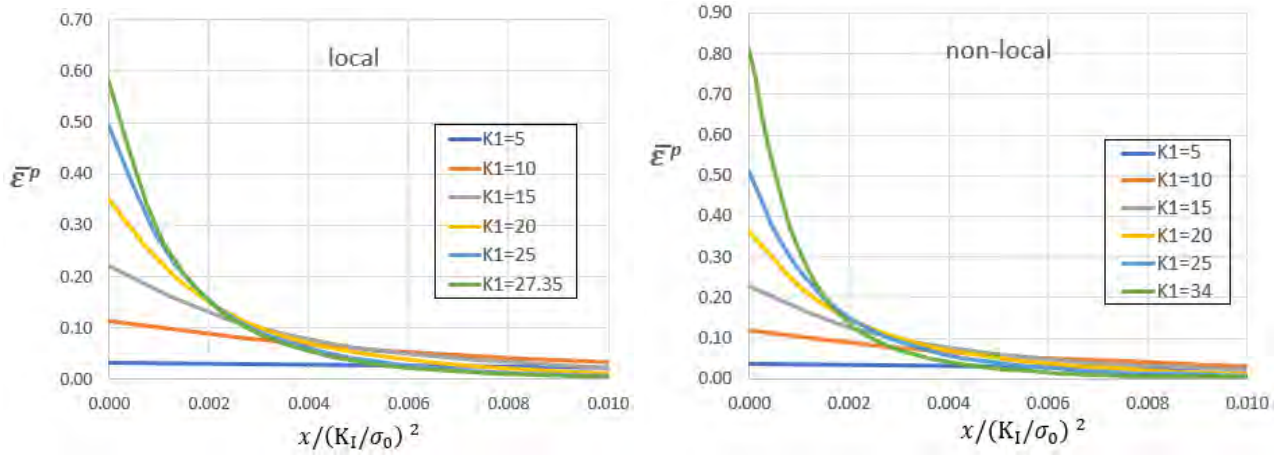

Figure 6.13: Distribution of the equivalent plastic strain ahead of the crack tip at different load levels.

Remarks

Figures 6.12 and 6.13 show that the porosity f and the equivalent plastic strain $\bar{\varepsilon}^p$ in the material take a maximum value at the root of the blunt crack and become progressively smaller ahead of the crack tip. On the other hand figures 6.10 and 6.11 show that the opening stress σ_{22} and the hydrostatic pressure p increase until they reach a maximum a little further from the crack tip and then progressively decrease again. This maximum which occurs at some distance of the crack tip (and not at the crack tip) happens since the blunt crack tip is traction-free, i.e. it has to do with the boundary conditions of the problem. Lastly, the results for the calculated fields are the same for both meshes (A and B) i.e., the numerical solution of the non-local formulation is mesh independent.

6.3 Necking and Failure of a Round Tensile Bar

Description of the Problem

The non-local anisotropic model for porous metals, which was presented in Chapter 4 is used to study the problem of necking and failure of a cylinder with circular cross-section subjected to uniaxial tension. The specimen has dimensions $L_0/R_0 = 2$, where $2\,L_0$ is its initial length in

the direction of the applied loads and R_0 is its initial radius. A cylindrical reference coordinate system (r, θ, z) is used for the analysis of the round tensile bar, with its origin placed in the centre of the bar ((i.e., $r = 0$ and $z = 0$)). Due to the symmetry of the problem only one quarter of the bar is considered in the analysis. To promote necking a small initial geometric imperfection ΔR of the form

$$\Delta R = -\xi R_0 \cos \frac{\pi z}{L_0}\,, \tag{6.12}$$

is introduced, such that the initial radius of the cylindrical bar varies with the relation

$$R(z) = R_0 - \xi R_0 \cos \frac{\pi z}{L_0}\,. \tag{6.13}$$

Boundary conditions

Regarding the boundary conditions of the problem, the bottom face of the bar at $z = 0$ is held fixed (i.e., $\mathbf{u}(r, \theta, z = 0) = \mathbf{0}$), while the upper face is subjected to a prescribed uniform displacement $\hat{u}$ in the axial direction of z (i.e., $u_z(r, \theta, z = L_0) = \hat{u}$). The lateral faces of the cylindrical bar are kept traction free. However, since one quarter of the bar is considered in the analysis then the specimen has the boundary conditions as shown in Fig. 6.14.

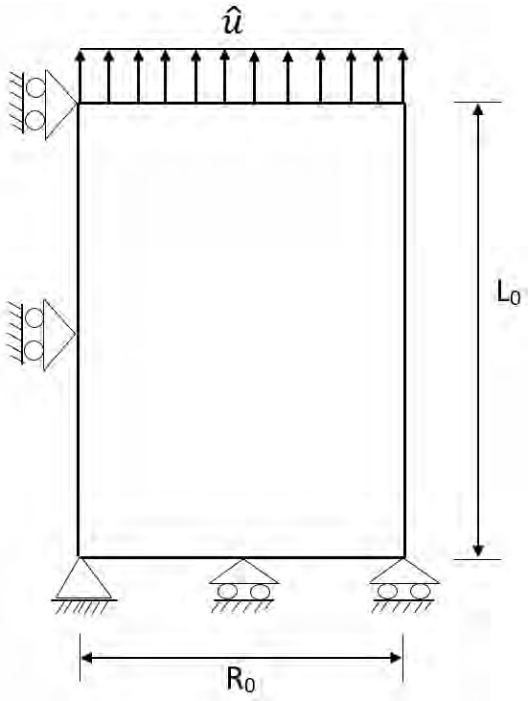

Figure 6.14: Schematic representation of the boundary conditions imposed.

Material

The material matrix is assumed to behave elastoplastically and harden with respect to the relation (4.20). A void nucleation model is assumed as described in Eqs. (6.7)-(6.11). The initial porosity of the material is chosen to be $f_0 = 0.04$ and the value of the intrinsic material length $\ell = 0.01\, R_0$. The material parameters are summarized in table 6.1.

E	ν	n	f_N	ε_n	s_N
$396.22\,\sigma_0$	0.3	12	0.04	0.4	0.1

Table 6.1: Material properties for the problem of necking

Material failure

To account for material failure at a material point, [27] replaced the porosity f in the Gurson yield condition with a "modified porosity" $f^*(f)$ defined as

$$f^*(f) = \begin{cases} f & \text{for} \quad f \le f_c\,, \\ f_c + \dfrac{1-f_c}{f_f - f_c}\,(f - f_c) & \text{for} \quad f > f_c\,, \end{cases} \tag{6.14}$$

where f_c and f_f are material parameters determined from experimental data involving specimen failure. In the present formulation, the *non-local* porosity f is replaced by f^* in the yield function (4.19) and the flow rule (4.21). Calculations are carried out with the modified non-local version of the anisotropic model. The values $f_c = 0.10$ and $f_f = 0.15$ are used in the calculations.

Numerical Implementation

ABAQUS/Standard has convergence difficulties with the element deletion, so ABAQUS/-Explicit together with user subroutines VUMAT and VDFLUX [18] is used. Four-node bilinear displacement and temperature, reduced integration with hourglass control (CAX4RT) elements are used and a mesh of 50x200 (where the first and second numbers denote the number of elements in the direction of the lengths R_0 and L_0 respectively). The material is assumed to fail locally when the non-local porosity f^* reaches the value of 0.99 (instead of exactly 1). When the value $f^* = 0.99$ is reached at a Gauss point, the material is assumed to lose its load carrying capacity and the element is removed.

Results

A plot for the normalized load $\hat{F} = F/(A\,\sigma_0)$, where $A = \pi R_0^2$, over the normalized displacement $\hat{u}/L_0$ is shown in Fig. 6.15.

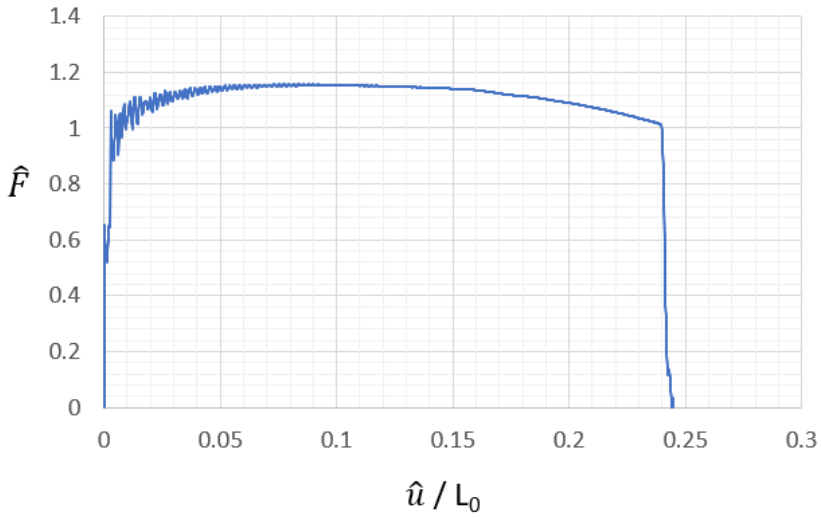

Figure 6.15: The load-displacement diagram of the axisymmetric analysis.

Figures 6.16 and 6.17 show contours of the equivalent plastic strain $\bar{\varepsilon}^p$ and the non local porosity f as the crack at the center of the specimen grows leading progressively to failure.

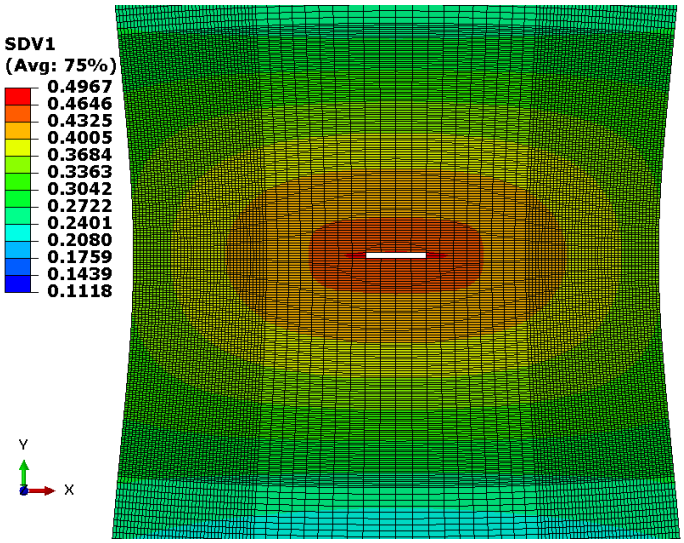

(a) Contour plot of $\bar{\varepsilon}^p$ for $\hat{u}/L_0 = 0.238$.

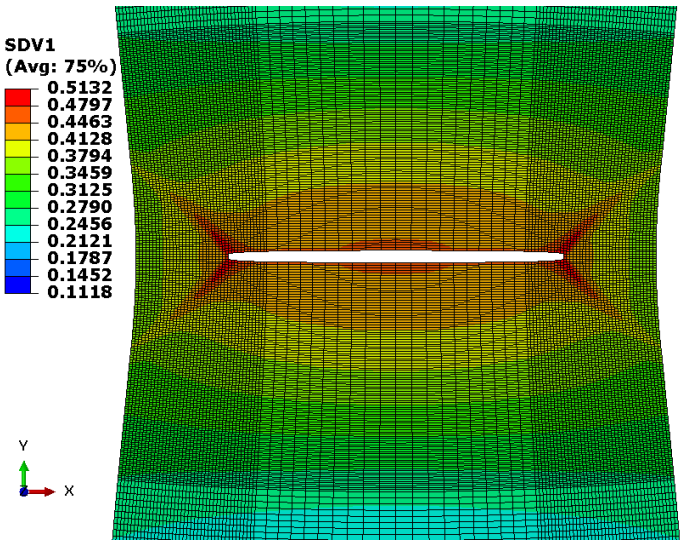

(b) Contour plot of $\bar{\varepsilon}^p$ for $\hat{u}/L_0 = 0.241$.

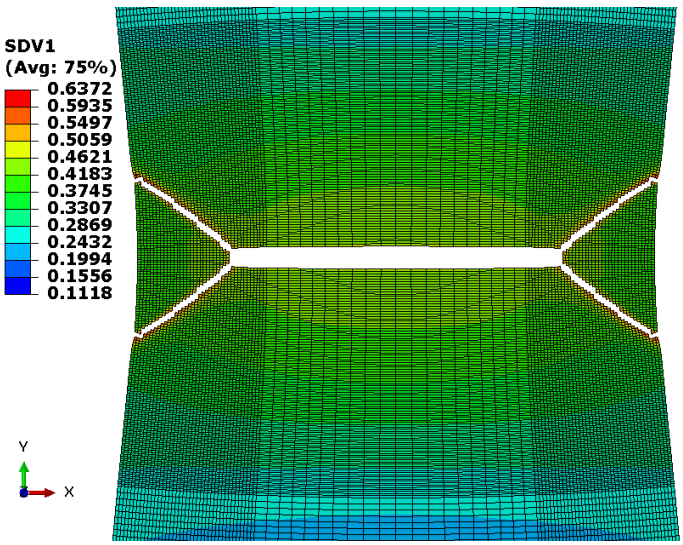

(c) Contour plot of $\bar{\varepsilon}^p$ for $\hat{u}/L_0 = 0.248$.

Figure 6.16: Contour plots of $\bar{\varepsilon}^p$ as the specimen leads progressively to failure. Whole specimen is shown.

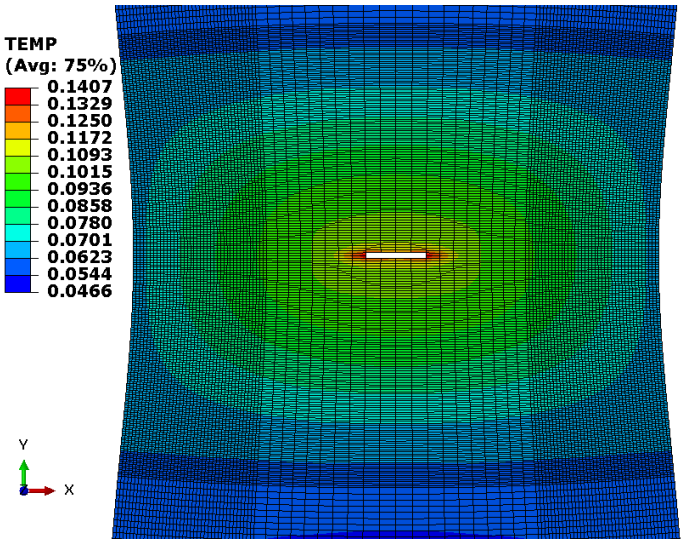

(a) Contour plot of $\bar{\varepsilon}^p$ for $\hat{u}/L_0 = 0.238$.

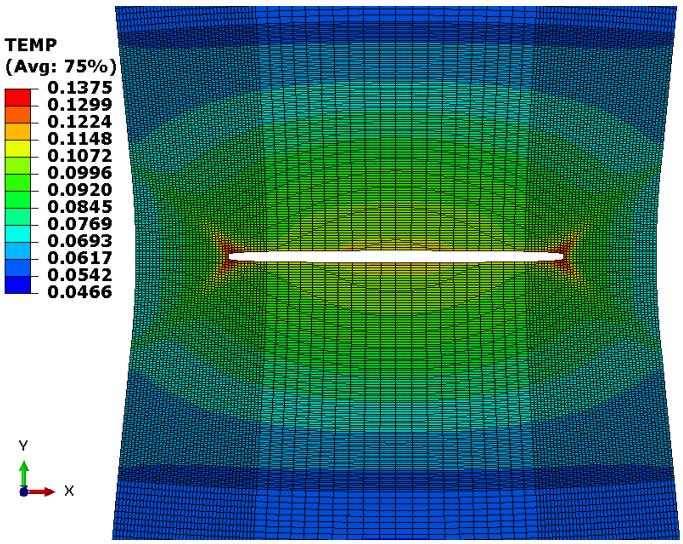

(b) Contour plot of f for $\hat{u}/L_0 = 0.241$.

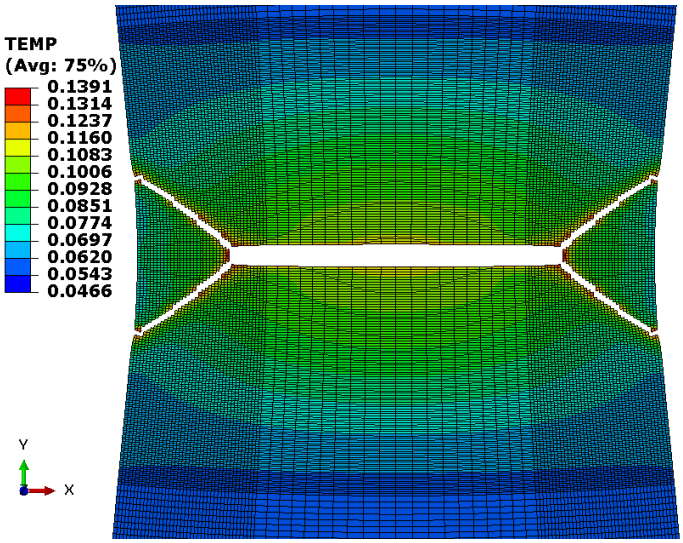

(c) Contour plot of f for $\hat{u}/L_0 = 0.248$.

Figure 6.17: Contour plots of f as the specimen leads progressively to failure. Whole specimen is shown.

6.4 Localization in Plane-Strain Tension

Description of the Problem

Consider the quasi-static problem of plastic flow localization in a tension specimen under plane strain conditions. It is known in the literature that, at large strains all the deformation progressively localizes into narrow shears bands. Due to this phenomenon when in the softening region, the governing equations of the problem are said to loose "ellipticity", which means that even after the refinement of the mesh, the numerical solution of the problem does not converge at any value. To overcome this difficulties, additional terms are introduced to restore the so-called "ellipticity", increasing the order of the governing equations. The non-local model presented in Chapter 4 is used in this application.

Boundary conditions

Due to symmetry one quarter of the specimen is considered in the analysis. Fig. 6.18 shows a schematic representation of one quarter of the specimen with the imposed boundary conditions. The right side of the specimen is traction free and the upper side is subjected to a prescribed displacement $\hat{u}$. The dimensions of the specimen are $h = 0.75w$, where h is the height of the specimen in the direction of the applied loads, and w is the width of the specimen.

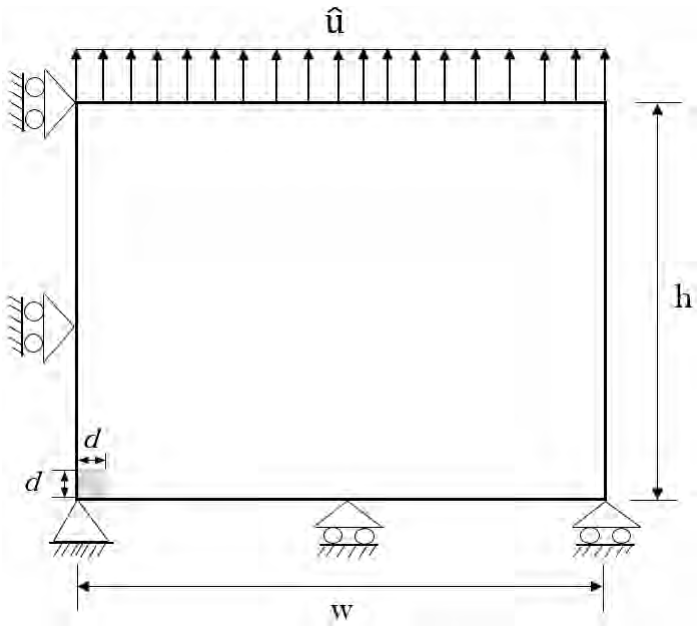

Figure 6.18: Schematic representation of one quarter of the rectangular specimen with the boundary conditions.

Numerical Implementation

To trigger the initiation of non-uniform deformation in the specimen, an imperfection in the material properties is introduced over as small square region of side $d = 0.05w$ at the center of the specimen, as shown in Fig. 6.18. In particular, the stress σ_0 in (4.20) is replaced by $0.99\sigma_0$ in the imperfect region.

The finite elements used are 4-node plane strain CPE4RT coupled temperature-displacement elements in ABAQUS/Explicit with reduced integration and hourglass control. The following three meshes are used in the analysis:

- **mesh A**: 20x20, elements = 400

- **mesh B**: 40x40, elements = 1600
- **mesh C**: 80x80, elements = 6400 .

Material

Again, the material matrix is assumed to behave elastoplastically and harden with respect to the relation (4.20). A void nucleation model is assumed as described in Eqs. (6.7)-(6.11). The initial porosity is selected to be $f_0 = 0.04$ and the non-local analysis is carried out for an intrinsic material length $\ell = 0.05w$. In addition, the the material parameters are summarized in table 6.2.

E	ν	n	f_N	ε_n	s_N	f_c	f_f
$396.22\,\sigma_0$	0.3	12	0.04	0.4	0.1	0.1	0.15

Table 6.2: Material properties for the problem of localization in plane strain tension.

The material, as in the previous example, is assumed to fail locally when the non-local porosity f^* reaches the value of 0.99. When the value $f^* = 0.99$ is reached at a Gauss point, the material in the element is assumed to lose its load carrying capacity, and the element is removed.

Results

Figure 6.19 shows the plot of the normalized load $\hat{F} = F/(\sigma_0 A)$ (where $A = wt$, w is the width and $t = 1\,\text{mm}$ the thickness of the specimen) to the normalized applied displacement $\hat{u}/h$ for the three different meshes 20×20, 40×40, and 80×80. It is readily seen that the non-local solutions converge to the exact one as the mesh is refined.

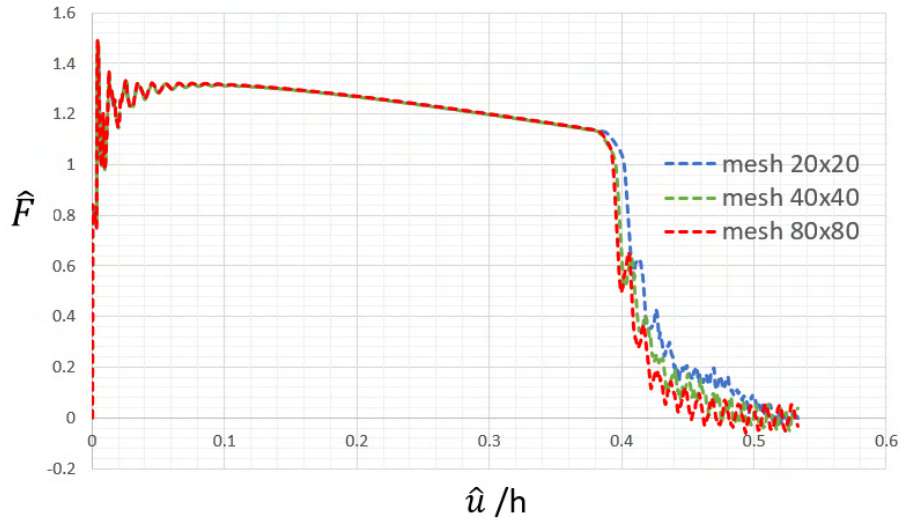

Figure 6.19: Load-displacement curves in plane strain tension for the three different meshes: 20×20, 40×40, and 80×80.

Figure 6.20 shows the contour plot of $\hat{\varepsilon}^p$ at a prescribed displacement $\hat{u}/h = 0.44$ for the three different mesh sizes. A further note is that the shear band seems to form at an angle of 40° from the axis in the direction of w.

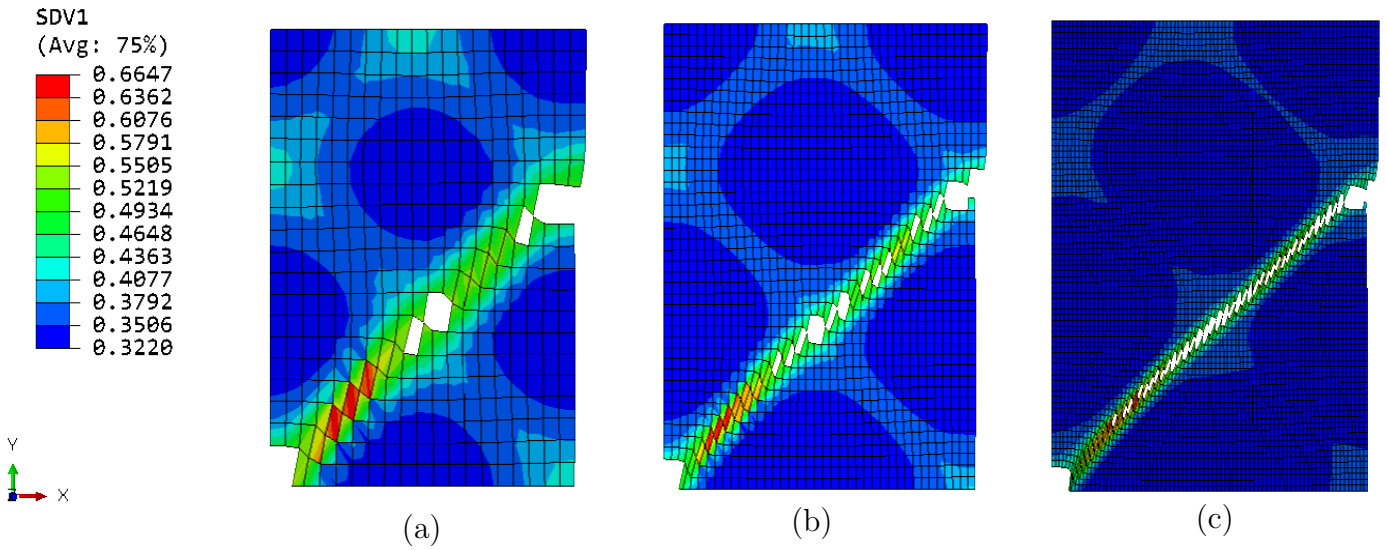

(a) (b) (c)

Figure 6.20: Contour plots of $\bar{\varepsilon}^p$ at $\hat{u}/h = 0.44$ for the three different meshes; (a) mesh 20x20; (b) mesh 40x40 (c) mesh 80x80;

Appendices

Appendix A - Expressions for the Eshelby Tensors

Willis [28, 30] has shown that the Eshelby tensor $\mathbf{S}$ and $\mathbf{\Pi}$ can be written in the form

$$\mathbf{S} = \frac{1}{4\pi w_1 w_2}\int_{|\xi|=1} \mathbf{H}(\boldsymbol{\xi}) : \boldsymbol{\mathcal{L}}\, \frac{dS(\xi)}{|\mathbf{Z}^{-1}\cdot\boldsymbol{\xi}|^3}, \quad \mathbf{\Pi} = \frac{1}{4\pi w_1 w_2}\int_{|\xi|=1} \hat{\mathbf{H}}(\boldsymbol{\xi}) : \boldsymbol{\mathcal{L}}\, \frac{dS(\xi)}{|\mathbf{Z}^{-1}\cdot\boldsymbol{\xi}|^3} \tag{A.1}$$

and the tensors $\mathbf{P} = \mathbf{S} : \boldsymbol{\mathcal{M}}$ and $\mathbf{R} = \mathbf{\Pi} : \boldsymbol{\mathcal{M}}$, and by noting that $\boldsymbol{\mathcal{L}} : \boldsymbol{\mathcal{M}} = \boldsymbol{\mathcal{M}} : \boldsymbol{\mathcal{L}} = \mathbf{I}$, then

$$\mathbf{P} = \frac{1}{4\pi w_1 w_2}\int_{|\xi|=1} \mathbf{H}(\boldsymbol{\xi})\, \frac{dS(\xi)}{|\mathbf{Z}^{-1}\cdot\boldsymbol{\xi}|^3}, \quad \mathbf{R} = \frac{1}{4\pi w_1 w_2}\int_{|\xi|=1} \hat{\mathbf{H}}(\xi)\, \frac{dS(\xi)}{|\mathbf{Z}^{-1}\cdot\boldsymbol{\xi}|^3} \tag{A.2}$$

where

$$H_{ijkl}(\boldsymbol{\xi}) = \left[\mathcal{L}_2^{-1}(\boldsymbol{\xi})\right]_{ik}\xi_j\xi_l|_{(ij)(kl)}, \quad \hat{H}_{ijkl}(\boldsymbol{\xi}) = \left[\mathcal{L}_2^{-1}(\boldsymbol{\xi})\right]_{ik}\xi_j\xi_l|_{[ij](kl)}, \tag{A.3}$$

$$|\mathcal{L}_2(\boldsymbol{\xi})|_{ik} = \mathcal{L}_{ijkl}\xi_j\xi_l, \quad \mathbf{Z} = w_1\mathbf{n}^{(1)}\mathbf{n}^{(1)} + w_2\mathbf{n}^{(2)}\mathbf{n}^{(2)} + \mathbf{n}^{(3)}\mathbf{n}^{(3)} \tag{A.4}$$

and the notations

$$A_{(ij)(kl)} = \frac{1}{4}(A_{ijkl} + A_{ijlk} + A_{jikl} + A_{jilk}), \quad A_{[ij](kl)} = \frac{1}{4}(A_{ijkl} + A_{ijlk} - A_{jikl} - A_{jilk}) \tag{A.5}$$

are used. Note that in (A.1) and (A.2) the integrals are evaluated along the surface of a unit sphere and $\boldsymbol{\xi}$ is the position vector on that surface. Recall that $w_1 = a_3/a_1$ and $w_2 = a_3/a_2$ are the aspect ratios of the local ellipsoid with lengths $(2a_1, 2a_2, 2a_3)$.

For isotropic metals $\mathbf{L} = 2\mu\mathbf{K} + 3k\mathbf{J}$, so that

$$\boldsymbol{\mathcal{L}}_2(\boldsymbol{\xi}) = \mu\left(|\boldsymbol{\xi}|^2\boldsymbol{\delta} + \frac{1}{1-2\nu}\boldsymbol{\xi}\boldsymbol{\xi}\right) \quad \text{and} \quad \boldsymbol{\mathcal{L}}_2^{(-1)}(\boldsymbol{\xi}) = \frac{1}{\mu|\boldsymbol{\xi}|^4}\left[|\boldsymbol{\xi}|^2\boldsymbol{\delta} - \frac{1}{2\,(1-\nu)}\boldsymbol{\xi}\boldsymbol{\xi}\right]. \tag{A.6}$$

Using (A.2) and (A.6), one can obtain after some algebra that

$$\begin{aligned}\left(\mathbf{H}(\boldsymbol{\xi}) : \boldsymbol{\mathcal{L}}\right)_{ijkl}(\boldsymbol{\xi},\nu) =& \frac{1}{2|\boldsymbol{\xi}|^2}\left(\delta_{ik}\xi_j\xi_l + \delta_{jk}\xi_i\xi_l + \delta_{il}\xi_j\xi_k + \delta_{jl}\xi_i\xi_k\right) \\ &- \frac{1}{|\boldsymbol{\xi}|^4}\frac{1}{1-\nu}\xi_i\xi_j\xi_k\xi_l + \frac{1}{|\boldsymbol{\xi}|^2}\frac{\nu}{1-\nu}\xi_i\xi_j\delta_{kl}\end{aligned} \tag{A.7}$$

and

$$\left(\hat{\mathbf{H}}(\boldsymbol{\xi}) : \boldsymbol{\mathcal{L}}\right)_{ijkl}(\boldsymbol{\xi}) = \frac{1}{2|\boldsymbol{\xi}|^2}\left(\delta_{ik}\xi_j\xi_l - \delta_{jk}\xi_i\xi_l + \delta_{il}\xi_j\xi_k - \delta_{jl}\xi_i\xi_k\right) \tag{A.8}$$

Kailasam et al. [14] have shown that $\mathbf{Q}$ can be written in the form

$$\frac{1}{\mu}\mathbf{Q} = \frac{1}{4\pi w_1 w_2}\int_{|\boldsymbol{\xi}|} \mathbf{E}(\boldsymbol{\xi})\, \frac{dS(\boldsymbol{\xi})}{|\mathbf{Z}^{-1}\cdot\boldsymbol{\xi}|^3}, \tag{A.9}$$

where

$$E_{ijkl}(\boldsymbol{\xi},\nu) = \delta_{ik}\delta_{jl} + \delta_{il}\delta_{jk} - \frac{1}{|\boldsymbol{\xi}|^2}\left(\delta_{ik}\xi_j\xi_l + \delta_{il}\xi_j\xi_k + \delta_{jk}\xi_i\xi_l + \delta_{jl}\xi_i\xi_k\right) + \frac{2\nu}{1-\nu}\left[\delta_{ij}\delta_{kl} - \frac{1}{|\boldsymbol{\xi}|^2}\left(\delta_{ij}\xi_k\xi_l + \delta_{kl}\xi_i\xi_j\right)\right] + \frac{2}{|\boldsymbol{\xi}|^4}\frac{1}{1-\nu}\xi_i\xi_j\xi_k\xi_l. \tag{A.10}$$

Making use of (A.9) and (A.10) one can derive analytic expressions for the corresponding components Q'_{ijkl} of $\mathbf{Q}$. Let $\alpha_1 = \alpha_3/w_1$, $\alpha_2 = \alpha_3/w_2$ with $\alpha_3 = 1$, and arrange the numbering so that $\alpha_1 \geq \alpha_2 \geq \alpha_3$. In particular, it can be shown that the nonzero components Q'_{ijkl} of $\mathbf{Q}$ relative to the local coordinate system defined by the $\mathbf{n}^{(i)}$'s, and for $a \equiv \alpha_1 > b \equiv \alpha_2 \equiv> c \equiv \alpha_3$ are

$$Q'_{1111} = \frac{\mu}{4\pi(1-\nu)}\left(8\pi - I_a - 3a^2 I_{aa}\right), \tag{A.11}$$

$$Q'_{1122} = \frac{\mu}{8\pi(1-\nu)}\left[16\pi\nu + (1-4\nu)(I_a + I_b) - 3\left(a^2+b^2\right)I_{ab}\right], \tag{A.12}$$

$$Q'_{1212} = \frac{\mu}{8\pi(1-\nu)}\left[8\pi + (1-2\nu)(I_a + I_b) - 3\left(a^2+b^2\right)I_{ab}\right], \tag{A.13}$$

where

$$I_a = \frac{4\pi abc}{(a^2-b^2)\sqrt{a^2-c^2}}\left[F(\theta,k) - E(\theta,k)\right], \tag{A.14}$$

$$I_c = \frac{4\pi abc}{(b^2-c^2)\sqrt{a^2-c^2}}\left[\frac{b\sqrt{a^2-c^2}}{ac} - E(\theta,k)\right], \tag{A.15}$$

$$I_b = 4\pi - I_a - I_c, \tag{A.16}$$

$$I_{ab} = \frac{I_b - I_a}{3(a^2-b^2)}, \quad I_{ac} = \frac{I_c - I_a}{3(a^2-c^2)}, \quad I_{aa} = \frac{4\pi}{3a^2} - I_{ab} - I_{ac}, \tag{A.17}$$

$$\theta = \sin^{-1}\sqrt{1 - \frac{a^2}{c^2}}, \quad k = \sqrt{\frac{a^2-b^2}{a^2-c^2}} \tag{A.18}$$

and

$$F(\theta,k) = \int_0^\theta \frac{d\phi}{\sqrt{1-k^2\sin^2\phi}}, \quad E(\theta,k) = \int_0^\theta \sqrt{1-k^2\sin^2\phi}\, d\phi \tag{A.19}$$

are the elliptic integrals of left and second kinds. All other nonzero components Q'_{ijkl} are found by simultaneous cyclic interchange of $(1,2,3)$ and (a,b,c). In the special cases where $a = b > c$ or $a > b = c$, the quantities $I_a, I_b, I_c, I_{ab}, I_{ac}$ and I_{aa} take the values given on page 385 of Eshelby's original article [10]. The special case of isotropy $a = b = c$ is discussed in page 3801 in [3].

Appendix B[1]

The Proof of the Kinematic Relation: $\omega_{ij} = W_{ij} - \frac{\lambda_i^2+\lambda_j^2}{\lambda_i^2-\lambda_j^2}D_{ij}$

Recall from chapter 2 that the deformation gradient $\mathbf{F}$ can be written in spectral form as

$$\mathbf{F} = \sum_{i=1}^{3} \lambda_i\, \mathbf{n}_i \otimes \mathbf{N}_i, \tag{B.1}$$

[1]This proof is found in [16].

and by differentiating

$$\dot{\mathbf{F}} = \sum_{i=1}^{3} \left[\dot{\lambda}_i \, \mathbf{n}_i \otimes \mathbf{N}_i + \lambda_i \left(\dot{\mathbf{n}}_i \otimes \mathbf{N}_i + \mathbf{n}_i \otimes \dot{\mathbf{N}}_i \right) \right] . \tag{B.2}$$

Therefore, in view of (B.2) an expression must be found for the derivatives of the triads $\mathbf{n}_i$ and $\mathbf{N}_i$. If $\mathbf{e}_i$ $(i = 1, 2, 3)$ are fixed reference unit vectors, the unit vectors $\mathbf{N}_i$ of the principal directions of $\mathbf{U}$ can be expressed as (see Fig. B.1)

$$\mathbf{N}_i = \mathbf{R}_0 \cdot \mathbf{e}_i \, , \tag{B.3}$$

where $\mathbf{R}_0$ is the rotation tensor that carries the orthogonal triad $\{\mathbf{e}_i\}$ into the Lagrangian triad $\{\mathbf{N}_i\}$. Defining the spin of the Lagrangian triad by

$$\boldsymbol{\Omega}_0 = \dot{\mathbf{R}}_0 \cdot \mathbf{R}_0^{-1} , \tag{B.4}$$

it follows that

$$\dot{\mathbf{N}}_i = \dot{\mathbf{R}}_0 \cdot \mathbf{e}_i = \boldsymbol{\Omega}_0 \cdot \mathbf{N}_i = -\mathbf{N}_i \cdot \boldsymbol{\Omega}_0 \, . \tag{B.5}$$

Note that on the axes of the Lagrangian triad $\mathbf{N}_i$ the spin tensor $\boldsymbol{\Omega}_0$ is expressed as

$$\boldsymbol{\Omega}_0 = \sum_{i \neq j} \Omega_{ij}^0 \, \mathbf{N}_i \otimes \mathbf{N}_j \, . \tag{B.6}$$

Now the principal directions $\mathbf{n}_i$ of the left stretch tensor $\mathbf{V}$, are related to the principal directions $\mathbf{N}_i$ of the right stretch tensor $\mathbf{U}$ by

$$\mathbf{n}_i = \mathbf{R} \cdot \mathbf{N}_i = \boldsymbol{\mathcal{R}} \cdot \mathbf{e}_i \, , \quad \boldsymbol{\mathcal{R}} = \mathbf{R} \cdot \mathbf{R}_0 \, . \tag{B.7}$$

Recall that the rotation tensor $\mathbf{R}$ is from the polar decomposition of the deformation gradient $\mathbf{F} = \mathbf{V} \cdot \mathbf{R} = \mathbf{R} \cdot \mathbf{U}$. By differentiating (B.7) there follows

$$\dot{\mathbf{n}}_i = \boldsymbol{\omega} \cdot \mathbf{n}_i \, , \tag{B.8}$$

where the spin of the Eulerian triad $\mathbf{n}_i$ is defined by

$$\boldsymbol{\omega} = \dot{\boldsymbol{\mathcal{R}}} \cdot \boldsymbol{\mathcal{R}}^{-1} = \dot{\mathbf{R}} \cdot \mathbf{R}^{-1} + \mathbf{R} \cdot \boldsymbol{\Omega}_0 \cdot \mathbf{R}^T \, . \tag{B.9}$$

On the axes $\mathbf{n}_i$, the spin $\boldsymbol{\omega}$ can be decomposed as

$$\boldsymbol{\omega} = \sum_{i \neq j} \omega_{ij} \, \mathbf{n}_i \otimes \mathbf{n}_j \, . \tag{B.10}$$

Making use of (B.1), (B.2), (B.5) and (B.8) it readily follows that

$$\dot{\mathbf{F}} = \sum_{i=1}^{3} \left(\dot{\lambda}_i \, \mathbf{n}_i \otimes \mathbf{N}_i + \boldsymbol{\omega} \cdot \mathbf{F} - \mathbf{F} \cdot \boldsymbol{\Omega}_0 \right) . \tag{B.11}$$

In view of (B.6) and (B.10) then (B.11) is written as

$$\dot{\mathbf{F}} = \sum_{i=1}^{3} \dot{\lambda}_i \, \mathbf{n}_i \otimes \mathbf{N}_i + \sum_{i \neq j} \left(\lambda_j \omega_{ij} - \lambda_i \Omega_{ij}^0 \right) \mathbf{n}_i \otimes \mathbf{N}_j \, . \tag{B.12}$$

In correspondence with (B.1) the inverse of the deformation gradient can be written in terms of the principal stresses as

$$\mathbf{F}^{-1} = \sum_{i=1}^{3} \frac{1}{\lambda_i} \mathbf{N}_i \otimes \mathbf{n}_i \, . \tag{B.13}$$

Using (B.13) and (2.43) from chapter 2 an expression for the velocity gradient $\mathbf{L}$ is obtained

$$\mathbf{L} = \dot{\mathbf{F}} \cdot \mathbf{F}^{-1} = \sum_{i=1}^{3} \frac{\dot{\lambda}_i}{\lambda_i} \mathbf{n}_i \otimes \mathbf{n}_i + \sum_{i \neq j} \left(\omega_{ij} - \frac{\lambda_i}{\lambda_j} \Omega^0_{ij} \right) \mathbf{n}_i \otimes \mathbf{n}_j \,. \tag{B.14}$$

The symmetric part of $\mathbf{L}$ is the rate of deformation tensor,

$$\mathbf{D} = \sum_{i=1}^{3} \frac{\dot{\lambda}_i}{\lambda_i} \mathbf{n}_i \otimes \mathbf{n}_i + \sum_{i \neq j} \frac{\lambda_j^2 - \lambda_i^2}{2\lambda_i \lambda_j} \Omega^0_{ij} \mathbf{n}_i \otimes \mathbf{n}_j \,, \tag{B.14}$$

while the antisymmetric part is the spin tensor,

$$\mathbf{W} = \sum_{i \neq j} \left(\omega_{ij} - \frac{\lambda_i^2 + \lambda_j^2}{2\lambda_i \lambda_j} \Omega^0_{ij} \right) \mathbf{n}_i \otimes \mathbf{n}_j \,. \tag{B.15}$$

For $i \neq j$ from (B.14) we have

$$\Omega^0_{ij} = \frac{2\lambda_i \lambda_j}{\lambda_j^2 - \lambda_i^2} D_{ij}, \quad \lambda_i \neq \lambda_j \,, \tag{B.16}$$

which is an expression for the components of Lagrangian spin $\mathbf{\Omega}_0$ in terms of the stretch ratios and the components of the rate of deformation tensor. Substituting (B.16) into (B.15) the following expression is obtained

$$\omega_{ij} = W_{ij} - \frac{\lambda_i^2 + \lambda_j^2}{\lambda_i^2 - \lambda_j^2} D_{ij}, \quad \lambda_i \neq \lambda_j \,. \tag{B.17}$$

A final note is that the expressions derived here are generalizations of continuum mechanics based on appropriate kinematic relations and hold for every point in a material's medium. The theory of a porous materials, takes into consideration only mean values. Thus, $\mathbf{W}^v$ and $\mathbf{D}^v$ are the average spin and rate deformation tensors, respectively, so that (B.17) takes the form

$$\omega'_{ij} = W^{\nu'}_{ij} - \frac{\lambda_i^2 + \lambda_j^2}{\lambda_i^2 - \lambda_j^2} D^{\nu'}_{ij} \,, \tag{B.25}$$

where the superscript 'ν' denotes for 'void' and primed quantities is just a notation used in the context to indicate that they are expressed in the Eulerian triad $\{\mathbf{n}_i\}$.

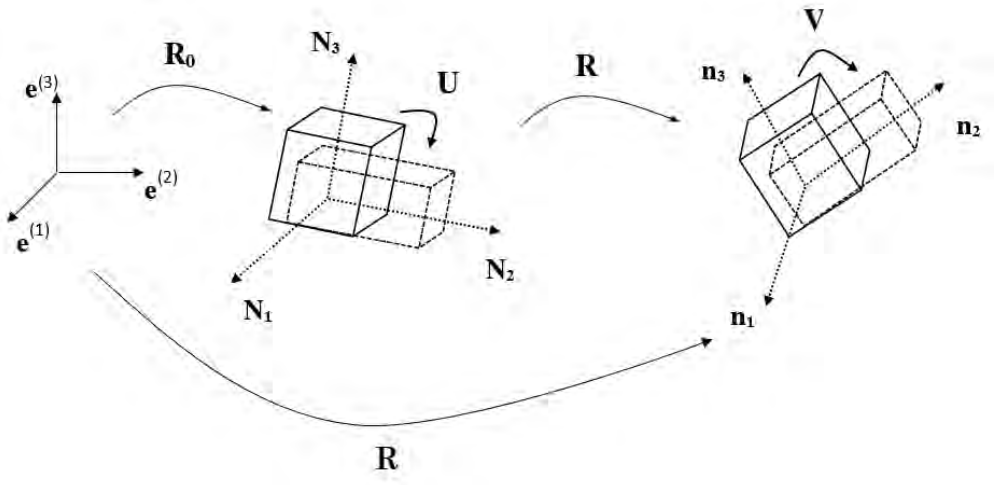

Figure B.1: Schematic representation for the rotation of the orthogonal base $\{\mathbf{e}_i\}$ to the Lagrangian and Eulerian triad $\{\mathbf{N}_i\}$ and $\{\mathbf{n}_i\}$ from the polar decomposition of $\mathbf{F}$.

Bibliography

[1] N. *Αράβας*. *Καρτεσιανοί Τανυστές*. Πανεπιστημιακές Εκδόσεις Θεσσαλίας.

[2] N. *Αράβας*. *Εισαγωγή στη Μηχανική των Παραμορφώσιμων Σωμάτων και τη Γραμμική Ελαστικότητα*. Πανεπιστημιακές Εκδόσεις Θεσσαλίας.

[3] N. Aravas and P. Ponte Castañeda. Numerical methods for porous metals with deformation-induced anisotropy. *Computer methods in applied mechanics and engineering*, 193(36-38):3767–3805, 2004.

[4] H. Cheng and K. Gupta. An historical note on finite rotations. 1989.

[5] C. Chu and A. Needleman. Void nucleation effects in biaxially stretched sheets. 1980.

[6] Y. Dafalias. The plastic spin. 1985.

[7] K. Danas. *Homogenization-based constitutive models for viscoplastic porous media with evolving microstructure*. PhD thesis, University of Pennsylvania, 2008.

[8] K. Danas and N. Aravas. Numerical modeling of elasto-plastic porous materials with void shape effects at finite deformations. *Composites Part B: Engineering*, 43(6):2544–2559, 2012.

[9] A. Elliott. Chapter 7: Dislocations and strengthening mechanisms in metal. https://slideplayer.com/slide/10855681/.

[10] J. D. Eshelby. The determination of the elastic field of an ellipsoidal inclusion, and related problems. *Proceedings of the royal society of London. Series A. Mathematical and physical sciences*, 241(1226):376–396, 1957.

[11] J. D. Eshelby. Elastic inclusions and inhomogeneities. *I.N. Sneddon, R. Hill (Eds.) Progress in Solid Mechanics*, vol. II:87–140, 1961.

[12] F. Fritzen, S. Forest, T. Böhlke, D. Kondo, and T. Kanit. Computational homogenization of elasto-plastic porous metals. *International Journal of Plasticity*, 29:102–119, 2012.

[13] M. Kailasam. *A general constitutive theory for particulate composites and porous materials with evolving microstructures*. PhD thesis, Ph. D. thesis, University of Pennsylvania, 1998.

[14] M. Kailasam, N. Aravas, and P. Ponte Castaneda. Porous metals with developing anisotropy: Constitutive models, computational issues and applications to deformation processing. 2000.

[15] M. Kailasam and P. Ponte Castaneda. A general constitutive theory for linear and nonlinear particulate media with microstructure evolution. *Journal of the Mechanics and Physics of Solids*, 46(3):427–465, 1998.

[16] V. A. Lubarda. *Elastoplasticity theory*. CRC press, 2001.

[17] J. Michel and P. Suquet. The constitutive law of nonlinear viscous and porous materials. *Journal of the Mechanics and Physics of Solids*, 40(4):783–812, 1992.

[18] I. Papadioti, N. Aravas, J. Lian, and S. Münstermann. A strain-gradient isotropic elasto-plastic damage model with j3 dependence. *International Journal of Solids and Structures*, 174:98–127, 2019.

[19] K. Piaras. Mechanics lecture notes part iii: Foundations of continuum mechanics. http://homepages.engineering.auckland.ac.nz/~pkel015/SolidMechanicsBooks/Part_III/index.html.

[20] P. Ponte Castañeda. The effective mechanical properties of nonlinear isotropic composites. *Journal of the Mechanics and Physics of Solids*, 39(1):45–71, 1991.

[21] P. Ponte Castañeda. Effective properties in power-law creep. In *Mechanics of Creep Brittle Materials 2*, pages 218–229. Springer, 1991.

[22] P. Ponte Castañeda and J. R. Willis. The effect of spatial distribution on the effective behavior of composite materials and cracked media. *Journal of the Mechanics and Physics of Solids*, 43(12):1919–1951, 1995.

[23] P. Ponte Castañeda and M. Zaidman. Constitutive models for porous materials with evolving microstructure. *Journal of the Mechanics and Physics of Solids*, 42(9):1459–1497, 1994.

[24] M. D. Rintoul and S. Torquato. Reconstruction of the structure of dispersions. *Journal of colloid and interface science*, 186(2):467–476, 1997.

[25] J. Schöberl. Netgen an advancing front 2d/3d-mesh generator based on abstract rules. *Computing and visualization in science*, 1(1):41–52, 1997.

[26] J. Segurado and J. Llorca. A numerical approximation to the elastic properties of sphere-reinforced composites. *Journal of the Mechanics and Physics of Solids*, 50(10):2107–2121, 2002.

[27] V. Tvergaard and A. Needleman. Analysis of the cup-cone fracture in a round tensile bar. *Acta metallurgica*, 32(1):157–169, 1984.

[28] J. Willis. Bounds and self-consistent estimates for the overall properties of anisotropic composites. *Journal of the Mechanics and Physics of Solids*, 25(3):185–202, 1977.

[29] J. Willis. Variational principles and bounds for the overall properties of composites. *Continuum models for discrete systems*, pages 185–215, 1978.

[30] J. R. Willis. Variational and related methods for the overall properties of composites. In *Advances in applied mechanics*, volume 21, pages 1–78. Elsevier, 1981.

[31] O. Xavier. Multimedia course: Continuum mechanics for engineers. http://oliver.rmee.upc.edu/xo/vpage/1/0/Teaching/Continuum-Mechanics.

[32] S. Xenos. Computational non-local plasticity of porous metals. B.S. thesis, 2018.